GRAPHENE REINFORCED ECO-FRIENDLY WATER SOLUBLE POLYMERS

BY

Osamah Awadh Bin Dahman

A Dissertation Presented to the

DEANSHIP OF GRADUATE STUDIES

KING FAHD UNIVERSITY OF PETROLEUM & MINERALS

DHAHRAN, SAUDI ARABIA

In Partial Fulfillment of the

Requirements for the Degree of

DOCTOR OF PHILOSOPHY

In

CHEMICAL ENGINEERING

December, 2016

KING FAHD UNIVERSITY OF PETROLEUM & MINERALS

DHAHRAN- 31261, SAUDI ARABIA

DEANSHIP OF GRADUATE STUDIES

This thesis, written by **Osamah Awadh Bin Dahman** under the direction his thesis advisor and approved by his thesis committee, has been presented and accepted by the Dean of Graduate Studies, in partial fulfillment of the requirements for the degree of **DOCTOR OF PHILOSOPHY IN CHEMICAL ENGINEERING.**

Dr. Mamdouh A. Al-Harthi
(Advisor)

Dr. Mohammed S. Ba-Shammakh
Department Chairman

Dr. Mohamed B. Amin
(Member)

Dr. Salam A. Zummo
Dean of Graduate Studies

Dr. Mohammed S. Ba-Shammakh
(Member)

29/11/16
Date

Dr. M. Mozahar Hossain
(Member)

Shaikh Abdur Razzak

Dr. Shaikh Abdur Razzak
(Member)

This work is dedicated to my beloved parents, my wife, my sons and daughters, my sisters, and my best friends.

ACKNOWLEDGMENTS

I express my gratitude and praise to ALMIGHTY ALLAH, the Most Merciful and the Most Gracious, for giving me the courage to complete this work successfully.

I am extremely thankful to Department of chemical Engineering, King Fahad University of Petroleum & Minerals (KFUPM), Saudi Arabia for awarding me scholarship to complete my PhD. Special thanks to the Deanship of Scientific Research (DSR), KFUPM, for financial support under project # IN121016.

I express my sincere thanks to my advisor Prof. Mamdouh Ahmed Al-Harthi for supervising my research. Without his invaluable support and guidance I would not have been able to complete my work. My hearties thanks to my committee members: Prof. Mohamed B. Amin, Dr. Mohammed Ba-Shammakh, Dr. M. Mozahar Hossain and Dr. Shaikh Abdur Razzak for their useful comments and suggestion. I would also like to thank Prof. Sadhan Kumar De, Dr. Jobin Jose, and Dr. Mostafizur Rahaman for their helpful suggestions. I am thankful to Mr. Sarath Perumpadappil for helping me in the experimentation. I would also like to acknowledge the Center of Research Excellence in Nanotechnology (CENT) at KFUPM for providing me the laboratory facility.

TABLE OF CONTENTS

LIST OF TABLES

LIST OF FIGURES

ABSTRACT

Full Name : Osamah Awadh Bin Dahman

Thesis Title : Graphene Reinforced Eco-Friendly Water Soluble Polymers

Major Field : Chemical Engineering

Date of Degree : December, 2016

During the last four decades, the daily usage of polyolefinic thermoplastics and different types of thermosets has increased tremendously. These materials are non-biodegradable and their waste causes serious environmental problems. Landfilling, incineration and recycling are common techniques used to solve the disposal problems. However, these methods have their own disadvantages and limitations. Development of biodegradable polymers based on natural resources is a good option for the fabrication of products such as films and packaging materials where high strength is not essential as far as applications are concerned.

In this study, graphene reinforced poly(vinyl alcohol) (PVA)/starch composites were developed using solution mixing and casting technique. After identifying the material combinations with optimum nanofiller, weathering and non-isothermal crystallization kinetics studies have been conducted. Furthermore, electrical and dielectric properties of graphene reinforced PVA/starch composites have been studied extensively. The incorporation of graphene into PVA/starch blend made both the polymers less vulnerable to environmental degradation with a remarkable retention in total crystallinity. Also, the addition of graphene to the PVA/starch system improved its electrical and dielectric properties at different frequencies. Moreover, blends of poly(acrylic acid) (PAA)/starch

were successfully prepared using glycerol as a plasticizer. The prepared PAA/starch composites have good thermal and mechanical properties compared to the individual components. The composites are likely to emerge as materials to find applications in indoor and outdoor applications such as household items, thin films for agriculture and packaging industries.

ملخص الرسالة

الاسم الكامل: أسامه عوض خميس بن دحمان

عنوان الرسالة: البوليمرات الذائبة في الماء الصديقة للبيئة والمدعمة بالجرافين

التخصص: هندسة كيميائية

تاريخ الدرجة العلمية: ديسمبر 2016

خلال الأربعة العقود الأخيرة زاد الاستخدام اليومي للمواد البلاستيكية المختلفة بشكل متسارع. هذه المواد غير قابلة للتحلل، وأصبحت مخلفاتها تسبب مشاكل خطيرة للبيئة. اقترحت العديد من الطرق للتخلص من المخلفات البلاستيكية مثل طريق الطمر والحرق وإعادة التدوير، إلا أن هذه الطرق لها العديد من السلبيات. يُعدُّ تطوير مواد بلاستيكية من مواد عضوية طبيعية قابلة للتحلل هو الخيار المناسب لتصنيع الرقائق ومواد التغليف البلاستيكية.

في هذه الدراسة، تم تطوير مواد مركبة باستخدام متعدد فينيل الكحول مع النشا والمدعمة بالجرافين باستخدام تقنية مزج المحاليل والصب. بعد تحديد التركيز الأمثل للمواد المركبة، تم دراسة تأثير العوامل الجوية وحركيات التبلور للمواد المركبة التي تم تحضيرها. بالإضافة إلى ذلك، تم دراسة الخصائص الكهربائية والعزل للمواد المحضرة.

أظهرت نتائج الدراسة أن إضافة الجرافين إلى المزيج المكون من متعدد فينيل الكحول و النشا أدى إلى تحسين مقاومة المزيج للظروف البيئية مع الاحتفاظ بنسبة عالية من درجة التبلور. كذلك أظهرت النتائج أن وجود الجرافين أدى إلى تحسين الخصائص الحراية والعزل لمزيج متعدد فينيل الكحول و النشا عند ترددات مختلفة. تم أيضاً في هذه الدراسة تحضير مزيج مركب مكون من متعدد حامض الإكريليك مع النشا بنجاح باستخدام مُـلَـدِّن الجليسيرول بخصائص حرارية وميكانيكية جيدة بالمقارنة مع المواد المكونة للمزيج.

من المتوقع أن تجد المواد المركبة التي تم تحضيرها العديد من التطبيقات العملية مثل الادوات المنزلية ومواد التغليف المختلفة.

CHAPTER 1

INTRODUCTION

1.1 Polymeric materials

Polymeric materials offer numerous benefits and the modern life without the use of such materials is nearly impossible. They are being used for the manufacturing of household articles, tote bags, packaging materials, and construction materials. Rising income and growing population have increased the demand for the usage of polymeric materials. Manipulations of processing and final properties contributed their usage tremendously in diverse applications starting from toothbrush to spacecraft.

However, these polymeric materials are hydrophobic and largely non-biodegradable, hence their wastes have severe disposal problem and are hazardous to environment. As an example, plastic bags have a short lifetime of usage and subsequently being thrown away as wastes. Careless dumping of synthetic polymers used in bags, agricultural mulch films, water bottles and food packaging is environmentally hazardous as the conventional polymeric materials are not degraded by micro-organisms and it takes hundreds of years to degrade.

Land filling, incineration and recycling are the universally used techniques to minimize the disposal problems. However, these methods have their own disadvantages and

limitations. Landfilling causes in the contamination of water sources and impediments of groundwater flow and the growth of plant roots, apart from threatening the animals that swallow plastic wastes along with their food. Eventually, considerable part of the waste materials finds their way into rivers and seas that cause polluting of the marine life. Furthermore, plastic wastes clog the drains thus disrupting the urban sewage system. The alternative method of burning of polymer wastes releases poisonous gases in the atmosphere. Next alternative is recycling, which is difficult from practical point of view, as thermoset polymers are not recyclable due to the presence of cross-linked network and the different thermoplastics are not compatible with each other, making the separation process in wastes unattainable and the recycling process uneconomical.

1.2 Biodegradable Polymer Nanocomposites

The long term concerns over the exponential decrease of natural petroleum resources and the environmental pollution has forced the researchers all over the world to think about biodegradable plastics products. Biodegradation is a process in which the substances are broken down by microorganisms, and it is comprised of four major steps; bio-deterioration, bio-fragmentation, assimilation and mineralization. In many ways biopolymers are the best candidates for replacing current synthetic plastics due to their attractive combinations of biodegradability, abundance and renewability. However, lack of basic properties and performance limit their usage in many applications.

The emergence of nanotechnology and reinforcement using nanomaterials in recent years has opened a window to the development of polymer composites for many crucial application areas. Numerous studies have been carried out in the past few years on the preparation and characterization of biopolymer nanocomposites based on layered-silicate

(clay), metal nanoparticles, carbon nanotubes (CNTs), and recently on graphene. The nanometer dimension of reinforcing filler could provide some rooms for manipulation of material composition to impart synergetic effects and thereby many fold improvements on engineering properties.

1.3 Work motivation

In this laboratory, poly(vinyl alcohol) (PVA)/starch blends have been studied extensively by Sreekumar et al. and it has been found that the mechanical integrity and strength are the weakness of the systems and hence they need a reinforcement. Recently, graphene has emerged as promising nanofiller in making novel nanocomposites with unique functional properties. The surface groups present on the graphene surface have been reported to interact with PVA, thus causing exfoliation of graphene nanosheets. Accordingly, we have chosen the development of graphene reinforced biodegradable composites based on PVA/starch as the topic for this project. We are further motivated by the fact that the hydroxyl groups present in both PVA and starch are expected to interact strongly with the oxygen-containing functional groups in graphene oxide (GO). Both starch and PVA are hydrophilic and biodegradable in nature. The advantage of the adding nanofiller such as graphene as a small amount of filler is enough to enhance the strength of the otherwise weak PVA/starch blend system.

1.4 Thesis Summary

This section focuses on the summary of each chapter. Each chapter is presented in manuscript formatting.

Chapter 2 describes the comprehensive review on importance of graphene as a highly rated material for forthcoming research. It focuses on the outstanding mechanical, electrical, thermal, optical and chemical properties of graphene. The applications of graphene based polymer nanocomposites are highlighted. Also, in this chapter the environment friendly polymer nanocomposites based on graphene as the nanofiller are reviewed.

Chapter 3 describes the degradation of a poly(vinyl alcohol)/starch blend and its nanocomposites with graphene under natural weather conditions in Dhahran, Saudi Arabia. After identifying the material combinations with optimum nanofiller in this laboratory, weathering study is conducted. Changes in crystallinity, molecular structure and morphology of the nanocomposites during the period of ageing are observed and reported.

Chapter 4 describes the non-isothermal crystallization behaviors of poly(vinyl alcohol)/starch/graphene nanocomposites using differential scanning calorimetry (DSC). Ozawa and Mo models are employed to study the non-isothermal kinetics. Activation energy (E_A) of these nanocomposites is determined using the differential Friedman method.

Chapter 5 describes electrical and dielectric properties of PVA/starch/graphene nanocomposites. It highlights the effects of graphene loading, and glycerol and starch addition on the DC and AC electrical conductivities and the percolation threshold. Moreover, the influence of these parameters on dielectric properties is investigated in this chapter.

In chapter 6, the compatibility of poly(acrylic acid) and corn starch blend is studied at different blend ratios in the presence of glycerol as a plasticizer. Comprehensive characterizations using different techniques are presented in this chapter.

In chapter 7, the conclusions and recommendations for future work are presented.

CHAPTER 2

LITERATURE REVIEW

2.1 Graphene: A highly rated material for forthcoming research

Graphene has a two-dimensional arrangement of carbon atoms in a hexagonal lattice (honeycomb structure) with sheet having a thickness of just one atom (0.33 nm). Graphene combines the layered structure of clays with excellent mechanical, thermal and electrical properties of carbon nanotubes, which eventually provides exceptional functional properties of the final products. The unique properties of graphene that make it a high potential material for near future research are summarized below:

2.1.1 Electrical properties

- Graphene is an excellent conductor, even better than copper.
- An electron can travel through the graphene sheet as if they carry no mass and as fast as 1/100th speed of light.
- The existence of an anomalous quantum Hall Effect and Klein tunnelling due to the 2-D motion of electrons on graphene sheets.

2.1.2 Thermal properties

- Graphene has got the best thermal conductivity (> 5000 W/m K) compared to all other isotopes of carbon.

- Its thermal conductance is isotropic; same in all directions in a two-dimensional plane.
- It can be easily used in electronic devices to dissipate heat formation.

2.1.3 Mechanical properties

- It is the strongest material human has ever made (stronger than steel and diamond).
- It is also stretchable up to 20% of its original length.
- Graphene can be used to manufacture super strong composites, flexible displays, etc.

2.1.4 Optical properties

- Graphene absorbs 2.3% of the light passes through it and hence it can be visible to the naked eyes.
- Graphene has a high degree of optical transmittance (≈ 98%) with high mobility which makes it a suitable material for fabricating transparent conductive electrodes.

2.1.5 Chemical properties

- Under normal conditions graphene behaves as an inert material, however, it can be functionalized by chemicals to render more reactive.
- Different atoms or molecules can be attached to graphene surface and can be exploited for application as sensors for chemicals.

Since the isolation of single sheet of graphene by Novoselov et al. [1], graphene has attracted attention of researchers in making novel nanocompsites [2]. In recent years, graphene has advanced one step ahead of nanoclays and carbon nanotubes and other nanofillers due to its unique characteristics. Graphene is known to be mixed with graphene oxide [3–6]. The initial development of graphene from graphite was via acid treatment [7] to exfoliate graphene sheets. This usually results in graphene sheets; rich with oxygen containing functionalities or in other words graphene oxide (GO). In order to get impurity free graphene sheets, GO can be reduced (rGO) by using reducing agents such as glucose, hydrazine etc. The use of GO or rGO in the polymer matrix largely depends on the intended applications of the final product. For example, better conductivity or transparency will be better for rGO rather than GO. However, the strong hydrogen bonding interaction derived from the oxygen functionalities in GO imparts better mechanical properties. Several models have been proposed for graphene oxide and one such model is reproduced in Figure 2-1.

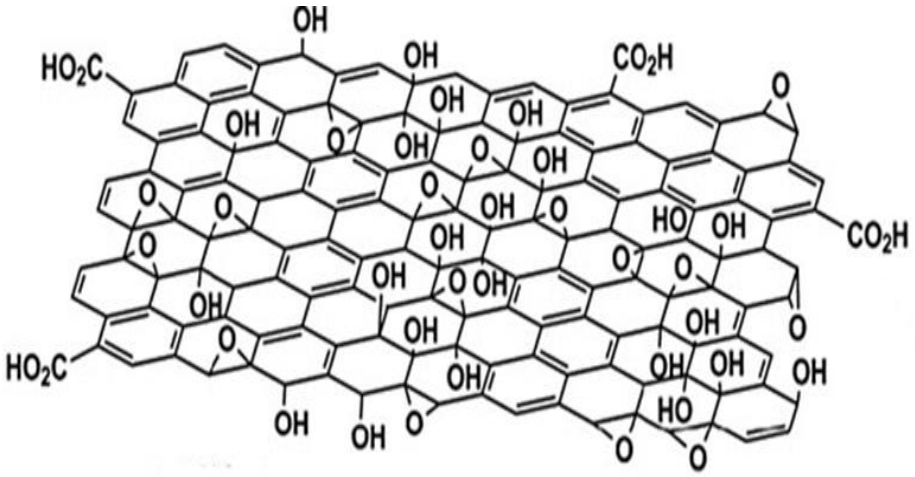

Fig 2-1: A model structure of graphene oxide showing different functional groups on the surface [8].

2.2 Applications of graphene based polymer nanocomposites

The unique properties of graphene make it an ideal candidate for a wide range of applications. These include fabrication of lightweight gasoline tanks, fuel efficient aircraft, hydrogels, aerospace and vehicle parts, stronger wind turbines, sport equipments, solar cells and displays as well as in biocompatible applications such as fabrication of smart packaging materials to keep food fresh and medical implants. Its toxicity issues are negligible as compared to carbon nanotube which has a degree of toxicity quite similar to that of mica or asbestos.

2.3 Dispersion of graphene

In order to achieve full potential in regard to enhancement in mechanical properties of the graphene/polymer composite, the layered nanofiller must be uniformly dispersed the matrix after exfoliation [9]. Ultrasonication is a commonly used method to achieve the exfoliation apart from the rapid heating method [10]. The optimum levels of ultrasonication time and energy is required for a fine dispersion and final product with optimum properties. Lack of sufficient ultrasonication time can cause the existence of graphene clusters in the polymer matrix whereas excess sonication leads to reduction of graphene sheet size [11].

The influence of ultrasonication pretreatment on the mechanical properties of GO/PVA composites was studied by Li at al. It was concluded that the optimum amount of input energy for ultrasonication pretreatment was 15 W h/L [11]. Graphene can be mixed with polymers by solution mixing, melt blend or in situ polymerization [12]. Percolation can be achieved at very low loadings of graphene nanofillers due to high aspect ratio and

large surface area [13,14]. Graphene/PVA nanocomposites have been generated interest in view of its excellent mechanical and electrical properties [15,16].

The optimum properties of the final products largely depend on the homogeneity of the dispersant (nanofiller) in the dispersing medium (polymer) because the large surface area of the nanofiller available for interaction with polymer makes better transfer of the load, mobility of charges or heat. The important factors that affect the performance of a polymer nanocomposite based on any nanofiller are; polymer matrix properties, functionality of filler surface, the quality of nanofiller dispersion in the medium and the processing method. Since the graphene sheets tend to form a curved structure, it is extremely difficult to obtain individual flat graphene sheets. Moreover, the hydrophobic nature of the synthesized graphene especially at their edges makes them further difficult to get into an aqueous medium. It is very important to have a fine dispersion of graphene in the medium of mixing in order to avoid the agglomeration in the final product. Different techniques standardized to make a good dispersion of graphene such as shear force or ultra-sonication, compatibilization using different surfactants and covalent bonding using grafted polymer chains or small molecules [17]. A perfect dispersion of graphene nanosheets in polymers causes less aggregation of the filler and provides extra surface area for the interaction between the nanofiller and the polymer matrix. Consequently, better mechanical and electrical properties can be achieved at low loadings of nanofiller due to the effective transfer of stress or charge through connected networks. Graphene can be made water soluble or stable dispersion with the aid of different functional modifiers. While making a stable dispersion of graphene in aqueous media, the stabilizer can have different functional groups which may facilitate the initial absorption

and then subsequent dispersion in the medium. Care must be taken into account while modifying the graphene so that it will retain its inherent properties especially excellent conductivity and optical properties. A dispersing agent such as 7,7,8,8–tetracyanoquinodimethane (TCNQ) is found to be very efficient in retaining the electrical property due to its highly conjugated system with abundant pi electrons (powerful electron acceptor) [18].

A highly water soluble graphene can be made by repetitive derivatization of graphene nanomaterial with p-carboxyphenyl diazonium tetrafluroborate salt. A series of reactions such as the initiation of the reaction using hypophophorous acid, neutralizing by NaOH, and finally repeat washing with acetoniotrile and water are involved [19]. Graphene water soluble solution can be produced without any aggregation by introducing a small amount of p-phenyl-SO_3H groups into partially-reduced graphene oxide [20]. It is to be noted that the functionalized graphene could form quality dispersion even in the mixture of water and various organic solvents such as methanol and, hence allowed to modify the surface along with polymers for reinforcing applications. It was also possible to control the level of sulfonation with minimal impact on the unique properties of the host polymer matrix and graphene nanofiller. The electrical conductivity of the modified graphene is found to be similar to that of graphite.

Pham et al., [21] made the sulphonic group modification of graphene by covalent functionalization using poly(3-amino benzene sulphonic acid) (PABS). The PABS-g-Graphene had shown better electrical conductivity than that of GO based composite. The reduction reaction enabled to recover the electron mobility on graphene sheets which was hindered by the presence of oxygen functionalities present in the GO. Xue et al., [22]

functionalized graphene oxide with polyhedral oligomeric silsesquioxane (POSS) and they found that the prepared POSS-graphene hybrid was highly soluble in several organic solvents, such as acetone, toluene, tetrahydrofuran (THF), hexane, chloroform and dichloromethane. Moreover, the prepared POSS-modified graphene was found to be useful nanofiller in host polymers such as PMMA. Zhang et al., [23] used a zwitterion intermediate cycloaddition approach to prepare a dispersible graphene. It was found that the functionalized graphene has a good level of dispersion in different solvents, such as water, DMF and $CHCl_3$. Also, the prepared films from the functionalized graphene displayed higher conductivity compared to those prepared from graphene oxide. Wang et al., [24] performed functionalization of graphene using tricobalt tetraoxide (Co_3O_4) to decrease the fire hazards of aliphatic polyester. Co_3O_4 has recognized to reduce the carbon monoxide (CO) content of the pyrolysis gases when burning. Consequently, decreasing the poisonousness of pyrolysis gases which has considerable attention in safety and engineering applications [25].

2.4 Environment friendly polymer nanocomposites based on graphene as the nanofiller

The major applications of biodegradable polymers are in three areas; agricultural, medical and packaging. There are varieties of biodegradable or biocompatible polymer/copolymer matrices or polymer blends available for specific applications. They are further modified by incorporating fillers or crosslinking to suit particular application. The emergence of nanotechnology has improved this area of research and recently main focus has been given for the utilization of the nanofillers in these polymers. Only a very low concentration of filler is required to obtain desired properties while keeping different characteristics such as transparency, less weight and higher mechanical and thermal properties. Compared to other nanofillers, graphene possess the least toxicity issues on bio related applications.

Solution mixing and casting method is the widely suggested and accepted method to prepare the biodegradable polymer nanocomposite, in which water is often employed as the dispersing medium. Different biodegradable polymer based graphene nanocomposites reported in the literature. These biodegradable polymer matrices including poly(vinyl alcohol) [2,17,26–43], poly(lactic acid) [44–53], poly(caprolactone) [54–57], cellulose [58–63], different varieties of starch [64,67], poly(hydroxybutyrate) [68–70], poly(butylene succinate) [71–74], chitosan [75–80] and so on.

Graphene based nanocomposites of different polysaccharides were developed by Gonzalez et al., [81]. The matrices were chitosan/Starch, carboxy methyl cellulose/starch and keratine. The chitosan/starch system showed an improvement in mechanical

properties whereas an opposite trend was observed for the other two systems. This enhancement in the mechanical properties was attributed to the presence of a strong hydrogen bonding interaction in the interface of the former system. Hence it is important to analyse the compatibility and the degree of interaction between graphene and the host polymer matrix in order to achieve the desired properties. The amount of graphene in polymer matrix is expected to be very low in quantity and even more than 3 wt. % of graphene content in polymer matrix can lead to considerable agglomeration [59].

2.5 PVA based graphene nanocomposites

Poly(vinyl alcohol) (PVA) is a synthetic water soluble polymer which possesses unique properties. These include biocompatibility, biodegradability, hydrophilicity, and also it has good mechanical and barrier properties [82]. PVA can be easily blended with biopolymers and fillers to make biodegradable composites owing to its processability and hydrophilicity. The properties of PVA are mainly controlled by the molecular weight, crystallinity and the degree of hydrolysis [83]. Xu et al., [26] reported the preparation of PVA/graphene oxide (GO) nanocomposite by using vacuum filtration. The composites had higher tensile strength and elongation at break compared to the virgin polymer. The absence of graphene peak in the X-ray diffractions (XRD) and the scanning electron microscope (SEM) images of the fracture surface confirmed the homogeneous dispersion of the GO in PVA matrix. The thermal studies (TGA) confirmed the improved stability of the nanocomposites. The optimum improvements in tensile properties were achieved at a GO concentration of 3 wt. %. The homogeneous dispersion and alignment of GO sheets in the PVA matrix along with strong interfacial hydrogen bonding interaction among the components were contributed to the enhancement in nanocomposites properties. Liang et

al., [2] prepared PVA/graphene oxide nanocomposites via simple solution mixing in water and casting method. The molecular level dispersion of graphene in the polymer matrix had significantly improved the mechanical strength properties. They achieved an increase of 76 % in tensile strength and a 62 % enhancement in Young's modulus by using only 0.7 wt. % of GO. They attributed these enhancements in the mechanical properties to two reasons; one is the interaction between PVA and graphene oxide through H-bonding due to oxygen-containing groups on the graphene surface and PVA chains. The second reason is the very large aspect ratio of graphene which favours an efficient stress transfer across the graphene/PVA interface. In a more sophisticated study, Cheng et al., [29] used PVA-g-Graphene Oxide (PVA-g-GO) instead of pristine GO to further improve the PVA based nanocomposite properties. The results were too remarkable as compared to the unfilled PVA , by using 1 wt. % of PVA-g-GO they achieved an increase of 88 % in tensile strength and 150 % improvement in Young's modulus. Also, they got 22 % increase in elongation at break, whereas they observed 15% reduction in elongation at break in the case of GO/PVA nanocomposite with 1 wt. % pristine GO, even though there was some significant improvement in strength properties. Zhao et al., [30] prepared graphene/PVA nanocomposites by introducing graphene oxide into PVA matrix and followed by reducing GO into graphene nanosheets using a facial aqueous solution. The morphology results showed the exfoliated graphene sheets in the bulk matrix and the Raman study confirmed the formation of graphene from GO via reduction reaction. They achieved a significant improvement in the mechanical properties at a low graphene loading. They obtained 10 times increase in Young's modulus and a 150 % enhancement in tensile strength at 1.8 vol. % lading of graphene.

Huang et al., [31] prepared GO/PVA nanocomposites by simple solution mixing process. The TEM and 2D-XRD measurements revealed that GO nanosheets were fully exfoliated and uniformly dispersed in PVA matrix. The FTIR and DSC measurements confirmed the strong hydrogen bonding interactions between GO nanosheets and PVA matrix. Dramatic changes were observed in the barrier properties of GO/PVA nanocomposites. At only 0.72 vol. % loading of graphene, the water vapor and O_2 permeability coefficients of PVA film were dropped by nearly 68% and 98%, respectively. This was ascribed to outstanding impermeable property of GO nanosheets, their full exfoliation, homogeneous dispersion and high orientation in the PVA matrix as well as the strong interfacial interaction between GO nanosheets and PVA matrix. The results had pointed towards a window of application of such materials for packaging industry. The water resistance capability of PVA polymer is very vital while considering them for biomedical and packaging applications. Wang et al. [32] achieved a significant improvement in water resistance by the addition of very low loading of graphene nanofiller. The contact angle measurements revealed that PVA character has been changed from hydrophilic to hydrophobic and hence better resistance against water absorption. They could also obtain a noteworthy improvement in mechanical properties. Also, Wang et al., [33] reported the preparation of PVA/GO nanocomposites via electrospinning method and its characterization. The nanofibers obtained for its mechanical, thermal and morphological analysis. They observed a decrease in decomposition temperature of GO/PVA nanocomposites compared to pristine PVA. They also got 42 times increase in tensile strength at a very low loading (0.02 wt. %). The presence of peroxides on the graphene nanosheets can form covalent bonds with the polymer chains along with strong physical

entanglements via hydrogen bonding eventually making the composite mechanically stronger. Zhang et al., [34] prepared GO/PVA hydrogel composites as a novel biomaterial by solution mixing and freeze/thaw technique. They have prepared GO from pristine graphite via modified Hummer method to attach oxide groups onto the graphene surface. They could obtain a 132 % enhancement in tensile strength and a 36 % increase in compressive strength compared to the pure PVA hydrogels by introducing only 0.8 wt. % of GO.

In case of graphene based nanocomposites, larger area of GO layers ensured perfect interaction with polymer molecules and thereby efficient stress transfer across the interface caused improvement in strength properties rather than crystallinity change. Similar observations were made by Yang et al., [35] for which they confirmed decrease in crystallinity by XRD, FTIR and DSC and also found considerable increase in glass transition temperature (T_g). PVA/graphene nanocomposites can also be prepared from non-covalently functionalized graphene. Wang et al., [36] made a graphene colloid using sodium deoxycholate (SDC) as the functionalizing component and then prepared PVA/Graphene composite via solution mixing and casting method. They optimized the properties at filler loading of 1.0 wt. % and further increase in filler loading adversely affect the final product properties. The glass transition temperatures of the composites were found to increase with increase in graphene content (3.4 °C difference between pure PVA and PVA with 3.0 wt. % of graphene) due to the restricted chain mobility because of graphene. Tantis et al., [37] discovered that chemical functionalization of graphene nanosheets is very important to prevent particle aggregation and to improve the compatibility with the polymer matrix. On contrary to some previous studies, they

observed that a graphene induced crystallization for semi-crystalline PVA polymer at a filler loading of 2 wt. %. They also observed that an enhanced improvement in thermal stability and dielectric permittivity. The acid functionalization of graphene using nitric acid and sulphuric acid can cause extra polar groups (–CO_2H and –OH) on graphene surface and hence better interaction with polymer like PVA [84]. Lee et al., [38] have exclusively studied the change in crystallization behaviour of PVA/Graphene nanocomposites. The crystallinity of graphene/PVA nanocomposites was quantitatively measured using FTIR spectra and DSC. At very low concentrations (<1 wt. %) graphene plays a key role to enhance the crystallinity of the polymer by acting as a nucleating agent. However, the high concentration of graphene in the polymer matrix retarded the crystal formation due to the limited inter-particle distance between graphene nanosheets. In addition it was also found that at high concentration of graphene (>1 wt. %), the mechanical properties increased with respect to graphene content. Ma at al., [17] prepared nanocomposite films of poly(vinyl alcohol) (PVA) and glucose-reduced graphene oxide (RGO) using solution blending method. Surfactants such as sodium dodecyl benzene sulfonate (SDBS) and poly(N-vinyl-2-pyrrolidone) (PVP) was added to stabilize the desperation of RGO in water. The results demonstrated that PVP enhanced the dispersion of RGO in water better than SDBS. Also, it was found that the tensile strength and Young's modulus of nanocomposite film of PVA contains 0.7 wt. % P-RGO were 47 % and 48 %, respectively, higher than that of pristine PVA, respectively. This improvement in mechanical properties was attributed to hydrogen-bonding interaction between PVA and P-RGO. Shang et al., [42] produced poly (vinyl alcohol)/graphene nanoribbon nanocomposites by using a solution mixing technique. Graphene nanoribbon

was produced by unzipping the carbon nanotubes using oxidants. The prepared nanocomposites showed considerable improvements in terms of mechanical performance and thermal stability. The improved properties of the nanocomposites were attributed to the good interaction between graphene nanoribbon and PVA matrix due to hydrogen bonding.

Composite membranes made of PVA and graphene are gaining huge attention these days because the PVA can easily act as transparent carriers while the graphene part serves to enhance the mechanical, thermal and electrical properties of the polymer matrix. Ye et al., [40] observed significant improvements in ionic conductivity and methanol crossover for PVA membrane reinforced with graphene for fuel cell application. An optimum loading of 0.7 % of graphene caused a 126% enhancement in ionic conductivity, 55% reduction in methanol permeability which eventually enhanced the cell performance by a 148% increase in power density.

Latif et al., [39] prepared pectine/PVA/graphene composites and compared the dielectric properties of hydrated and dry films of the composites. It was found that the controlled hydration step had huge impact on dielectric permittivity of the composite and this effect was attributed to the formation of chain-bound water complexes among pectine, PVA and graphene. These types of composite films can find applications in the manufacturing of super capacitor. Jose et al., [43] prepared polymer films of PVA/starch/graphene using glycerol as a plasticizer. A solution mixing and casting technique was employed for preparing the films. The results showed that a graphene loading of 0.5 wt. % is an optimum loading in terms of best mechanical properties. The presence of starch and graphene led to an increase in the thermal stability of PVA and a decrease in the

crystallinity. These films have potential application in packaging purposes and biomedical applications.

2.6 Starch based graphene nanocomposite

Starch is the most abundant natural polymer which can be extracted from agricultural plants or trees and they are believed to be a substitute for petroleum based polymers. It is a biodegradable polymer and has several advantages such as wide availability, lower cost than synthetic materials, and total compostability without any toxic residue [85]. Starch is brittle in absence of an appropriate plasticizer and consequently plasticized starch or modified starch is frequently used to enhance the final features of products [86]. Use the blends of starch with polymers to upgrade the mechanical properties and compatibility as well as to impart a biodegradable property to polymeric materials was widely reported. Blends of starch with synthetic biodegradable polymers such as poly(lactic acid) (PLA) [87–89], polycaprolactone (PCL) [90,91], poly(vinyl alcohol) (PVA) [43,92–97] and poly(acrylic acid) (PAA) [98] have been comprehensively investigated. These blends have full biodegradability, and may be used in vital applications in modern life, such as packaging, agricultural, and medical applications.

Plasticized starch (PS)/graphene (GO or rGO) composites produced by Ma et al., [64] clearly showed the difference in properties between GO and rGO. The nanocomposites with the former showed better mechanical properties and stability against UV light whereas the rGO system showed better thermal stability and electrical conductivity. In another work, glycerol-plasticized pea starch/graphene oxide nanocomposites produced much improved results on several mechanical properties. These improvements were attributed to the formation of hydrogen bonding between the graphene oxide and

hydroxyl groups of starch granules. The GO nanosheets also enhanced the thermal stability and reduced the moisture uptake and UV transmittance of starch films [65]. Ma et al., [66] prepared novel nanocomposites of chitosan (CS)/oxidized starch (OST)/graphene oxide (GO) via solution mixing and casting technique followed by solvent evaporation and compared the characteristic properties against that of nanocomposites containing starch instead of oxidized starch. They found that the presence of acid groups in the oxidized starch enhanced the miscibility of the system. Also it was found that there is an enhancement in mechanical properties, reduction in moisture uptake with respect to graphene oxide content in the compound. Recently, Peregrino et al., [67] fabricated nanocomposites films of acetylated starch (ST) and graphene oxide (GO) using poly(vinyl alcohol) (PVA) as a plasticizer. The GO was converted to reduced graphene oxide (RGO) by using UV treatment. The films showed an enhancement in thermal and electrical properties.

References

[1] K. S. Novoselov, a K. Geim, S. V Morozov, D. Jiang, Y. Zhang, S. V Dubonos, I. V Grigorieva, and a a Firsov, "Electric field effect in atomically thin carbon films.," *Science* , vol. 306, no. 5696, pp. 666–9, Oct. 2004.

[2] J. Liang, Y. Huang, L. Zhang, Y. Wang, Y. Ma, T. Guo, and Y. Chen, "Molecular-Level Dispersion of Graphene into Poly(vinyl alcohol) and Effective Reinforcement of their Nanocomposites," *Adv. Funct. Mater.*, vol. 19, no. 14, pp. 2297–2302, Jul. 2009.

[3] H. Kim, A. Abdala, and C. W. Macosko, "Graphene/Polymer Nanocomposites," *Macromolecules*, vol. 43, no. 16, pp. 6515–6530, Aug. 2010.

[4] C. Gómez-Navarro, J. C. Meyer, R. S. Sundaram, A. Chuvilin, S. Kurasch, M. Burghard, K. Kern, and U. Kaiser, "Atomic structure of reduced graphene oxide.," *Nano Lett.*, vol. 10, no. 4, pp. 1144–8, Apr. 2010.

[5] J. T. Robinson, F. K. Perkins, E. S. Snow, Z. Wei, and P. E. Sheehan, "Reduced graphene oxide molecular sensors.," *Nano Lett.*, vol. 8, no. 10, pp. 3137–40, Oct. 2008.

[6] Y. Zhu, S. Murali, W. Cai, X. Li, J. W. Suk, J. R. Potts, and R. S. Ruoff, "Graphene and graphene oxide: synthesis, properties, and applications.," *Adv. Mater.*, vol. 22, no. 35, pp. 3906–24, Sep. 2010.

[7] W. S. Hummers and R. E. Offeman, "Preparation of Graphitic Oxide," *J. Am. Chem. Soc.*, vol. 80, no. 6, pp. 1339–1339, Mar. 1958.

[8] S. Stankovich, R. D. Piner, S. T. Nguyen, and R. S. Ruoff, "Synthesis and exfoliation of isocyanate-treated graphene oxide nanoplatelets," *Carbon N. Y.*, vol. 44, no. 15, pp. 3342–3347, Dec. 2006.

[9] E. THOSTENSON, C. LI, and T. CHOU, "Nanocomposites in context," *Compos. Sci. Technol.*, vol. 65, no. 3–4, pp. 491–516, Mar. 2005.

[10] S. Park and R. S. Ruoff, "Chemical methods for the production of graphenes.," *Nat. Nanotechnol.*, vol. 4, no. 4, pp. 217–24, Apr. 2009.

[11] Y. Li, R. Umer, Y. A. Samad, L. Zheng, and K. Liao, "The effect of the ultrasonication pre-treatment of graphene oxide (GO) on the mechanical properties of GO/polyvinyl alcohol composites," *Carbon N. Y.*, vol. 55, pp. 321–327, Apr. 2013.

[12] K. Kalaitzidou, H. Fukushima, and L. T. Drzal, "A new compounding method for exfoliated graphite–polypropylene nanocomposites with enhanced flexural

properties and lower percolation threshold," *Compos. Sci. Technol.*, vol. 67, no. 10, pp. 2045–2051, Aug. 2007.

[13] T. Ramanathan, a a Abdala, S. Stankovich, D. a Dikin, M. Herrera-Alonso, R. D. Piner, D. H. Adamson, H. C. Schniepp, X. Chen, R. S. Ruoff, S. T. Nguyen, I. a Aksay, R. K. Prud'Homme, and L. C. Brinson, "Functionalized graphene sheets for polymer nanocomposites.," *Nat. Nanotechnol.*, vol. 3, no. 6, pp. 327–31, Jun. 2008.

[14] P. Steurer, R. Wissert, R. Thomann, and R. Mülhaupt, "Functionalized Graphenes and Thermoplastic Nanocomposites Based upon Expanded Graphite Oxide.," *Macromol. Rapid Commun.*, vol. 30, no. 4–5, pp. 316–27, Feb. 2009.

[15] H. J. Salavagione, G. Martínez, and M. A. Gómez, "Synthesis of poly(vinyl alcohol)/reduced graphite oxide nanocomposites with improved thermal and electrical properties," *J. Mater. Chem.*, vol. 19, no. 28, p. 5027, Jul. 2009.

[16] J. Wu, Q. Tang, H. Sun, J. Lin, H. Ao, M. Huang, and Y. Huang, "Conducting film from graphite oxide nanoplatelets and poly(acrylic acid) by layer-by-layer self-assembly.," *Langmuir*, vol. 24, no. 9, pp. 4800–5, May 2008.

[17] H. L. Ma, Y. Zhang, Q. H. Hu, S. He, X. Li, M. Zhai, and Z. Z. Yu, "Enhanced mechanical properties of poly(vinyl alcohol) nanocomposites with glucose-reduced graphene oxide," *Mater. Lett.*, vol. 102–103, pp. 15–18, Jul. 2013.

[18] R. Hao, W. Qian, L. Zhang, and Y. Hou, "Aqueous dispersions of TCNQ-anion-stabilized graphene sheets.," *Chem. Commun. (Camb).*, no. 48, pp. 6576–8, Dec. 2008.

[19] A. Gizzatov, A. Dimiev, Y. Mackeyev, J. M. Tour, and L. J. Wilson, "Highly water soluble multi-layer graphene nanoribbons and related honey-comb carbon nanostructures.," *Chem. Commun.*, vol. 48, no. 45, pp. 5602–4, Jun. 2012.

[20] Y. Si and E. Samulski, "Synthesis of water soluble graphene," *Nano Lett.*, vol. 8, no. 6, pp. 1679–1682, 2008.

[21] T. A. Pham, J. S. Kim, D. Kim, and Y. T. Jeong, "Facile preparation of water-Dispersible graphene nanosheets by covalent functionalization with poly (3-aminobenzene sulfonic acid)," *Polym. Eng. Sci.*, vol. 52, no. 9, pp. 1854–1861, 2012.

[22] Y. Xue, Y. Liu, F. Lu, J. Qu, H. Chen, and L. Dai, "Functionalization of Graphene Oxide with Polyhedral Oligomeric Silsesquioxane (POSS) for Multifunctional Applications," *J. Phys. Chem. Lett.*, vol. 3, no. 12, pp. 1607–1612, Jun. 2012.

[23] X. Zhang, W. R. Browne, and B. L. Feringa, “Preparation of dispersible graphene through organic functionalization of graphene using a zwitterion intermediate cycloaddition approach,” *RSC Adv.*, vol. 2, no. 32, p. 12173, Nov. 2012.

[24] X. Wang, L. Song, H. Yang, W. Xing, H. Lu, and Y. Hu, “Cobalt oxide/graphene composite for highly efficient CO oxidation and its application in reducing the fire hazards of aliphatic polyesters,” *J. Mater. Chem.*, vol. 22, no. 8, p. 3426, Jan. 2012.

[25] X. Xie, Y. Li, Z. Q. Liu, M. Haruta, and W. Shen, “Low-temperature oxidation of CO catalysed by Co(3)O(4) nanorods.,” *Nature*, vol. 458, no. 7239, pp. 746–9, Apr. 2009.

[26] Y. Xu, W. Hong, H. Bai, C. Li, and G. Shi, “Strong and ductile poly(vinyl alcohol)/graphene oxide composite films with a layered structure,” *Carbon N. Y.*, vol. 47, no. 15, pp. 3538–3543, Dec. 2009.

[27] S. Mitra, S. Banerjee, and D. Chakravorty, “Tunneling conduction in graphene/(poly)vinyl alcohol composite,” *J. Appl. Phys.*, vol. 113, no. 15, p. 154314, 2013.

[28] S. Mitra, O. Mondal, D. R. Saha, A. Datta, S. Banerjee, and D. Chakravorty, “Magnetodielectric effect in Graphene-PVA nanocomposites,” *J. Phys. Chem. C*, vol. 115, no. 29, pp. 14285–14289, 2011.

[29] H. K. F. Cheng, N. G. Sahoo, Y. P. Tan, Y. Pan, H. Bao, L. Li, S. H. Chan, and J. Zhao, “Poly(vinyl alcohol) nanocomposites filled with poly(vinyl alcohol)-grafted graphene oxide,” *ACS Appl. Mater. Interfaces*, vol. 4, no. 5, pp. 2387–94, May 2012.

[30] X. Zhao, Q. Zhang, D. Chen, and P. Lu, “Enhanced Mechanical Properties of Graphene-Based Poly(vinyl alcohol) Composites,” *Macromolecules*, vol. 43, no. 5, pp. 2357–2363, Mar. 2010.

[31] H. D. Huang, P. G. Ren, J. Chen, W. Q. Zhang, X. Ji, and Z. M. Li, “High barrier graphene oxide nanosheet/poly(vinyl alcohol) nanocomposite films,” *J. Memb. Sci.*, vol. 409, no. 410, pp. 156–163, Aug. 2012.

[32] J. Wang, X. Wang, C. Xu, M. Zhang, and X. Shang, “Preparation of graphene/poly(vinyl alcohol) nanocomposites with enhanced mechanical properties and water resistance,” *Polym. Int.*, vol. 60, no. 5, pp. 816–822, May 2011.

[33] C. Wang, Y. Li, G. Ding, X. Xie, and M. Jiang, “Preparation and characterization of graphene oxide/poly(vinyl alcohol) composite nanofibers via electrospinning,” *J. Appl. Polym. Sci.*, vol. 127, no. 4, pp. 3026–3032, Feb. 2013.

[34] L. Zhang, Z. Wang, C. Xu, Y. Li, J. Gao, W. Wang, and Y. Liu, "High strength graphene oxide/polyvinyl alcohol composite hydrogels," *J. Mater. Chem.*, vol. 21, no. 28, pp. 10399–10406, 2011.

[35] X. Yang, L. Li, S. Shang, and X. Tao, "Synthesis and characterization of layer-aligned poly(vinyl alcohol)/graphene nanocomposites," *Polymer (Guildf).*, vol. 51, no. 15, pp. 3431–3435, Jul. 2010.

[36] L. Wang, R. Liao, Z. Tang, Y. Lei, and B. Guo, "Sodium deoxycholate functionalized graphene and its composites with polyvinyl alcohol," *J. Phys. D. Appl. Phys.*, vol. 44, no. 44, p. 445302, Nov. 2011.

[37] I. Tantis, G. Psarras, and D. Tasis, "Functionalized graphene–poly (vinyl alcohol) nanocomposites: Physical and dielectric properties," *eXPRESS Polym. Lett.*, vol. 6, no. 4, pp. 283–292, 2012.

[38] S. Lee, J. Y. Hong, and J. Jang, "The effect of graphene nanofiller on the crystallization behavior and mechanical properties of poly(vinyl alcohol)," *Polym. Int.*, vol. 62, no. 6, pp. 901–908, Jun. 2012.

[39] I. A. Latif, S. M. Abbas, and M. A. Kadhum, "Hydrogen Bonds Effects on the Electrical Properties of Pectin / Pva Graphene Nanocomposites," *Chem. Mater. Res.*, vol. 3, no. 1, pp. 1–12, 2013.

[40] Y. S. Ye, M. Y. Cheng, X. L. Xie, J. Rick, Y. J. Huang, F. C. Chang, and B. J. Hwang, "Alkali doped polyvinyl alcohol/graphene electrolyte for direct methanol alkaline fuel cells," *J. Power Sources*, vol. 239, pp. 424–432, Oct. 2013.

[41] S. D. Wu, W. Lv, J. Xu, D. Han, X. Chen, P. Wang, and Q. H. Yang, "A graphene/poly(vinyl alcohol) hybrid membrane self-assembled at the liquid/air interface: enhanced mechanical performance and promising saturable absorber," *J. Mater. Chem.*, vol. 22, no. 33, p. 17204, 2012.

[42] S. Shang, L. Gan, C. W. M. Yuen, S. Jiang, and N. M. Luo, "The synthesis of graphene nanoribbon and its reinforcing effect on poly (vinyl alcohol)," *Compos. Part A Appl. Sci. Manuf.*, vol. 68, pp. 149–154, Jan. 2015.

[43] J. Jose, M. A. Al-Harthi, M. A.-A. AlMa'adeed, J. Bhadra Dakua, and S. K. De, "Effect of graphene loading on thermomechanical properties of poly(vinyl alcohol)/starch blend," *J. Appl. Polym. Sci.*, vol. 132, no. 16, p. n/a–n/a, Jan. 2015.

[44] Y. Shen, T. Jing, W. Ren, J. Zhang, Z. G. Jiang, Z. Z. Yu, and A. Dasari, "Chemical and thermal reduction of graphene oxide and its electrically conductive polylactic acid nanocomposites," *Compos. Sci. Technol.*, vol. 72, no. 12, pp. 1430–1435, Jul. 2012.

[45] I. H. Kim and Y. G. Jeong, "Polylactide/exfoliated graphite nanocomposites with enhanced thermal stability, mechanical modulus, and electrical conductivity," *J. Polym. Sci. Part B Polym. Phys.*, vol. 48, no. 8, pp. 850–858, Apr. 2010.

[46] E. Narimissa, R. K. Gupta, H. J. Choi, N. Kao, and M. Jollands, "Morphological, mechanical, and thermal characterization of biopolymer composites based on polylactide and nanographite platelets," *Polym. Compos.*, vol. 33, no. 9, pp. 1505–1515, Sep. 2012.

[47] B. W. Chieng, N. A. Ibrahim, W. M. Z. W. Yunus, M. Z. Hussein, and V. S. Giita Silverajah, "Graphene Nanoplatelets as Novel Reinforcement Filler in Poly(lactic acid)/Epoxidized Palm Oil Green Nanocomposites: Mechanical Properties.," *Int. J. Mol. Sci.*, vol. 13, no. 9, pp. 10920–34, Jan. 2012.

[48] B. W. Chieng, N. A. Ibrahim, W. Zin, W. Yunus, and M. Z. Hussein, "Poly(lactic acid)/Poly(ethylene glycol) Polymer Nanocomposites: Effects of Graphene Nanoplatelets," *Polymers (Basel).*, vol. 6, no. 1, pp. 93–104, 2014.

[49] Y. Chen, X. Yao, X. Zhou, Z. Pan, and Q. Gu, "Poly(lactic acid)/Graphene Nanocomposites Prepared via Solution Blending Using Chloroform as a Mutual Solvent," *J. Nanosci. Nanotechnol.*, vol. 11, no. 9, pp. 7813–7819, Sep. 2011.

[50] L. Lei, J. Qiu, and E. Sakai, "Preparing conductive poly(lactic acid) (PLA) with poly(methyl methacrylate) (PMMA) functionalized graphene (PFG) by admicellar polymerization," *Chem. Eng. J.*, vol. 209, pp. 20–27, Oct. 2012.

[51] A. M. Pinto, J. Cabral, D. a. P. Tanaka, A. M. Mendes, and F. D. Magalhães, "Effect of incorporation of graphene oxide and graphene nanoplatelets on mechanical and gas permeability properties of poly(lactic acid) films," *Polym. Int.*, vol. 62, no. 1, pp. 33–40, Jan. 2013.

[52] H. Wang and Z. Qiu, "Crystallization behaviors of biodegradable poly(l-lactic acid)/graphene oxide nanocomposites from the amorphous state," *Thermochim. Acta*, vol. 526, no. 1–2, pp. 229–236, Nov. 2011.

[53] W. Li, Z. Xu, L. Chen, M. Shan, X. Tian, C. Yang, H. Lv, and X. Qian, "A facile method to produce graphene oxide-g-poly(L-lactic acid) as an promising reinforcement for PLLA nanocomposites," *Chem. Eng. J.*, vol. 237, pp. 291–299, Feb. 2014.

[54] W. Kai, Y. Hirota, L. Hua, and Y. Inoue, "Thermal and mechanical properties of a poly(ε-caprolactone)/graphite oxide composite," *J. Appl. Polym. Sci.*, vol. 107, no. 3, pp. 1395–1400, Feb. 2008.

[55] D. Cai and M. Song, “A simple route to enhance the interface between graphite oxide nanoplatelets and a semi-crystalline polymer for stress transfer.,” *Nanotechnology*, vol. 20, no. 31, p. 315708, Aug. 2009.

[56] S. Sayyar, E. Murray, B. C. Thompson, S. Gambhir, D. L. Officer, and G. G. Wallace, “Covalently linked biocompatible graphene/polycaprolactone composites for tissue engineering,” *Carbon N. Y.*, vol. 52, pp. 296–304, Feb. 2013.

[57] T. Nezakati, A. Tan, and A. M. Seifalian, “Enhancing the electrical conductivity of a hybrid POSS-PCL/graphene nanocomposite polymer.,” *J. Colloid Interface Sci.*, vol. 435, pp. 145–55, Dec. 2014.

[58] N. D. Luong, N. Pahimanolis, U. Hippi, J. T. Korhonen, J. Ruokolainen, L. S. Johansson, J. D. Nam, and J. Seppälä, “Graphene/cellulose nanocomposite paper with high electrical and mechanical performances,” *J. Mater. Chem.*, vol. 21, no. 36, p. 13991, Aug. 2011.

[59] G. W. Jeon, J. E. An, and Y. G. Jeong, “High performance cellulose acetate propionate composites reinforced with exfoliated graphene,” *Compos. Part B Eng.*, vol. 43, no. 8, pp. 3412–3418, Dec. 2012.

[60] Y. Feng, X. Zhang, Y. Shen, K. Yoshino, and W. Feng, “A mechanically strong, flexible and conductive film based on bacterial cellulose/graphene nanocomposite,” *Carbohydr. Polym.*, vol. 87, no. 1, pp. 644–649, Jan. 2012.

[61] X. Zhang, X. Liu, W. Zheng, and J. Zhu, “Regenerated cellulose/graphene nanocomposite films prepared in DMAC/LiCl solution,” *Carbohydr. Polym.*, vol. 88, no. 1, pp. 26–30, Mar. 2012.

[62] M. Yadav, K. Y. Rhee, I. H. Jung, and S. J. Park, “Eco-friendly synthesis, characterization and properties of a sodium carboxymethyl cellulose/graphene oxide nanocomposite film,” *Cellulose*, vol. 20, no. 2, pp. 687–698, Jan. 2013.

[63] R. K. Layek, A. Kundu, and A. K. Nandi, “High-Performance Nanocomposites of Sodium Carboxymethylcellulose and Graphene Oxide,” *Macromol. Mater. Eng.*, vol. 298, no. 11, pp. 1166–1175, Nov. 2013.

[64] T. Ma, P. R. Chang, P. Zheng, and X. Ma, “The composites based on plasticized starch and graphene oxide/reduced graphene oxide.,” *Carbohydr. Polym.*, vol. 94, no. 1, pp. 63–70, Apr. 2013.

[65] R. Li, C. Liu, and J. Ma, “Studies on the properties of graphene oxide-reinforced starch biocomposites,” *Carbohydr. Polym.*, vol. 84, no. 1, pp. 631–637, Feb. 2011.

[66] J. Ma, C. Liu, R. Li, and J. Wang, “Properties and structural characterization of oxide starch/chitosan/graphene oxide biodegradable nanocomposites,” *J. Appl. Polym. Sci.*, vol. 123, no. 5, pp. 2933–2944, Mar. 2012.

[67] P. P. Peregrino, M. J. A. Sales, M. F. P. da Silva, M. A. G. Soler, L. F. L. da Silva, S. G. C. Moreira, and L. G. Paterno, “Thermal and electrical properties of starch-graphene oxide nanocomposites improved by photochemical treatment.,” *Carbohydr. Polym.*, vol. 106, pp. 305–11, Jun. 2014.

[68] X. Jing and Z. Qiu, “Effect of Low Thermally Reduced Graphene Loadings on the Crystallization Kinetics and Morphology of Biodegradable Poly(3-hydroxybutyrate),” *Ind. Eng. Chem. Res.*, vol. 51, no. 42, pp. 13686–13691, Oct. 2012.

[69] V. Sridhar, I. Lee, H. H. Chun, and H. Park, “Graphene reinforced biodegradable poly(3-hydroxybutyrate-co-4-hydroxybutyrate) nano-composites,” *eXPRESS Polym. Lett.*, vol. 7, no. 4, pp. 320–328, 2013.

[70] C. R. Arza, P. Jannasch, and F. H. J. Maurer, “Network formation of graphene oxide in poly(3-hydroxybutyrate) nanocomposites,” *Eur. Polym. J.*, vol. 59, pp. 262–269, Oct. 2014.

[71] C. Wan and B. Chen, “Reinforcement of biodegradable poly(butylene succinate) with low loadings of graphene oxide,” *J. Appl. Polym. Sci.*, vol. 127, no. 6, pp. 5094–5099, Mar. 2013.

[72] X. Wang, S. Xuan, L. Song, H. Yang, H. Lu, and Y. Hu, “Synergistic Effect of POSS on Mechanical Properties, Flammability, and Thermal Degradation of Intumescent Flame Retardant Polylactide Composites,” *J. Macromol. Sci. Part B*, vol. 51, no. 2, pp. 255–268, Feb. 2012.

[73] X. Wang, H. Yang, L. Song, Y. Hu, W. Xing, and H. Lu, “Morphology, mechanical and thermal properties of graphene-reinforced poly(butylene succinate) nanocomposites,” *Compos. Sci. Technol.*, vol. 72, no. 1, pp. 1–6, Dec. 2011.

[74] X. W. Wang, C. Zhang, P. L. Wang, J. Zhao, W. Zhang, J. H. Ji, K. Hua, J. Zhou, X. B. Yang, and X. P. Li, “Enhanced performance of biodegradable poly(butylene succinate)/graphene oxide nanocomposites via in situ polymerization,” *Langmuir*, vol. 28, no. 18, pp. 7091–5, May 2012.

[75] Y. Chen, L. Chen, H. Bai, and L. Li, “Graphene oxide–chitosan composite hydrogels as broad-spectrum adsorbents for water purification,” *J. Mater. Chem. A*, vol. 1, no. 6, pp. 1992–2001, 2013.

[76] J. H. Lee, J. Marroquin, K. Y. Rhee, S. J. Park, and D. Hui, "Cryomilling application of graphene to improve material properties of graphene/chitosan nanocomposites," *Compos. Part B Eng.*, vol. 45, no. 1, pp. 682–687, Feb. 2013.

[77] J. S. Cheng, J. Du, and W. Zhu, "Facile synthesis of three-dimensional chitosan–graphene mesostructures for reactive black 5 removal," *Carbohydr. Polym.*, vol. 88, no. 1, pp. 61–67, 2012.

[78] N. Zhang, H. Qiu, Y. Si, W. Wang, and J. Gao, "Fabrication of highly porous biodegradable monoliths strengthened by graphene oxide and their adsorption of metal ions," *Carbon N. Y.*, vol. 49, no. 3, pp. 827–837, Mar. 2011.

[79] G. Yang, J. Cao, L. Li, R. K. Rana, and J. J. Zhu, "Carboxymethyl chitosan-functionalized graphene for label-free electrochemical cytosensing," *Carbon N. Y.*, vol. 51, pp. 124–133, Jan. 2013.

[80] R. Justin and B. Chen, "Characterisation and drug release performance of biodegradable chitosan-graphene oxide nanocomposites.," *Carbohydr. Polym.*, vol. 103, pp. 70–80, Mar. 2014.

[81] C. Rodríguez-González, A. L. Martínez-Hernández, V. M. Castaño, O. V. Kharissova, R. S. Ruoff, and C. Velasco-Santos, "Polysaccharide nanocomposites reinforced with graphene oxide and keratin-grafted graphene oxide," *ndustrial Eng. Chem. Res.*, vol. 51, no. 9, pp. 3619–3629, 2012.

[82] M. I. Baker, S. P. Walsh, Z. Schwartz, and B. D. Boyan, "A review of polyvinyl alcohol and its uses in cartilage and orthopedic applications.," *J. Biomed. Mater. Res. B. Appl. Biomater.*, vol. 100, no. 5, pp. 1451–7, Jul. 2012.

[83] N. A. Peppas and E. W. Merrill, "Development of semicrystalline poly(vinyl alcohol) hydrogels for biomedical applications.," *J. Biomed. Mater. Res.*, vol. 11, no. 3, pp. 423–34, May 1977.

[84] B. Das, K. Eswar Prasad, U. Ramamurty, and C. N. R. Rao, "Nano-indentation studies on polymer matrix composites reinforced by few-layer graphene.," *Nanotechnology*, vol. 20, no. 12, p. 125705, Mar. 2009.

[85] F. Xie, E. Pollet, P. J. Halley, and L. Avérous, "Starch-based nano-biocomposites," *Prog. Polym. Sci.*, vol. 38, no. 10–11, pp. 1590–1628, Oct. 2013.

[86] M. Maiti, B. S. Kaith, R. Jindal, and A. K. Jana, "Synthesis and characterization of corn starch based green composites reinforced with Saccharum spontaneum L graft copolymers prepared under micro-wave and their effect on thermal, physio-chemical and mechanical properties," *Polym. Degrad. Stab.*, vol. 95, no. 9, pp. 1694–1703, Sep. 2010.

[87] H. Oza, M. R. Thompson, A. N. Hrymak, and Q. Liu, “Influence of di-functional versus multi-functional chain extenders on the foamability of a potato starch-based biopolymer,” *Starch - Stärke*, vol. 64, no. 12, pp. 944–954, Dec. 2012.

[88] C. Ouyang, Y. Wang, N. Zhao, X. Liu, S. Li, and Z. Zhang, “Preparation of poly(lactic acid) and modified starch composites,” *Polym. Bull.*, vol. 68, no. 7, pp. 2009–2019, Jan. 2012.

[89] Z. Xiong, Y. Yang, J. Feng, X. Zhang, C. Zhang, Z. Tang, and J. Zhu, “Preparation and characterization of poly(lactic acid)/starch composites toughened with epoxidized soybean oil.,” *Carbohydr. Polym.*, vol. 92, no. 1, pp. 810–6, Jan. 2013.

[90] F. M. Nor, D. Kurniawan, Y. K. Seo, J. K. Park, H. Y. Lee, and J. Y. Lim, “Polycaprolactone-starch blends with corn-based coupling agent: physical properties and in vitro analysis.,” *Proc. Inst. Mech. Eng. H.*, vol. 226, no. 9, pp. 693–8, Sep. 2012.

[91] S. Ali Akbari Ghavimi, M. H. Ebrahimzadeh, M. Solati-Hashjin, and N. A. Abu Osman, “Polycaprolactone/starch composite: Fabrication, structure, properties, and applications.,” *J. Biomed. Mater. Res. A*, Nov. 2014.

[92] H. M. Palma-Rodríguez, G. Aguirre-Álvarez, N. Chavarría-Hernández, A. I. Rodríguez-Hernández, L. A. Bello-Pérez, and A. Vargas-Torres, “Oxidized banana starch-polyvinyl alcohol film: Partial characterization,” *Starch - Stärke*, vol. 64, no. 11, pp. 882–889, Nov. 2012.

[93] P. Sreekumar, M. a. Al-Harthi, and S. De, “Reinforcement of starch/polyvinyl alcohol blend using nano-titanium dioxide,” *J. Compos. Mater.*, vol. 46, no. 25, pp. 3181–3187, Feb. 2012.

[94] P. A. Sreekumar, M. A. Al-Harthi, and S. K. De, “Effect of glycerol on thermal and mechanical properties of polyvinyl alcohol/starch blends,” *J. Appl. Polym. Sci.*, vol. 123, no. 1, pp. 135–142, 2012.

[95] P. A. Sreekumar, M. A. Al-Harthi, and S. K. De, “Studies on compatibility of biodegradable starch/polyvinyl alcohol blends,” *Polym. Eng. Sci.*, vol. 52, no. 10, pp. 2167–2172, Oct. 2012.

[96] S. P. Appu, S. K. De, M. J. Khan, and M. A. Al-Harthi, “Natural weather ageing of starch/polyvinyl alcohol blend: effect of glycerol content,” *J. Polym. Eng.*, vol. 33, no. 3, pp. 1–7, Jan. 2013.

[97] J. Jose, S. K. De, M. A. AlMa’adeed, J. B. Dakua, P. A. Sreekumar, R. Sougrat, and M. A. Al-Harthi, “Compatibilizing role of carbon nanotubes in poly(vinyl alcohol)/starch blend,” *Starch /Stärke*, vol. 66, pp. 1–7, Oct. 2014.

[98] O. A. Bin-Dahman, J. Jose, and M. A. Al-Harthi, “Compatibility of poly(acrylic acid)/starch blends,” *Starch - Stärke*, p. n/a–n/a, Jun. 2015.

CHAPTER 3

EFFECT OF NATURAL WEATHER AGING ON THE CRYSTALLINITY OF POLY(VINYL ALCOHOL)/STARCH/GRAPHENE NANOCOMPOSITE

Osamah A. Bin-Dahman[1], Jobin Jose[2] and Mamdouh A. Al-Harthi[1, 3]

[1]Department of Chemical Engineering, King Fahd University of Petroleum & Minerals, Dhahran, Saudi Arabia

[2]Center for Engineering Research, King Fahd University of Petroleum & Minerals, Dhahran, Saudi Arabia

[3]Center for Research Excellence in Nanotechnology, King Fahd University of Petroleum & Minerals, Dhahran, Saudi Arabia

[*]Corresponding Author: Mamdouh A. Al-Harthi, E-mail address: mamdouh@kfupm.edu.sa

This chapter has been published in "Starch/Stärke" on July 4, 2016

Abstract

Degradation has a significant impact on the crystallinity of biodegradable polymers. This chapter was undertaken to investigate the degradation of a poly(vinyl alcohol) (PVA)/starch blend and its nanocomposites with graphene under natural weathering conditions in Dhahran, Saudi Arabia. Changes in crystallinity, mechanical properties, molecular structure and morphology of the nanocomposites during the aging period have been observed and inferred. The thermal and spectroscopic results demonstrated the dissolution of the amorphous phase during early stages of exposure followed by the deterioration of the crystalline phase in later stages. Morphological micrographs showed that the surface of the nanocomposites had fewer defects compared to the PVA/starch blend. Poly(vinyl alcohol)/starch/graphene nanocomposites showed a remarkable retention in total crystallinity compared to the PVA/starch blend during the aging period. The incorporation of graphene into the PVA/starch blend made both the polymers less vulnerable to environmental degradation, and these nanocomposites could therefore be suitable as packaging films for use in outdoor applications.

Keywords:

Natural weathering / Crystallinity / PVA-starch blend / Graphene / Nanocomposites.

3.1 Introduction

Polymeric materials are widely used for the manufacturing of tote bags, household articles, and packaging materials. However, as they are hydrophobic and largely non-biodegradable, these materials present a significant waste disposal problem and are hazardous to the environment. Land-filling, incineration, and recycling are universal techniques used to solve the problem of disposal of plastic products. However, these approaches each have their own shortcomings and limitations. The long-term concern over the problem of environmental pollution has led researchers to consider biodegradable plastic products. Efforts have been made to overcome these environmental problems by blending synthetic biodegradable polymers with biopolymers [1–7].

Poly(vinyl alcohol) (PVA) is a synthetic, water-soluble polymer that possesses unique properties. These include biocompatibility, biodegradability, hydrophilicity, and good mechanical and barrier properties [8]. Poly(vinyl alcohol) can be easily blended with biopolymers and fillers to make biodegradable composites due to its easy processing and hydrophilicity. The properties of PVA are primarily controlled by its molecular weight, crystallinity and the degree of hydrolysis [9]. Poly(vinyl alcohol) has been used in a wide range of applications including the fabrication of biomedical materials [10,11], membranes [12,13], and drug delivery systems [14,15].

Pure PVA films have two primary limitations: high cost and a low biodegradation rate [16,17]. These shortcomings can be mitigated by blending PVA with cheap, renewable, widely available, and fully biodegradable materials such as starch [18,19]. Starch can be used to improve the properties and reduce the cost of final products [20]. The blend ratio between PVA and starch can be modified to obtain the desired mechanical properties. We

observed that the optimal properties of the PVA/starch system in terms of compatibility and mechanical properties can be obtained with a ratio of 70/30 by weight. Glycerol was used as a plasticizer in this study [7,21].

The degradability of PVA with several biopolymers under different environmental conditions has been reported in the literature [22–25]. It has been reported that the biodegradation of a starch/PVA mixture depends on the composition and the nature of the microorganism [23]. Biodegradation increased the transparency of a soy protein isolate/PVA composite and converted it into small parts [26]. The degradation of PVA and starch/PVA blends under natural weathering conditions increased with a high glycerol content of [25].

The emergence of nanotechnology and reinforcement using nanomaterials has allowed for the development of polymer composites used for diverse applications. Recently, the thermal and mechanical properties of the PVA/starch system using carbon nanotubes and graphene as nanofillers have been studied [27,28].

The study of polymer degradation under natural weathering is imperative because it has environmental significance and because of the increased use of polymer products in outdoor applications. Natural weathering is a complex process due to the presence of several variable parameters, including sunlight, humidity, wind, and rain. In this chapter, we studied the progress of natural weather aging of a PVA/starch blend and its graphene nanocomposites at our University premises in Dhahran, Saudi Arabia. Special emphasis was given to the study of the changes in crystallinity, mechanical properties, molecular structure, and morphology.

3.2 Materials and methods

3.2.1 Materials

Poly(vinyl alcohol) (CAS Number: 9002-89-5) with a molecular weight of 27,000 and glycerol (CAS number: 56-81-5) were procured from Sigma Aldrich Company. Corn starch (CAS number: 9005-25-8) with a 27% Amylose was delivered by ARASCO Corn Products, Dammam, Saudi Arabia. Graphene (CAS Number: 1034343-98-0) with oxygen content of 1 %, surface area of about 13-15 m^2/g and thickness from 50 to 100 nm was purchased from Grafen Chemical Industries Co, Turkey.

3.2.2 Preparation of composites

Poly(vinyl alcohol)/starch/graphene nanocomposites were prepared via solution mixing and casting techniques. The details of sample preparation were given by Jose et al. [28]. The weight ratio between PVA and starch was kept constant (70:30). Graphene was added based on the formulations shown in Table 3-1.

Table 3-1: Formulations used for the preparation of PVA/starch/graphene nanocomposites

Sample code	PVA/starch (wt. %) [a)]	Graphene	
		Wt. % based on polymer blend	Actual weight (g)
PS	70/30	0	0
PSG (0.25%)	70/30	0.25	0.015
PSG (0.5%)	70/30	0.5	0.03
PSG (1%)	70/30	1	0.06

a) Each of the composition contains 4.8 g of PVA, 1.8 g of starch and 3 g (2.4 mL) of glycerol.

3.2.3 Natural weather aging

Sheets of PVA/starch blend and its nanocomposites with graphene were used for the natural weather aging studies. Before exposure, the sheets were conditioned at a temperature of 50 °C in an air oven for 24 h. The samples were exposed to an outdoor environment in Dhahran, Saudi Arabia. Strips of samples cut from the sheets (average thickness of about 0.30 mm) were fixed on a rack at an angle of 45° on the rooftop of our research building. The sample rack was placed facing East for maximum exposure to sunlight (Latitude: 26° 17′ 0″ N, Longitude: 50° 12′ 0″ E). The weathering study was conducted from the first week of October until first week of December, and samples were collected at regular intervals (0, 1, 3, 5, 7, and 9 wk) to analyze the extent of degradation with respect to exposure time. Details of the average temperature, humidity, and rainfall during these periods are shown in Fig. 3-1.

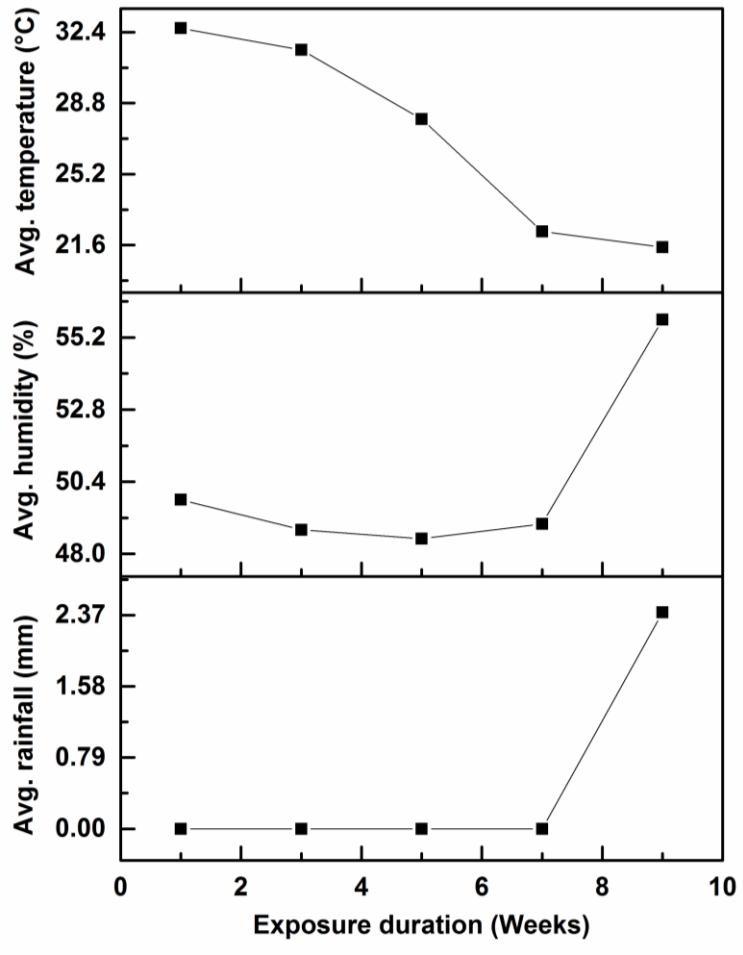

Fig 3-1: Climate data for Dhahran, Saudi Arabia, from October until December

3.2.4 Differential scanning calorimeter (DSC) analysis

Differential scanning calorimetric (DSC) studies were conducted using a DSC-Q1000, Universal V4.2E TA instrument. The melting and crystallization behaviors of the blends were studied at a heating rate of 10 °C/min and at a range of temperatures between -50 °C and 240 °C in a nitrogen atmosphere. The percentage of crystallinity was estimated using the following expression [29,30]:

$$\%\ of\ crystallinity = \left(\frac{\Delta H_{fus}/\emptyset_{PVA}}{\Delta H^{o}_{fus}}\right) \times 100 \qquad (3\text{-}1)$$

Where, ΔH_{fus} is the enthalpy of fusion of the composites, ΔH^{o}_{fus} is the enthalpy of fusion of the 100 % crystalline PVA, and $\emptyset_{PVA}$ is the PVA fraction in the composites. The value of ΔH^{o}_{fus} of PVA was taken as 142 J/g [31].

3.2.5 Tensile properties

Tensile tests were performed according to ASTM D 882-12 at a crosshead speed of 50 mm/min by using a Universal Testing Instrument (INSTRON 3366). The samples were prepared by cutting strip samples of 100 mm length and 15 mm width. Five samples of each composition were tested, and the average values were taken.

3.2.6 Fourier transform infrared spectroscopy (FTIR)

A Thermo NICOLET 6700 FTIR Spectrometer was used to obtain the FTIR spectra. The spectra of samples were collected from an average of 32 scans, at a resolution of 4 cm^{-1} from 500 to 4000 cm^{-1}.

3.2.7 X-ray diffraction (XRD)

X-ray diffraction (XRD) analysis was conducted by using a LABX XRD-6000, Shimadzu Diffractometer operating at 40 kV, 40 mA. X-rays with 1.541 A° wavelength were generated by Cu Kα source. In order to detect the changes in the crystal structure the diffraction angle (2θ) was varied from 2° to 40°.

3.2.8 Field emission scanning electron microscopy (FESEM)

Field emission scanning electron micrographs were obtained using MIRA3 TESCAN. Untouched pieces of samples were collected after each week of exposure, and the surfaces were coated with platinum (5 nm thickness) before scanning.

3.3 Results and discussion

3.3.1 Thermal study

Thermal analysis of the PVA/starch blend and its nanocomposites with graphene as a function of ageing time was carried out by the DSC technique. Degradation has a significant impact on the crystallinity of biodegradable polymers [32]. Sreekumar et al. studied the effect of glycerol on the degradation of PVA and starch/PVA blends under natural weathering conditions [25].

The percentage of crystallinity was calculated from equation (3-1). Variations in the crystalline melting temperature (T_m) and the percentage of crystallinity with ageing time are shown in Figs. 3-2 and 3-3, respectively. The addition of graphene into the PVA/starch blend in the control samples caused a decrease in the crystalline melting temperature, as shown in Fig. 3-2. This result may be due to a weakening of the hydrogen bonding between the PVA and starch in the presence of graphene. However, there was an increase in the percentage of crystallinity after incorporation of graphene into PVA/starch matrix. The sample containing 0.5 wt. % loading of graphene showed the highest percentage of crystallinity (Fig. 3-3). It was reported that graphene serves as a nucleating agent for PVA polymer [33,34].

UV radiation from sunlight can cause several changes in the chemical structure of polymers over time. These include a formation of new groups, crosslinking, main chain scission, and oxidation, which eventually causes changes in the physical and mechanical properties of polymers [35].

There is a significant increase in the crystalline melting temperature and the percentage of crystallinity for the PVA/starch blend and its nanocomposites within the first 3 wk of exposure to an outdoor environment. In this period of aging, the degradation is mainly due to degradation of the amorphous phase (secondary bonds). In the early period of exposure, the temperature was relatively high, which caused the partial removal of moisture and glycerol from the weathered samples. This removal led to a breakage of hydrogen bonding between the PVA and starch molecules. This breakage in turn contributed to the increase of ΔH_{fus} and consequently increased the percentage of crystallinity [25]. However, after the 3rd week of aging, the PVA/starch blend and its nanocomposites displayed a decrease in T_m and percentage of crystallinity. This may be due to the reduction of the amorphous phase and the beginning of the degradation of the crystalline phase.

During the first 7 wk of exposure, there was no rain. After the 7th week, there was a heavy rain which caused the dissolution of a large amount of the amorphous portion. This dissolution may have been due to the severe deterioration of the secondary bonds. Also, in the last stage of aging, chain scissions seemed to occur upon exposure to sunlight, which led to an increase in the free volume of polymers [36]. As a result, the molecules re-arranged themselves, resulting in an increase in the percentage of crystallinity of the samples after the 7th week (Fig. 3-3). The percentage of crystallinity of the PVA/starch blend and the nanocomposite of 1 wt. % graphene were close to each other in the last week of exposure. The rainfall during the last 2 wk of exposure caused the dissolution of polymer phases, especially in the amorphous region. The change in crystallinity is more pronounced with PVA/starch blends, which indicates a high degree of deterioration. In

the case of the 1 wt. % graphene nanocomposite, the agglomerated graphene particles in the PVA/starch matrix held the matrix together and hence the change in its crystallinity was minimal compared to the other cases.

The PVA/starch/graphene nanocomposite showed a significant increase in the value of the change in the percentage of crystallinity compared to the PVA/starch blend during the aging test as shown in Fig. 3-4. The presence of graphene seems to accelerate the dissolution rate of the amorphous portion of the PVA/starch blend. This may be due to the weakening of the interaction between the PVA and starch molecules. The existence of oxygen-containing groups on the surface of graphene may also contribute to the acceleration of chain scissions of molecules during the exposure.

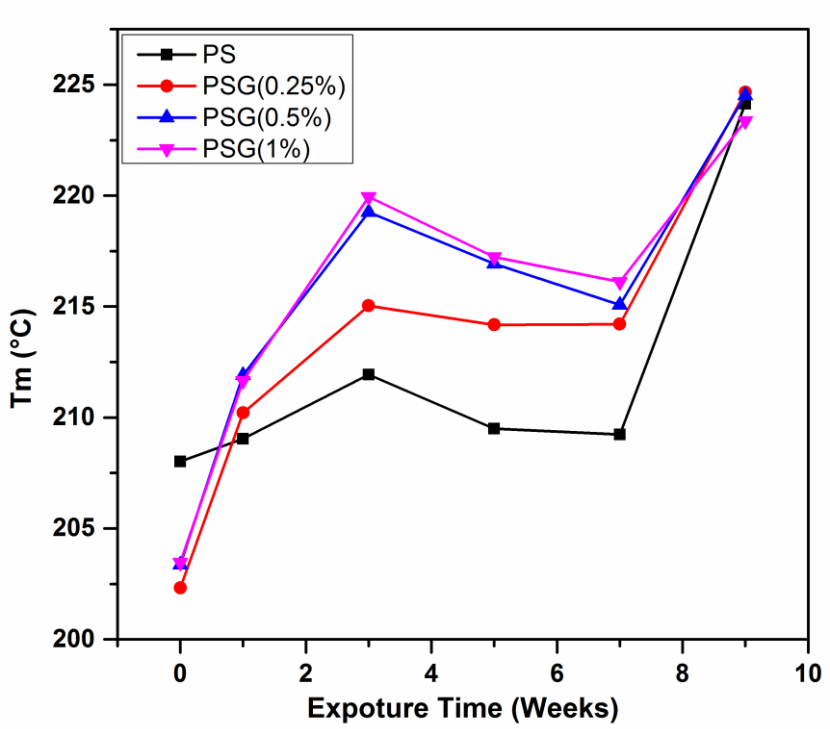

Fig 3-2: Effect of aging time on the crystalline melting temperature of the PVA/starch blend and its nanocomposites with graphene

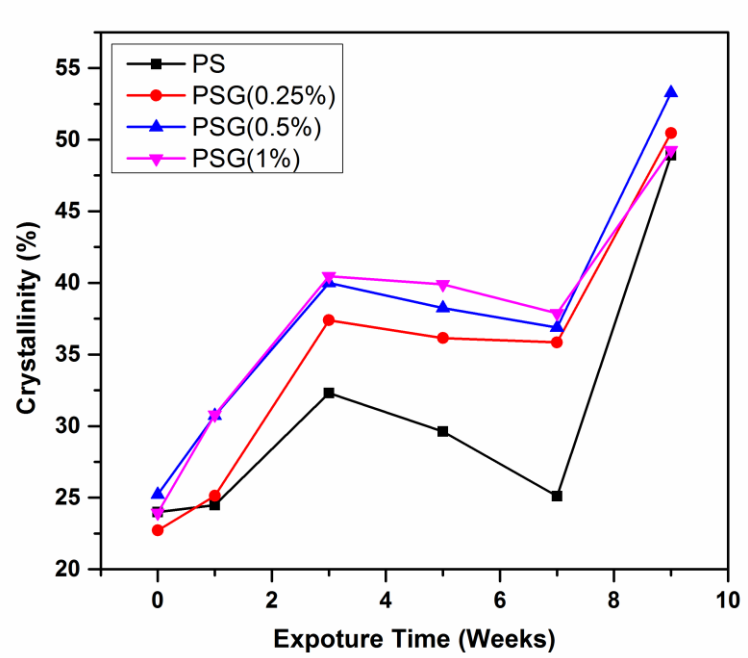

Fig 3-3: Effect of aging time on the percentage of crystallinity of the PVA/starch blend and its nanocomposites with graphene

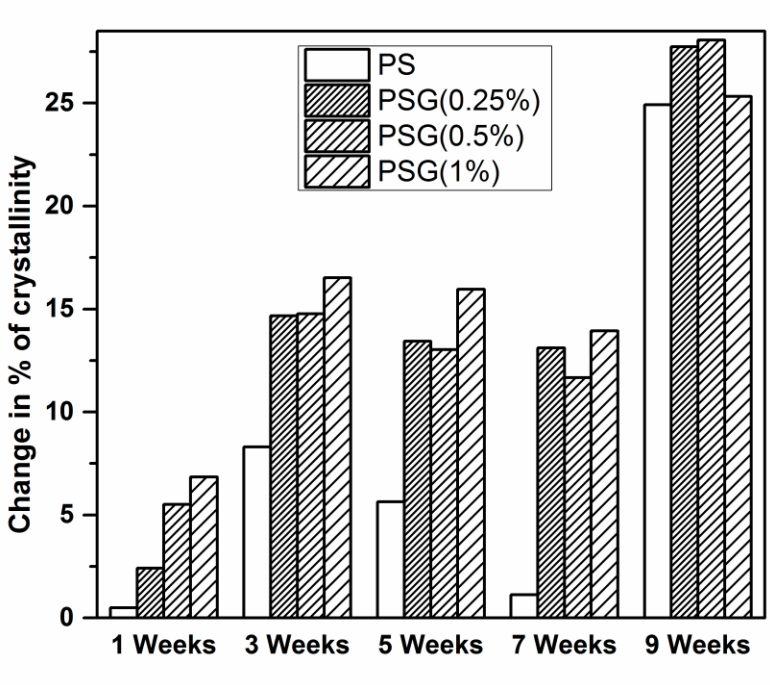

Fig 3-4: Effect of graphene on the crystallinity of the PVA/starch blend under natural weather condition

3.3.2 Mechanical properties

The mechanical properties of the PVA/starch blend and its nanocomposites with graphene are listed in Table 3-2.

Table 3-2: Effect of graphene loading on mechanical properties of PVA/starch/graphene nanocomposites

Sample	Tensile strength (MPa)	Tensile modulus (MPa)	Elongation at break (%)
PS	8.2	170.0	19.1
PSG(0.25%)	8.7	179.4	21.7
PSG(0.5%)	9.3	200.1	67.3
PSG(1%)	9.1	198.1	25.8

It is clear that the introduction of graphene into the PVA/starch matrix led to an improvement in the tensile strength, tensile modulus, and percentage elongation at break of the PVA/starch blend. This result may be attributed the homogeneous dispersion of graphene in PVA/starch matrix along with a strong interfacial interaction between the components which caused an efficient transfer of the mechanical load. The percentage elongation at break reached its maximum value at 0.5% loading of graphene, indicating the improved ductility of the sample. However, further increase in graphene loading, PSG (1%), resulted in a decrease in mechanical properties due to the agglomeration of graphene nanosheets inside the PVA/starch matrix; hence, the load transfer between the polymer matrices and the nanofiller was not proficient.

Effects of environmental weathering on the mechanical properties of the PS blend and PSG (0.5%) nanocomposite are summarized in Table 3-3. Data from the samples after 7 wk of exposure were not reported because they were severely degraded and the mechanical test became too difficult.

Table 3-3: Effect of environmental weathering on mechanical properties of PS and PSG (0.5%)

Exposure time (Weeks)	Tensile strength (MPa)		Tensile modulus (MPa)	
	PS	PSG(0.5%)	PS	PSG(0.5%)
0	8.2	9.3	170.0	200.1
3	11.2	13.2	411.7	692.4
5	10.2	12.1	367.7	478.3
7	9.1	11.6	200.8	285.6

The tensile strength of PS and PSG (0.5%) increased by 37% and 42%, respectively, after 3 wk of exposure and then decreased gradually as the exposure time increased. The corresponding increases in tensile modulus in the same period were 142% and 246%, respectively. This result is due to the fact that the total crystallinity of the exposed samples increased after the dissolution of the amorphous phase, which contributed to the enhancement of the mechanical properties. This result is consistent with the results obtained from the DSC studies (Fig. 3-3). Further degradation caused damage in the crystalline portion, and the mechanical properties were degraded after extended exposure.

3.3.3 Spectroscopic study

The infrared spectra of the PS blend and PSG (0.5%) nanocomposite before and after different times of exposure are shown in Figs. 3-5 and 3-6, respectively. The spectrum of the control sample (PS) shows a clear absorption carbonyl peak at 1710 cm^{-1}. This peak comes from the residual acetate groups during the synthesis process of the PVA polymer [37]. The characteristic absorption peak at 1650 cm^{-1}, which is assigned to bound water, indicates the presence of strong hydrogen bonds between PVA and starch as well as between their individual components [38].

At the first 3 wk of exposure, there are no new peaks found in the infrared spectra of the PVA/starch blend and its graphene nanocomposites. This result is because the degradation in this period was primarily due to the dissolution of the amorphous phase. The intensities of the hydroxyl peak (3200-3500 cm^{-1}) and the bound water peak (1650 cm^{-1}) decreased in the third week. This result is due to the reduction of hydroxyl groups due to the breakdown of hydrogen bonds. At the 9th week of exposure, the spectra of the weathered samples had demonstrated significant changes compared to those of control samples due to several chemical reactions during this period of aging. Also, at the ninth week of exposure, the intensities of the hydroxyl and carbonyl (at 1710 cm^{-1}) peaks increased due to the increase in the amount of photo-oxidation degradation products [37]. The characteristic absorption peak at 1140 cm^{-1}, which arises from the stretching vibration of the C–O group, is strongly associated with the crystalline phase [39,40]. The intensity of this peak in all samples increased in the final week of aging. This result indicates of an increase in the crystalline phase of the samples, which agrees with the results of crystallinity discussed in the thermal analysis (Fig. 3-3).

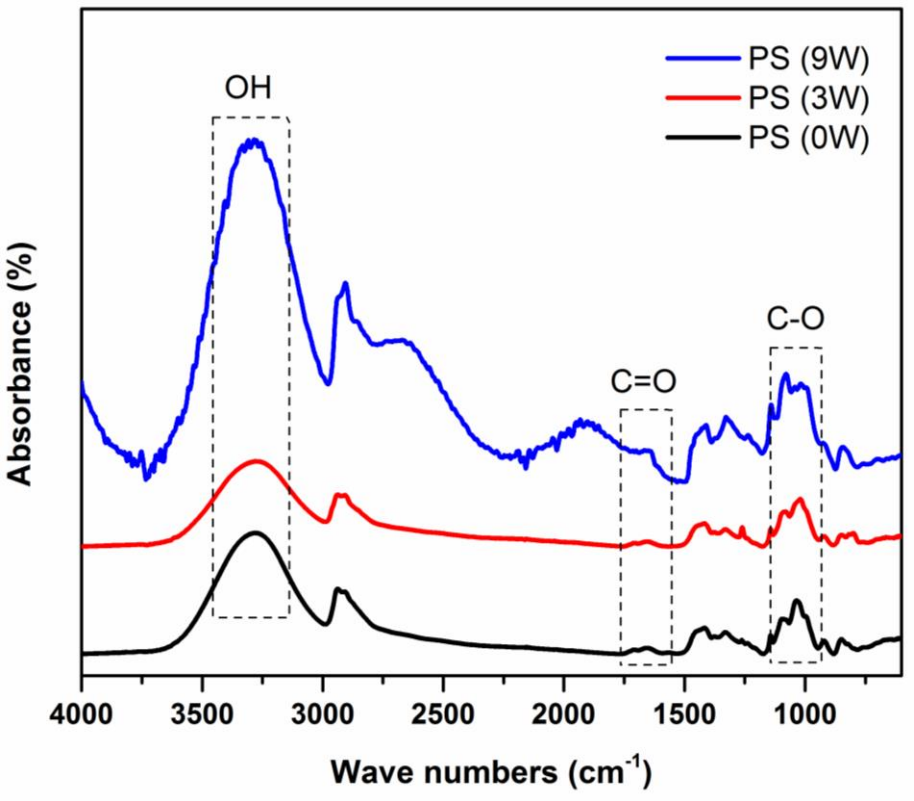

Fig 3-5: FTIR spectra of the PVA/starch blend before and after different times of exposure

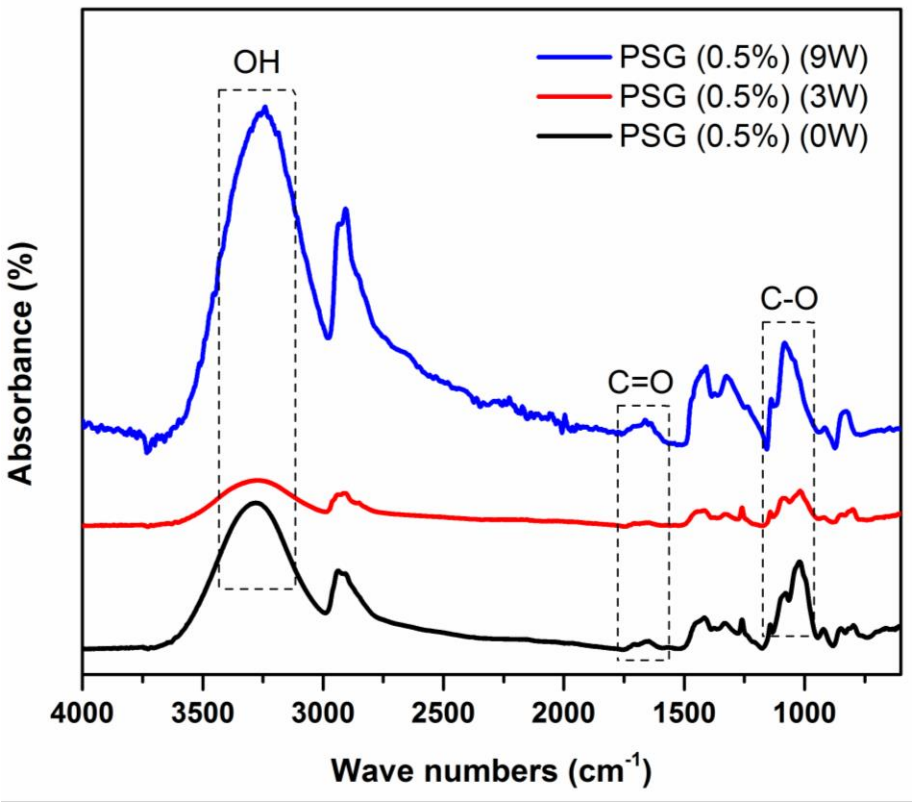

Fig 3-6: FTIR spectra of the PVA/starch nanocomposite containing 0.5 wt. % of graphene before and after different times of exposure

3.3.4 X-ray diffraction studies

The x-ray diffraction diagrams of the PS blend and PSG (0.5%) nanocomposite before and after different exposure times are shown in Figs. 3-7 and 3-8, respectively. The characteristic peak at 19.9° 2θ represents the XRD pattern of PVA and the one at 23° 2θ represents the XRD pattern of a mixture of A-category and V-hydrate category crystal structure in starch [6,7,21]. The XRD characteristic peak of graphene nanosheets (26.6° 2θ) did not appear in PSG (0.5%) nanocomposite, indicating that graphene was exfoliated and homogeneously dispersed in the PVA/starch matrix.

In the 3rd week of exposure, the intensity of the PVA peak only marginally changed. This result may be because the degradation in this period took place primarily in the amorphous region of the specimen. However, after the 5th week of aging, the intensity of the PVA peak was significantly decreased. This result may be attributed to the additional degradation of the crystalline phase. This result is corroborated by the DSC results as well as by the mechanical properties. However, although the trend was the same, the characteristic peak of PVA in the PSG (0.5%) nanocomposite has a higher intensity compared to the one in the PVA/starch blend (PS). Therefore, the presence of graphene in the polymer matrices has restricted degradation to some extent.

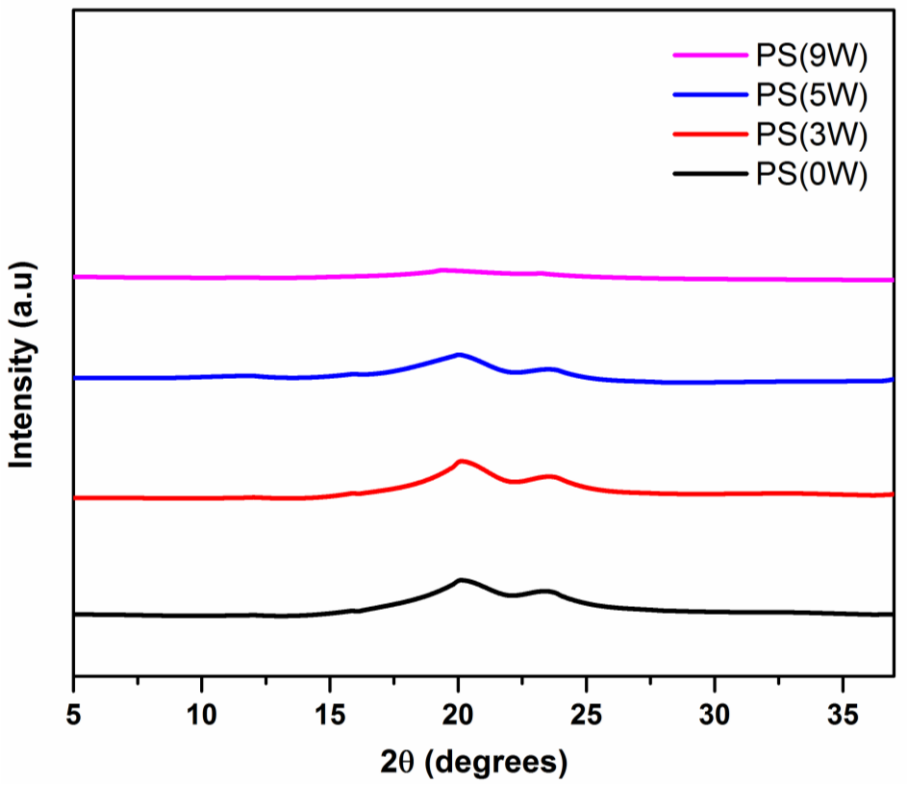

Fig 3-7: XRD diagrams of the PS blend before and after different times of exposure

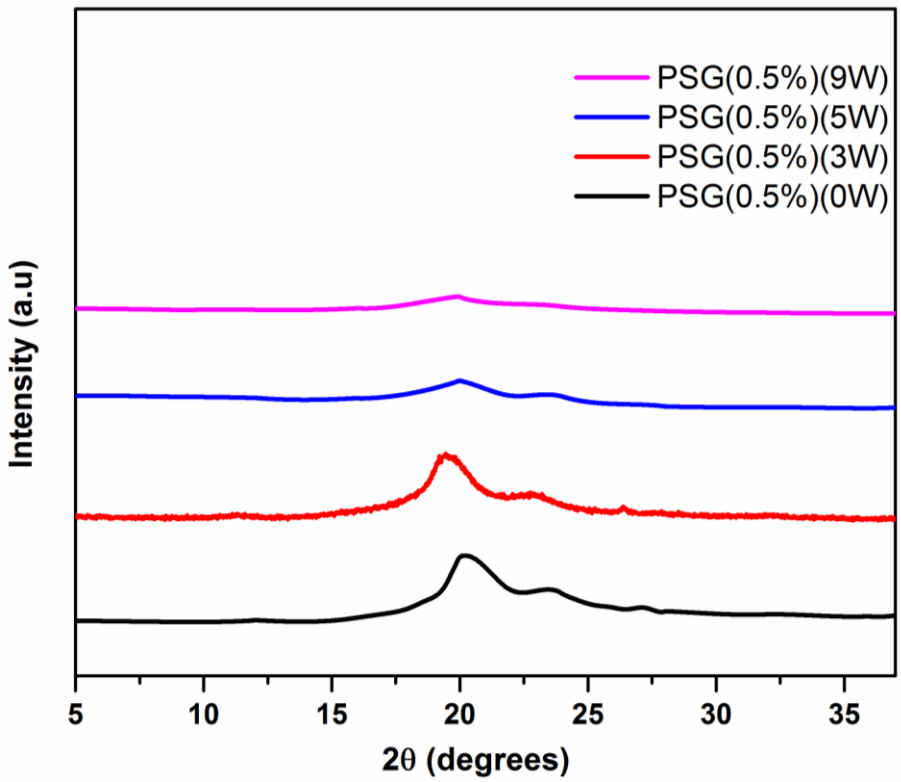

Fig 3-8: XRD diagrams of PSG (0.5%) before and after different times of exposure

3.3.5 Morphological study

Scanning electron microscopy is an effective and powerful technique for monitoring changes on the surface of polymers – such as cracks, crevices and bubbles – during degradation. The FESEM images of the surfaces of the PS blend and PSG (0.5%) before and after exposure are shown in Fig. 3-9. Before exposure, the surfaces of samples were smooth and free of any type of defects. After being exposed to natural weathering conditions, the surfaces become rough, and many defects are seen on the surfaces of samples. Some dust particles were also seen on the surfaces after exposure. The surfaces of the samples were well-maintained during the exposure period without any cracks forming due to the presence of water vapor in the air, which acts as a plasticizer. During the exposure period, the surfaces of the weathered samples having graphene showed less deterioration than the PVA/starch blend samples did. This result may be due to the increase in the percentage of crystallinity of these samples after aging, as was explained in the thermal analysis of these systems (Fig. 3-3). During the final stages of aging, the samples became brittle and lost their physical integrity.

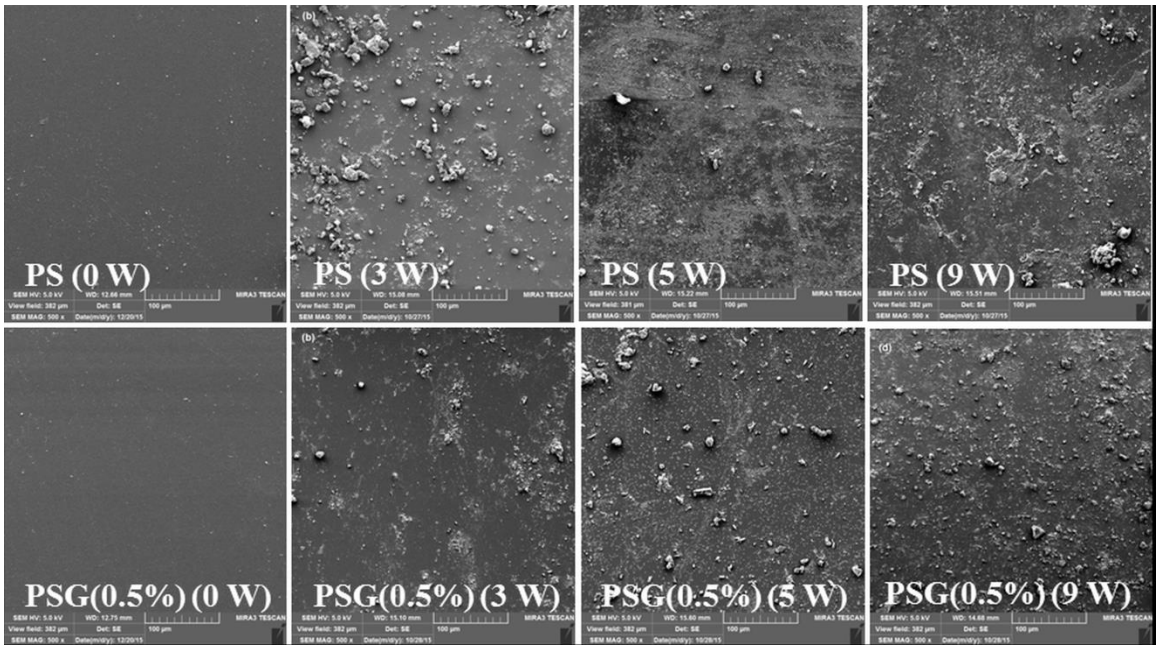

Fig 3-9: FESEM images for the surfaces of the PS blend and PSG (0.5%) before and after different times of exposure

3.4 Conclusions

Environmental effects primarily affect the crystallinity of all biodegradable polymers. In the early stages of exposure, the degradation was primarily due to the dissolution of the amorphous phase, while in the later stages even the crystalline phases was degraded. The incorporation of graphene into the PVA/starch matrix led to a significant increase in the rate of change in the crystallinity percentage during the exposure. Graphene accelerates the dissolution rate of the amorphous portion of the PVA/starch blend by weakening the interaction between the molecules. As the aging process progressed, polymer chain scission may have taken place due to exposure to sunlight. The shorter polymer chains that were generated could be easily re-arranged in the polymer matrix and hence increase the crystallinity percentage. The introduction of graphene into PVA/starch blends made both of the polymers less susceptible to environmental degradation.

Refernces

[1] Ouyang, C., Wang, Y., Zhao, N., Liu, X., et al., Preparation of poly(lactic acid) and modified starch composites. *Polym. Bull*. 2012, *68*,2009–2019.

[2] Xiong, Z., Yang, Y., Feng, J., Zhang, X., et al., Preparation and characterization of poly(lactic acid)/starch composites toughened with epoxidized soybean oil. *Carbohydr. Polym*. 2013, *92*,810–816.

[3] Nor, F. M., Kurniawan, D., Seo, Y. K., Park, J. K., et al., Polycaprolactone-starch blends with corn-based coupling agent: physical properties and in vitro analysis. *Proc. Inst. Mech. Eng. H*. 2012, *226*,693–698.

[4] Ali Akbari Ghavimi, S., Ebrahimzadeh, M. H., Solati-Hashjin, M., Abu Osman, N. A., Polycaprolactone/starch composite: Fabrication, structure, properties, and applications. *J. Biomed. Mater. Res. A* 2014, *103*,2482–2498.

[5] Bin-Dahman, O. A., Jose, J., Al-Harthi, M. A., Compatibility of poly(acrylic acid)/starch blends. *Starch/Stärke* 2015,*67*,1061-1069.

[6] Sreekumar, P., Al-Harthi, M. A., De, S. K., Reinforcement of starch/polyvinyl alcohol blend using nano-titanium dioxide. *J. Compos. Mater*. 2012, *46*,3181–3187.

[7] Sreekumar, P. A., Al-Harthi, M. A., De, S. K., Studies on compatibility of biodegradable starch/polyvinyl alcohol blends. *Polym. Eng. Sci*. 2012, *52*,2167–2172.

[8] Baker, M. I., Walsh, S. P., Schwartz, Z., Boyan, B. D., A review of polyvinyl alcohol and its uses in cartilage and orthopedic applications. *J. Biomed. Mater. Res. B Appl. Biomater*. 2012, *100*,1451–1457.

[9] Peppas, N. A., Merrill, E.W., Development of semicrystalline poly(vinyl alcohol) hydrogels for biomedical applications. *J. Biomed. Mater. Res.* 1977, 11,423–434.

[10] Kenawy, E. R., Kamoun, E. A., Mohy Eldin, M. S., El-Meligy, M. A., Physically crosslinked poly(vinyl alcohol)-hydroxyethyl starch blend hydrogel membranes: Synthesis and characterization for biomedical applications. *Arab. J. Chem.* 2014, *7*,372–380.

[11] Pawde, S. M., Deshmukh, K., Characterization of polyvinyl alcohol/gelatin blend hydrogel films for biomedical applications. *J. Appl. Polym. Sci.* 2008, *109*,3431–3437.

[12] Santos, C., Silva, C. J., Büttel, Z., Guimarães, R., et al. Preparation and characterization of polysaccharides/PVA blend nanofibrous membranes by electrospinning method. *Carbohydr. Polym*. 2014, *99*,584–592.

[13] Ahmad, J., Deshmukh, K., Hägg, M. B., Influence of TiO_2 on the Chemical, Mechanical, and Gas Separation Properties of Polyvinyl Alcohol-Titanium Dioxide (PVA-TiO_2) Nanocomposite Membranes. *Int. J. Polym. Anal. Charact*. 2013 ,*18*,287–296.

[14] Peppas, N. A., Tennenhouse, D., Semicrystalline poly(vinyl alcohol) films and their blends with poly(acrylic acid) and poly(ethylene glycol) for drug delivery applications. *J. Drug. Deliv. Sci. Technol.* 2004, *14*,291–297.

[15] Wang, X., Yucel, T., Lu, Q., Hu, X., Kaplan, D. L., Silk nanospheres and microspheres from silk/pva blend films for drug delivery. *Biomaterials* 2010, *31*,1025–1035.

[16] Mao, L., Imam, S., Gordon, S., Cinelli, P., Chiellini, E., Extruded cornstarch-glycerol-polyvinyl alcohol blends: mechanical properties, morphology, and biodegradability. *J. Polym. Environ*. 2000, *8*,205–211.

[17] Jayasekara, R., Harding, I., Bowater. I., Christie, G. B. Y., Lonergan, G. T. Biodegradation by Composting of Surface Modified Starch and PVA Blended Films. *J. Polym. Environ*. 2003, *11*,49–56.

[18] Liu, H., Xie, F., Yu, L., Chen, L., Li, L., Thermal processing of starch-based polymers. *Prog. Polym. Sci*. 2009, *34*,1348–1368.

[19] Yu, L., Dean, K., Li, L., Polymer blends and composites from renewable resources. *Prog. Polym. Sci*. 2006, *31*,576–602.

[20] Maiti, M., Kaith, B. S., Jindal, R., Jana, A. K., Synthesis and characterization of corn starch based green composites reinforced with Saccharum spontaneum L graft copolymers prepared under micro-wave and their effect on thermal, physio-chemical and mechanical properties. *Polym. Degrad. Stab*. 2010, *95*,1694–1703.

[21] Sreekumar, P. A., Al-Harthi, M. A., De, S. K., Effect of glycerol on thermal and mechanical properties of polyvinyl alcohol/starch blends. *J. Appl. Polym. Sci*. 2012, *123*,135–142.

[22] Guohua, Z., Ya, L., Cuilan, F., Min, Z., et al., Water resistance, mechanical properties and biodegradability of methylated-cornstarch/poly(vinyl alcohol) blend film. *Polym. Degrad. Stab*. 2006, *91*,703–711.

[23] Tudorachi, N., Cascaval, C., Rusu, M., Pruteanu, M., Testing of polyvinyl alcohol and starch mixtures as biodegradable polymeric materials. *Polym. Test*. 2000, *19*,785–799.

[24] Cinelli, P., Chiellini, E., Imam, S. H., Hybrid composite based on poly(vinyl alcohol) and fillers from renewable resources. *J. Appl. Polym. Sci*. 2008, *109*,1684–1691.

[25] Sreekumar, P. A., De, S. K., Khan, M. J., Al-Harthi, M.A., Natural weather ageing of starch/polyvinyl alcohol blend: effect of glycerol content. *J. Polym. Eng*. 2013, *33*,257–263.

[26] Su, J. F., Wang, S. S., Xia, W. L., Environmental-Friendly Soy Protein Isolate/Poly(Vinyl Alcohol) Blend Films: Biodegradation Behaviors. *Adv. Mater. Res*. 2010, *178*,151–155.

[27] Jose, J., De, S. K., AlMa'adeed, M. A., Dakua, J. B.,et al., Compatibilizing role of carbon nanotubes in poly(vinyl alcohol)/starch blend. *Starch /Stärke* 2014, *66*,1–7.

[28] Jose, J., Al-Harthi, M. A., AlMa'adeed, M. A., Dakua, J. B., De,S. K., Effect of graphene loading on thermomechanical properties of poly(vinyl alcohol)/starch blend. *J. Appl. Polym. Sci*. 2015, *132*,doi:10.1002/app.41827.

[29] Chieng, B., Ibrahim, N., Yunus, W., Hussein, M., Poly(lactic acid)/Poly(ethylene glycol) Polymer Nanocomposites: Effects of Graphene Nanoplatelets. *Polymers* 2013, *6*,93–104.

[30] Cheng, J., Zhang, J., Wang, X., Investigation on crystallization behavior and hydrophilicity of poly(vinylidene fluoride)/poly(methyl methacrylate)/poly(vinyl pyrrolidone) ternary blends by solution casting. *J. Appl. Polym. Sci*. 2013, *127*,3997–4005.

[31] Nishio, Y., Haratani, T., Takahashi, T., Manley, R. S. J., Cellulose/poly(vinyl alcohol) blends: an estimation of thermodynamic polymer-polymer interaction by melting-point-depression analysis. *Macromolecules* 1989, *22*,2547–2549.

[32] Zhou, W. Y.,Duan, B.,Wang, M., Cheung, W. L., *Isothermal and Non-isothermal Crystallization Kinetics of Poly(L-Lactide)/Carbonated Hydroxyapatite Nanocomposite Microspheres*. In Tech, 2011, pp. 231–260

[33] Lee, S., Hong, J. Y., Jang, J., The effect of graphene nanofiller on the crystallization behavior and mechanical properties of poly(vinyl alcohol). *Polym. Int*. 2012, *62*,901–908.

[34] Li, C., Vongsvivut, J., She, X., Li, Y., et al., New insight into non-isothermal crystallization of PVA-graphene composites. *Phys. Chem. Chem. Phys.* 2014, *16*,22145–22158.

[35] Kaczmarek, H., Podgórski, A., Bajer, K., Photochemical reactions in poly(vinyl chloride)/poly(vinyl alcohol) blends. *J. Photochem. Photobiol. A Chem.* 2005, *171*,187–195.

[36] Ramani, R., Ranganathaiah, C., Degradation of acrylonitrile-butadiene-styrene and polycarbonate by UV irradiation. Polym. Degrad. Stab. 2000, 69,347–354.

[37] Kaczmarek, H., Da ̨browska, A., Vuković-Kwiatkowska, I., Accelerated weathering of pectin/poly(vinyl alcohol) blends studied by spectroscopic methods. J. Appl. Polym. Sci. 2011, 122,1936–1945.

[38] Wolkers, W. F., Oliver, A. E., Tablin, F., Crowe, J. H., A Fourier-transform infrared spectroscopy study of sugar glasses. Carbohydr. Res. 2004, 339,1077–1085.

[39] Hong, P. D., Chou, C. M., Chuang, W. T., Effects of mixed solvent on gelation of poly(vinyl alcohol) solutions. J. Appl. Polym. Sci. 2001, 79,1113–1120.

[40] Senda, T., He, Y., Inoue, Y., Biodegradable blends of poly(ε-caprolactone) withα-chitin and chitosan: specific interactions, thermal properties and crystallization behavior. Polym. Int. 2002, 51,33–39.

CHAPTER 4

INFLUENCE OF GRAPHENE ON NON-ISOTHERMAL CRYSTALLIZATION KINETICS OF POLY(VINYL ALCOHOL)/STARCH COMPOSITE

Osamah A. Bin-Dahman[1], *Farrukh Shehzad*[1] *and Mamdouh A. Al-Harthi*[1, 2]

[1]Department of Chemical Engineering, King Fahd University of Petroleum & Minerals, Dhahran, Saudi Arabia

[2]Center for Research Excellence in Nanotechnology, King Fahd University of Petroleum & Minerals, Dhahran, Saudi Arabia

[*]Corresponding Author: Mamdouh A. Al-Harthi, E-mail address: mamdouh@kfupm.edu.sa

This chapter has been submitted to journal of "Journal of thermal analysis and calorimetry"

Abstract

The non-isothermal crystallization behaviors of poly(vinyl alcohol)/starch and poly(vinyl alcohol)/starch/graphene nanocomposites were studied by using differential scanning calorimetry (DSC). Ozawa and Mo models have been employed to analyze the non-isothermal kinetics. The differential Friedman method was used to evaluate the activation energy (E_A) of the nanocomposites. The Mo model showed a success in the whole investigated temperature range. It was found that graphene promoted the crystallization of a poly(vinyl alcohol)/starch composite by increasing the crystallization onset temperature (T_{on}) along with lowering the E_A. However, it was observed from the values of the half-crystallization time ($t_{1/2}$) that graphene hindered the growth of crystals, and consequently retarded the overall rate of crystallization.

Keywords:

Non-isothermal crystallization - Graphene - Poly(vinyl alcohol)/starch – Nanocomposites

4.1 Introduction

There are considerable concerns over the decline of natural petroleum resources and the environmental pollution during the last four decades. Most of the synthetic polymeric materials have hydrophobic characteristics and cannot be degraded by microorganisms. Therefore, their wastes have a severe risk to the environment. These issues forced the researchers to develop renewable and biodegradable polymer products that can be easily degraded by environmental effects and microorganisms. However, physical and mechanical properties of such kind of polymers are the major challenges and depend to a large extent on the crystalline structure of polymers. The crystallization behavior has a key role to study the physical and mechanical features of polymers [1]. The percent crystallinity is directly linked to several of the important properties showed by semi-crystalline polymers such as stiffness, toughness, brittleness, and optical clarity.

Poly(vinyl alcohol) (PVA) is a semi-crystalline polymer which is considered to be one of the most important polymers due to its outstanding properties. These include biocompatibility, hydrophilicity and non-toxicity [2]. PVA can be easily blended with polymers as well as with fillers to make biodegradable composites with excellent properties. The properties of PVA basically depend on its crystallinity, molecular weight, and level of hydrolysis [3]. PVA has been used in different industrial applications such as water-soluble packaging films, coatings, textile sizing, and membranes [4,5]. It has also been used in many biomedical applications, for example, drug delivery systems [6,7], enzyme immobilization [8], hydrogels [9,10], and artificial biomedical devices [11]. Starch is a renewable, biodegradable polymer which has plentiful benefits such as wider availability, lower cost compared to synthetic materials, and total compostability without

creating poisonous residues [12]. Starch can be utilized to enhance the rate of degradation as well as to reduce the overall cost of the final products [13–15]. Blends of poly(vinyl alcohol) with starch were extensively studied by Sreekumar et al. [16–19]. Recently, Jose at al. further studied the thermal and mechanical properties of this system using carbon nanotube [20] and graphene [21] as fillers.

Studies of the non-isothermal crystallization kinetics are beneficial for modeling of the industrial processes that take place under the non-isothermal conditions [22]. Moreover, the study of the crystallization behavior is essential to the performance of PVA products. The crystallization kinetics of PVA and PVA-based composites have been studied in the literature [23–31].

However, a comprehensive study about the crystallization kinetics of a ternary nanocomposite system by using graphene as nanofiller has not been reported in the literature. The present chapter mainly aims to study non-isothermal crystallization kinetics of a ternary system composed of poly(vinyl alcohol), starch and graphene as a nanofiller by using differential scanning calorimetry (DSC). Two models, such as Ozawa and Mo models have been employed to study the non-isothermal kinetics. The differential Friedman method was applied to assess the activation energy of nanocomposites.

4.2 Experimental

4.2.1 Materials

Poly(vinyl alcohol) (M_w 27000), and glycerol were purchased from the Sigma Aldrich, USA. Corn starch was obtained from ARASCO Corn Products, Saudi Arabia. Graphene

was obtained from Grafen Chemical Industries Co, Turkey. It has an oxygen content of 1 %, surface area of about 13-15 m^2/g and thickness from 50 to100 nm.

4.2.2 Preparation of the Blends

Nanocomposites of PVA/starch/graphene were prepared by means of solution mixing and casting method. The ratio of PVA/starch was held constant in all the samples, i.e. 70/30 parts by weight. It was corroborated that in this composition, the components of the blend were more compatible [16–18]. PVA (4.2 g) was fully dissolved in 50 ml DI water at 90 ^oC. Separately, an aqueous dispersion of starch (1.8 g) in the presence of a specified quantity of glycerol as a plasticizer was produced. Similarly, a stable aqueous dispersion of graphene was also formed by ultra-sonication. Sonication was done for 2 min at 30% amplitude by using the Ultrasonica Q 700 ultrasonicator probe. After that, all the three dispersion were mixed and stirred continuously at 400 rpm for 3 h. To eliminate any air traces, the mixture was degassed for 10 min. Afterwards, the mixture was transferred to flat glass surface and put overnight in an oven at 50 $^{\circ}C$ for drying. Once it was fully dried, the films were peeled out and stored in a desiccator.

4.2.3 Thermal analysis

The non-isothermal crystallization studies were conducted by using a DSC-Q1000, TA instrument in an inert gas atmosphere. Prior to the DSC test, the samples were dried in an oven at 50 °C for 24 h. In practice, 6 ± 0.5 mg of each sample was used for the test to minimize the effect of thermal gradient in the sample. As we have been studying the melt crystallization, the samples were at first heated up to 245 °C by using a programmed temperature ramp of 15 °C/min. The temperature was kept constant at 245 °C for 3 min to get rid of any possible nucleation. After that the samples were cooled down to 40 °C

using different cooling rates. In this study, we used four cooling rates i.e. 5, 10, 15 and 20 °C/min. Since, PVA is susceptible to thermal degradation; a new sample was used for each cooling rate to eliminate the effect of thermal degradation.

4.3 Results and discussions

4.3.1 Thermal properties

Differential scanning calorimetric (DSC) is a powerful analytical technique for studying the crystallization kinetics. The thermal characteristics of the PVA/starch blend and its nanocomposites obtained at cooling rates are listed in Table 4-1. The crystallization peak temperature (T_P), which corresponds to the maximum crystallization rate, is an important parameter for semi-crystallization polymers owing to the combination of nucleation and growth processes [32,33]. It is evident from Table 1 that as the cooling rate is increased, the crystallization peak temperature (T_p) decreases. This is because of polymer molecules get sufficient time at a lower cooling rate to transform from melt to crystalline form. Thus, the crystallization process can take place even at higher temperatures [1]. Conversely, the higher cooling rate doesn't provide sufficient time to the polymer molecules to follow the cooling rate and form crystal domains due to the effect of heat hysteresis [31]. As a result, the T_p is shifted to a lower value.

The addition of graphene enhanced the crystallization enthalpy (ΔH_{cry}) of PVA/starch blend and shifted its crystallization peak temperature to higher values for all the cooling rates as seen in Table 4-1. This indicates that graphene nucleates the crystallization of PVA/starch nanocomposites and crystallization occurs at high temperature. However, at a higher cooling i.e. 20 °C/min, a slight decrease in the crystallization peak temperature is observed, particularly at the higher loading of graphene (1wt. %). This might be ascribed

to the retardation of crystal growth by the limited interparticle space at higher loading of graphene [30].

Also, after the addition of graphene, the crystallization onset temperature (T_o) for the PVA/starch blend has been changed to a higher value. This gives an indication that the presence of graphene caused the crystallization process to start at higher temperatures [34].

Table 4-1: Summarized DSC results of the PVA/starch blend and its nanocomposites at different cooling rates

Samples	β (°C/min)	T_o (°C)	T_P (°C)	ΔH_{cry} (J/g)
PS	5	195.31	191.28	56.75
	10	187.29	182.55	51.88
	15	185.64	180.72	46.42
	20	180.08	173.84	43.94
PSG (0.25%)	5	196.59	192.33	59.65
	10	189.14	184.32	53.01
	15	187.61	180.81	48.85
	20	186.09	179.94	47.38
PSG (0.5%)	5	197.93	193.41	59.05
	10	189.99	185.12	53.33
	15	188.86	184.16	51.85
	20	187.68	182.65	48.63
PSG (1%)	5	199.79	196.04	63.09
	10	197.31	193.25	56.06
	15	189.39	184.67	53.8
	20	185.33	180.52	48.21

All the samples contain 3 g of glycerol. P refers to poly(vinyl alcohol), S to starch and G to graphene.

For further investigation of the crystallization mechanism, crystallization kinetics of the PVA/starch blend and its nanocomposites were studied. The fractional relative crystallinity (X_t) with respect to the crystallization temperature (T) was calculated by utilizing Eq. 4-1 [35,36]. The baseline and integral calculations were performed by the software, which was provided by the vendor, i.e. Universal Analysis 2000, TA Instruments.

$$X_t = \frac{\int_{T_0}^{T} (dH_c/dT)dT}{\int_{T_0}^{T\infty} (dH_c/dT)dT} \qquad (4\text{-}1)$$

In the above equation T_o stands for the onset crystallization temperature, T_∞ represents the end crystallization temperatures i.e. 40 ºC in this case, and dH represents the heat evolved in an infinitely small temperature interval dT. The instantaneous crystallization temperature (T) can be related to the elapsed time (t) by Eq. 4-2.

$$t = \frac{(T_0 - T)}{\beta} \qquad (4\text{-}2)$$

Where T_o is the onset crystallization temperature and β stands for the cooling ramp. In this way, the relative crystallinity versus time is plotted as shown in Figure 4-1.

To compare the rate of crystallization, values of the half-crystallization time ($t_{1/2}$) for all samples prepared in this study were estimated from Figure 4-1 and their respective values were listed in Table 4-2. This parameter, $t_{1/2}$ represents the time needed for the polymer to achieve 50 % relative crystallinity at a given temperature. A decreasing trend for the $t_{1/2}$ is evident with increasing cooling rate, meaning that the rate of crystallization has increased with increasing cooling rates.

Although, graphene acts as a nucleating agent [29,30], incorporation of graphene at low concentration into the PVA/starch matrix caused an increase in the values of $t_{1/2}$. This

indicates the slower crystallization rate that may be attributed to the role of graphene on retarding the diffusion of the crystal lattice. It is interesting to note that the values of $t_{1/2}$ decreased slightly at a further loading of graphene (1 wt. %) for all cooling rates (as shown in Table 4-2). This can be attributed to the agglomeration of graphene and hence reducing the retardation effect.

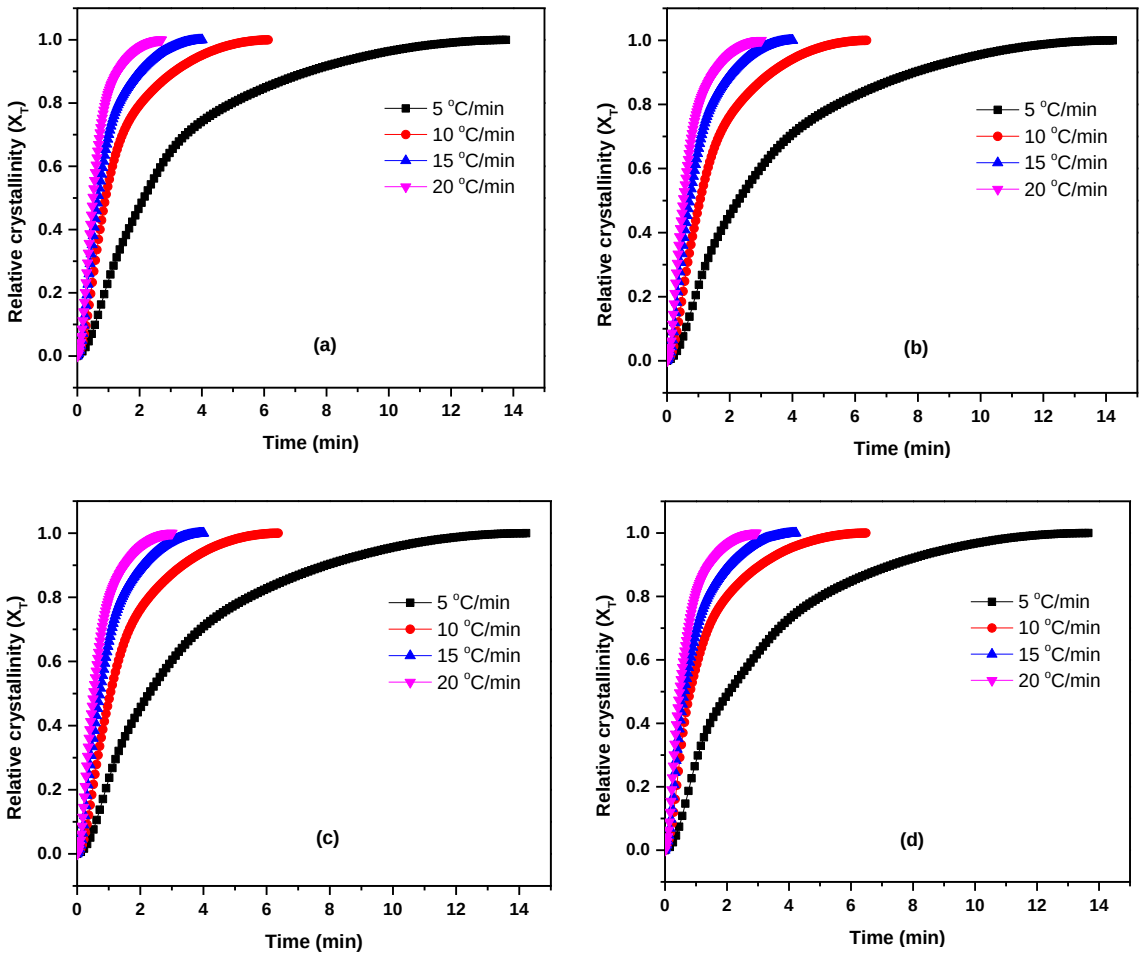

Fig 4-1: Variation of relative crystallinity (X_t) as a function of crystallization time for (a) PS, (b) PSG (0.25%), (c) PSG (0.5%) and (d) PSG (1%)

Table 4-2: Summarized values of half-crystallization time of the PVA/starch blend and its nanocomposites at different cooling rates

β (°C/min)	$t_{(1/2)}$ (min)			
	PS	PSG (0.25%)	PSG (0.5%)	PSG (1%)
5	2.140	2.276	2.284	2.179
10	0.907	1.052	1.059	0.924
15	0.665	0.714	0.723	0.681
20	0.502	0.523	0.547	0.511

The non-isothermal crystallization kinetics of PVA/starch and PVA/starch/graphene nanocomposites were further investigated using two methods, particularly the Ozawa and Mo equations.

4.3.2 Ozawa method

Ozawa [37] suggested a model to examine the non-isothermal crystallization kinetics of polymers. This model is extended from Avrami theory [38] by supposing that the non-isothermal crystallization process is made up of infinitely small isothermal stages of crystallization. According to Ozawa theory, the relative crystallinity, temperature, and β can interrelated as follows:

$$X_t = 1 - \exp(\frac{-K(T)}{\beta^m}) \quad (4\text{-}3)$$

By taking double logarithm, Eq. 4-3 can be linearized as shown in Eq. 4-4

$$Ln\big(-Ln(1 - X_t)\big) = Ln\big(K(T)\big) - mLn(\beta) \quad (4\text{-}4)$$

where m and K(T) are the Ozawa exponent and the Ozawa crystallization rate constant, respectively. Both m and K(T) parameters depending on a given crystalline morphology and type of nucleation.

The values of m and K(T) can be obtained by fitting straight line (Eq. 4-4) to a plot of $Ln\left(-Ln(1-X_t)\right)$ against $Ln(\beta)$.

The Ozawa plots for all the samples are shown in Figure (4-2) and the results are presented in Table 4-3. In the present system, Ozawa plots showed some extent of linearity only for samples with low content of graphene at the later stages of crystallization. This gives an indication of the complexity of crystallization process and its temperature dependence. It also indicates that the crystallization mechanism is not similar throughout the whole process [31]. In fact, Ozawa model ignored the secondary crystallization and dependency of m parameter and the fold length on temperature. Moreover, the thickness of lamella is considered to be dependent on temperature. Due to weak linear relation in the plots of Ozawa equation, the Mo method was applied to study the non-isothermal crystallization kinetics.

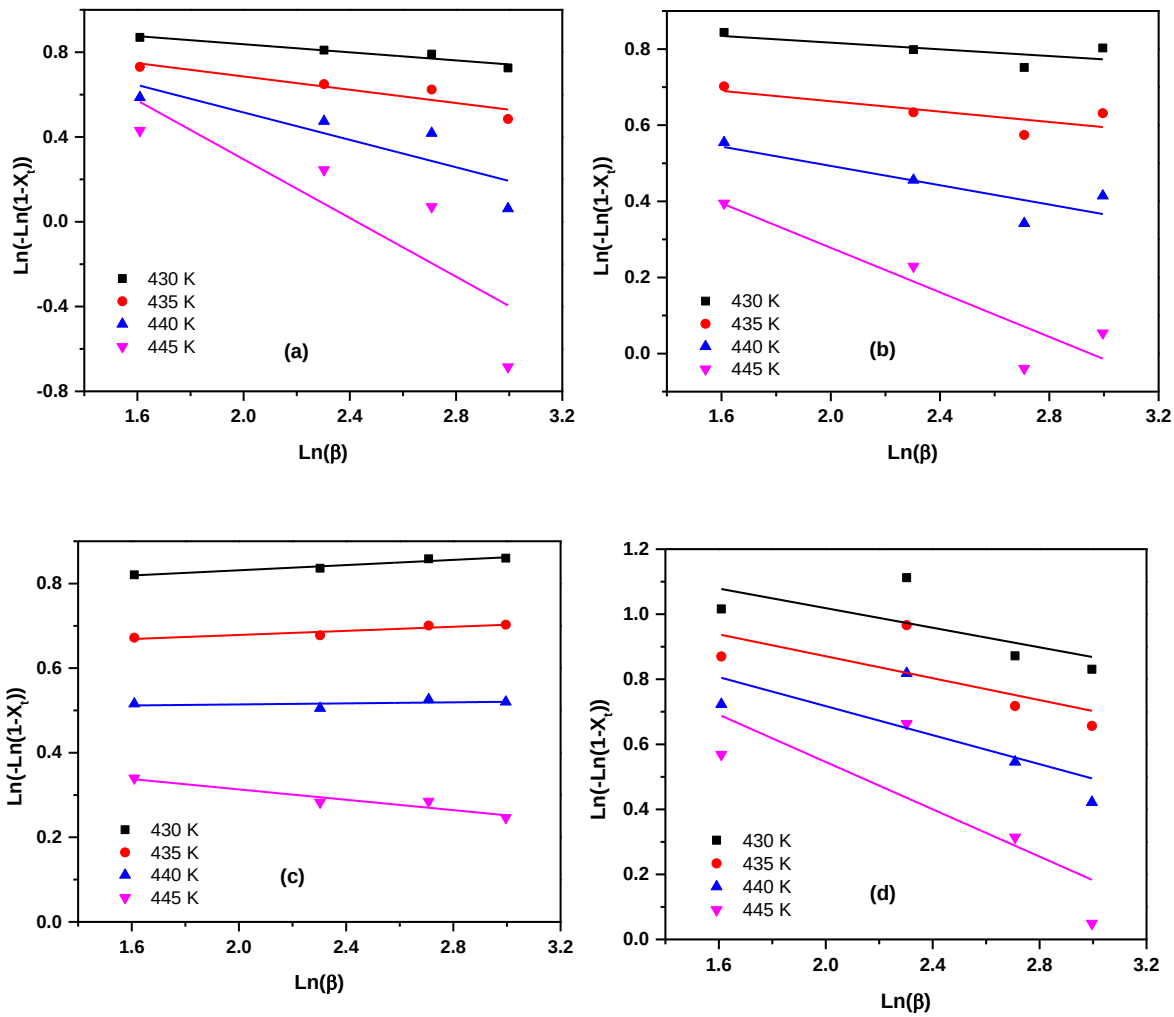

Fig 4-2: The Ozawa plots for (a) PS, (b) PSG (0.25%), (c) PSG (0.5%) and (d) PSG (1%)

Table 4-3: Summarized kinetics results obtained by Ozawa analysis

Sample	T(K)	m	Ln(K(T))
PS	430	0.10	1.03
	435	0.16	1.00
	440	0.32	1.16
	445	0.69	1.68
PSG (0.25%)	430	0.04	0.90
	435	0.07	0.80
	440	0.13	0.75
	445	0.29	0.86
PSG (0.5%)	430	-0.03	0.77
	435	-0.02	0.63
	440	-0.01	0.50
	445	0.06	0.44
PSG (1%)	430	0.15	1.32
	435	0.17	1.21
	440	0.22	1.16
	445	0.36	1.27

4.3.3 Mo method

Liu et al [39] proposed a model commonly known as Mo-model, to examine the non-isothermal crystallization of polymers. This model is actually the combined form of Avrami and Ozawa models. It is given by Eq. 4-5

$$nLn(t) + Ln(k_t) = Ln\big(K(T)\big) - mLn(\beta) \quad (4\text{-}5)$$

The above equation can be simplified to the following final form:

$$Ln[\beta] = Ln[F(T)] - \alpha Ln[t] \quad (4\text{-}6)$$

Where, $F(T) = [K(T)/k_t]^{1/m}$ represents the value super-cooling that required to attain certain degree of crystallization within a unit of crystallization time, and α = *n/m* represents the ratio of the Avrami exponent to Ozawa exponent, respectively.

According to Eq. 4-6, the plot of *Ln[β]* against *Ln[t]* at a certain degree of crystallization should be a straight line and the values of α and *F(T)* can be estimated by fitting Eq. 4-6 to the data. The Mo plots for the PVA/starch blend and its nanocomposites with graphene are shown in Figure 4-2. Unlike Ozawa model, Mo mode fits all the experimental data very accurately. The results of Mo analysis are listed in Table 4-4, which is clear that the value of *F(T)* increases with increasing the relative crystallinity for PVA/starch and its nanocomposites. This indicates that, in a given time higher super-cooling was needed to attain a higher level of crystallinity [28]. It was also observed that a constant relative crystallinity, *F(T)* for the PVA/starch blend increased after the addition of graphene. The results of *F(T)* match perfectly with the trend of $t_{(1/2)}$ that both values decreased at a higher loading of graphene (1 wt. %). It is also noticeable that the value of α parameter is relatively stable, indicating that Mo model is appropriately described the crystallization process.

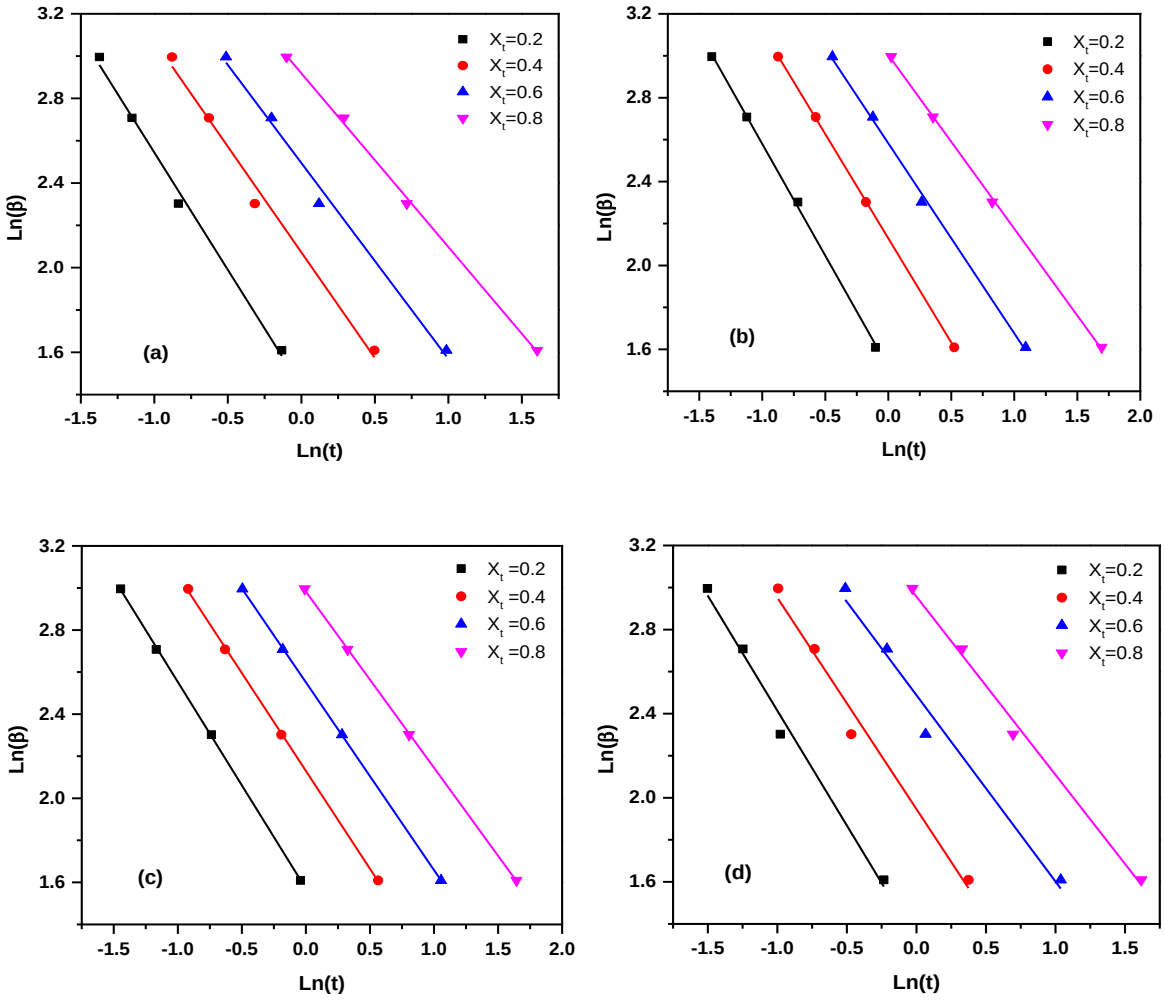

Fig 4-3: The Mo plots for (a) PS, (b) PSG (0.25%), (c) PSG (0.5%) and (d) PSG (1%)

Table 4-4: Summarized kinetics results obtained by Mo analysis

Sample	X_t	F(T)	α	R^2
PS	0.2	4.20	1.11	0.99
	0.4	7.94	1.00	0.99
	0.6	12.12	0.93	0.99
	0.8	18.52	0.82	1.00
PSG (0.25%)	0.2	4.55	1.07	1.00
	0.4	8.41	0.99	1.00
	0.6	13.23	0.91	1.00
	0.8	20.16	0.83	1.00
PSG (0.5%)	0.2	4.81	0.98	1.00
	0.4	8.41	0.93	1.00
	0.6	13.32	0.89	1.00
	0.8	20.24	0.84	1.00
PSG (1%)	0.2	3.95	1.09	0.99
	0.4	7.68	1.01	0.98
	0.6	12.04	0.89	0.98
	0.8	19.24	0.85	0.99

4.3.4 Effective activation energy

Activation energy (E_A) is an important parameter in the phase transformation process. It relates to the energy that is needed for the movement of the ordered chains from one phase to another [40,41]. In case of melt crystallization there are multiple steps involved and the medium of reaction undergoes various physical changes, therefore the activation energy should be termed as effective activation energy. The effective activation energy accounts for all the intermediate stages involved in the process and it depends on the temperature and the extent of conversion [42]. E_A can be determined by two different classes of methods, (1) model fitting method and (2) the model free methods, also known as the iso-conversional methods. In the latter case, E_A is determined independently of the

reaction model. However, for this purpose more cooling rate is required to obtain E_A vs. α dependence in case of melt crystallization. The model-free methods can also provide detailed insights of the reaction progress from the conversion and temperature dependence. For more details of the methods used for calculation of activation energy and their accuracy, the readers can refer to reference [43]. The most frequently used iso-conversional methods are differential Friedman method [44], integral Ozawa–Flynn–Wall method [45], Kissinger–Akahira–Sunose method [46,47] and advanced iso-conversional method [42,48]. In this study, we utilized the differential Friedman method given by Eq. 4-7 [44].

$$\ln\left(\beta_i\left(\frac{d\alpha}{dT}\right)\right)_\alpha = \left[lnf(\alpha) + \frac{-E}{RT_i}\right] \qquad (4\text{-}7)$$

Thus, for the experiments performed at variant cooling rates β, $f(a)$ is constant at a fixed degree of α. Therefore, by measuring the temperature (T_i) and the rate of conversion at a specific degree of α, E_A can be determined by fitting Eq. 4-7 to the data of $ln\left(\beta_i\left(\frac{d\alpha}{dT}\right)\right)$ versus $1/RTi$. The E_A vs α dependence of PVA/starch and PVA/starch/graphene nanocomposites are shown in Figure 4-4. Due to the exothermic nature of the melt crystallization, greater magnitude of absolute E_A favors the process [34,49]. It is observed that the addition of graphene lowers the E_A, which indicates that graphene promotes the crystallization of PVA/starch composite. Similar observations are reported by Li et al. in case of PVA/montmorillonite clay nanocomposites [28]. It is also evident from Figure 4-4 that the melt crystallization process of PVA/starch/graphene nanocomposites is a multistep and the activation energy changes with temperature and conversion. Therefore, the use of model-fitting method may lead to erroneous results.

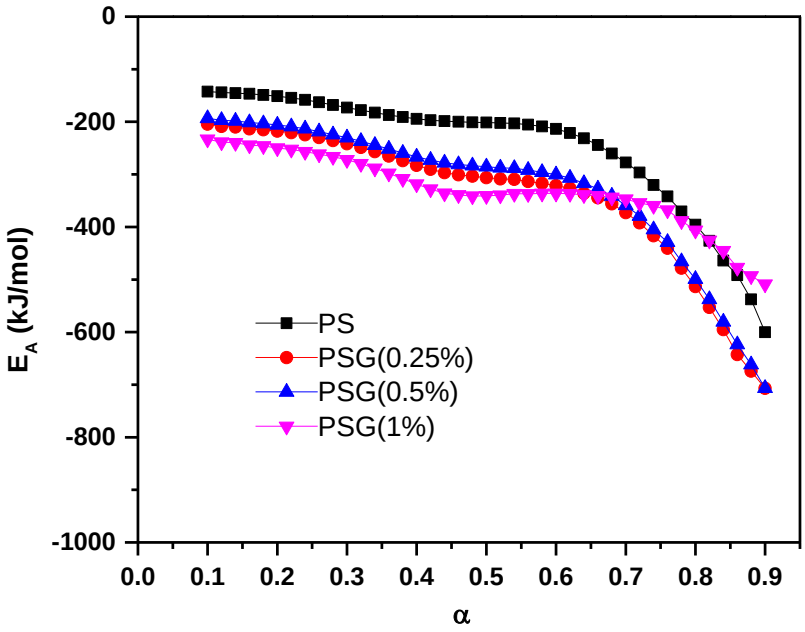

Fig 4-4: Comparison of effective activation energy at progressive conversion for PVA/starch and PVA/starch/graphene nanocomposites

4.4 Conclusion

Poly(vinyl alcohol)/starch/graphene nanocomposites were formed by using solution mixing and casting method. The non-isothermal crystallization behavior of the nanocomposites was investigated by using DSC. Ozawa and Mo models have been employed to analyze the non-isothermal kinetics. The Ozawa theory was failed to adequately describe the crystallization kinetics of the system owing to the inappropriate assumption of ignoring the secondary stage crystallization.

Mo model had successfully identified the non-isothermal crystallization process of poly(vinyl alcohol)/starch/graphene nanocomposites. Graphene nucleated the crystallization of PVA/starch and shifted its crystallization onset (T_{on}) and peak (T_p) temperatures to higher values as well as enhanced its crystallization enthalpy (ΔH_{cry}). However, the additions of graphene confined chain transfers from melt to crystalline form and hindered the growth of crystals, consequently, retarded the overall rate of crystallization.

The activation energy (E_A) was measured by applying the differential Friedman method. Thus the dependence of E_A on the temperature and the extent of the conversion was obtained. It was found that the addition of graphene into the PVA/starch composite considerably lowered the effective E_A, therefore favoring the crystallization process.

Refernces

1. Shi Y-H, Dou Q. Non-isothermal crystallization kinetics of β-nucleated isotactic polypropylene. J. Therm. Anal. Calorim. 2012;112:901–11.

2. Baker MI, Walsh SP, Schwartz Z, Boyan BD. A review of polyvinyl alcohol and its uses in cartilage and orthopedic applications. J. Biomed. Mater. Res. B. Appl. Biomater. 2012;100:1451–7.

3. Peppas NA, Merrill EW. Development of semicrystalline poly(vinyl alcohol) hydrogels for biomedical applications. J. Biomed. Mater. Res. 1977;11:423–34.

4. Santos C, Silva CJ, Büttel Z, Guimarães R, Pereira SB, Tamagnini P, et al. Preparation and characterization of polysaccharides/PVA blend nanofibrous membranes by electrospinning method. Carbohydr. Polym. 2014;99:584–92.

5. Ahmad J, Deshmukh K, Hägg MB. Influence of TiO 2 on the Chemical, Mechanical, and Gas Separation Properties of Polyvinyl Alcohol-Titanium Dioxide (PVA-TiO 2) Nanocomposite Membranes. Int. J. Polym. Anal. Charact. Taylor & Francis Group; 2013;18:287–96.

6. Peppas NA, Tennenhouse D. Semicrystalline poly(vinyl alcohol) films and their blends with poly(acrylic acid) and poly(ethylene glycol) for drug delivery applications. J. Drug Deliv. Sci. Technol. 2004;14:291–7.

7. Wang X, Yucel T, Lu Q, Hu X, Kaplan DL. Silk nanospheres and microspheres from silk/pva blend films for drug delivery. Biomaterials. 2010;31:1025–35.

8. Carbone K, Casarci M, Varrone M. Crosslinked poly(vinyl alcohol) supports for the immobilization of a lipolytic enzyme. J. Appl. Polym. Sci. John Wiley & Sons, Inc.; 1999;74:1881–9.

9. Kenawy E-R, Kamoun EA, Mohy Eldin MS, El-Meligy MA. Physically crosslinked poly(vinyl alcohol)-hydroxyethyl starch blend hydrogel membranes: Synthesis and characterization for biomedical applications. Arab. J. Chem. 2014;7:372–80.

10. Pawde SM, Deshmukh K. Characterization of polyvinyl alcohol/gelatin blend hydrogel films for biomedical applications. J. Appl. Polym. Sci. 2008;109:3431–7.

11. Costa LMM, de Olyveira GM, Cherian BM, Leão AL, de Souza SF, Ferreira M. Bionanocomposites from electrospun PVA/pineapple nanofibers/Stryphnodendron adstringens bark extract for medical applications. Ind. Crops Prod. 2013;41:198–202.

12. Xie F, Pollet E, Halley PJ, Avérous L. Starch-based nano-biocomposites. Prog. Polym. Sci. 2013;38:1590–628.

13. Chai W-L, Chow J-D, Chen C-C. Effects of Modified Starch and Different Molecular Weight Polyvinyl Alcohols on Biodegradable Characteristics of Polyvinyl Alcohol/Starch Blends. J. Polym. Environ. 2012;20:550–64.

14. Maiti M, Kaith BS, Jindal R, Jana AK. Synthesis and characterization of corn starch based green composites reinforced with Saccharum spontaneum L graft copolymers prepared under micro-wave and their effect on thermal, physio-chemical and mechanical properties. Polym. Degrad. Stab. 2010;95:1694–703.

15. Bin-Dahman OA, Jose J, Al-Harthi MA. Compatibility of poly(acrylic acid)/starch blends. Starch - Stärke. 2015;n/a – n/a.

16. Sreekumar P, Al-Harthi M a., De S. Reinforcement of starch/polyvinyl alcohol blend using nano-titanium dioxide. J. Compos. Mater. 2012;46:3181–7.

17. Sreekumar PA, Al-Harthi MA, De SK. Effect of glycerol on thermal and mechanical properties of polyvinyl alcohol/starch blends. J. Appl. Polym. Sci. 2012;123:135–42.

18. Sreekumar PA, Al-Harthi MA, De SK. Studies on compatibility of biodegradable starch/polyvinyl alcohol blends. Polym. Eng. Sci. 2012;52:2167–72.

19. Appu SP, De SK, Khan MJ, Al-Harthi MA. Natural weather ageing of starch/polyvinyl alcohol blend: effect of glycerol content. J. Polym. Eng. 2013;33:1–7.

20. Jose J, De SK, AlMa'adeed MA, Dakua JB, Sreekumar PA, Sougrat R, et al. Compatibilizing role of carbon nanotubes in poly(vinyl alcohol)/starch blend. Starch /Stärke. 2014;66:1–7.

21. Jose J, Al-Harthi MA, AlMa'adeed MA-A, Bhadra Dakua J, De SK. Effect of graphene loading on thermomechanical properties of poly(vinyl alcohol)/starch blend. J. Appl. Polym. Sci. 2015;132:n/a – n/a.

22. Piorkowska E, Galeski A, Haudin J-M. Critical assessment of overall crystallization kinetics theories and predictions. Prog. Polym. Sci. 2006;31:549–75.

23. Huang H, Gu L, Ozaki Y. Non-isothermal crystallization and thermal transitions of a biodegradable, partially hydrolyzed poly(vinyl alcohol). Polymer (Guildf). 2006;47:3935–45.

24. Peng Z, Kong LX, Li S-D. Non-isothermal crystallisation kinetics of self-assembled polyvinylalcohol/silica nano-composite. Polymer (Guildf). 2005;46:1949–55.

25. Zhu Y, Du Z, Li H, Zhang C. Preparation and crystallization behavior of multiwalled carbon nanotubes/poly(vinyl alcohol) nanocomposites. Polym. Eng. Sci. 2011;51:1770–9.

26. Probst O, Moore EM, Resasco DE, Grady BP. Nucleation of polyvinyl alcohol crystallization by single-walled carbon nanotubes. Polymer (Guildf). 2004;45:4437–43.

27. Peng Z, Chen D. Study on the nonisothermal crystallization behavior of poly(vinyl alcohol)/attapulgite nanocomposites by DSC analysis. J. Polym. Sci. Part B Polym. Phys. 2006;44:534–40.

28. Li C, Hou T, Vongsvivut J, Li Y, She X, She F, et al. Simultaneous crystallization and decomposition of PVA/MMT composites during non-isothermal process. Thermochim. Acta. 2015;618:26–35.

29. Li C, Vongsvivut J, She X, Li Y, She F, Kong L. New insight into non-isothermal crystallization of PVA-graphene composites. Phys. Chem. Chem. Phys. The Royal Society of Chemistry; 2014;16:22145–58.

30. Lee S, Hong J-Y, Jang J. The effect of graphene nanofiller on the crystallization behavior and mechanical properties of poly(vinyl alcohol). Polym. Int. 2012;62:901–8.

31. Hassanjani Roushan A, Omrani A, Motahari A, Rostami AA. Influence of Octasilane POSS on Non-Isothermal Crystallization, Thermal Stability and Conductivity of Poly(vinyl alcohol) Nanocomposite. Polym. Plast. Technol. Eng. Taylor & Francis; 2015;55:268–77.

32. Jang J, Lee DK. Plasticizer effect on the melting and crystallization behavior of polyvinyl alcohol. Polymer (Guildf). 2003;44:8139–46.

33. Bosq N, Guigo N, Persello J, Sbirrazzuoli N. Melt and glass crystallization of PDMS and PDMS silica nanocomposites. Phys. Chem. Chem. Phys. The Royal Society of Chemistry; 2014;16:7830–40.

34. Shehzad F, Thomas SP, Al-Harthi MA. Non-isothermal crystallization kinetics of high density polyethylene/graphene nanocomposites prepared by in-situ polymerization. Thermochim. Acta. 2014;589:226–34.

35. Pas SJ, Dargusch MS, MacFarlane DR. Crystallisation kinetics of some archetypal ionic liquids: isothermal and non-isothermal determination of the Avrami exponent. Phys. Chem. Chem. Phys. The Royal Society of Chemistry; 2011;13:12033–40.

36. Daud M, Shehzad F, Al-Harthi MA. Non-isothermal crystallization kinetics of LLDPE prepared by in situ polymerization in the presence of nano titania. Polym. Bull. 2015;72:1233–45.

37. Ozawa T. Kinetics of non-isothermal crystallization. Polymer (Guildf). 1971;12:150–8.

38. Avrami M. Kinetics of Phase Change. I General Theory. J. Chem. Phys. AIP Publishing; 1939;7:1103.

39. Liu T, Mo Z, Wang S, Zhang H. Nonisothermal melt and cold crystallization kinetics of poly(aryl ether ether ketone ketone). Polym. Eng. Sci. 1997;37:568–75.

40. Joshi M, Butola BS. Studies on nonisothermal crystallization of HDPE/POSS nanocomposites. Polymer (Guildf). 2004;45:4953–68.

41. Chafidz A, Ali I, Ali Mohsin ME, Elleithy R, Al-Zahrani S. Atomic Force Microscopy, thermal, viscoelastic and mechanical properties of HDPE/CaCO3 nanocomposites. J. Polym. Res. 2012;19:1–17.

42. Vyazovkin S. Is the Kissinger equation applicable to the processes that occur on cooling? Macromol. Rapid Commun. WILEY- VCH Verlag; 2002;23:771–5.

43. Starink M. The determination of activation energy from linear heating rate experiments: a comparison of the accuracy of isoconversion methods. Thermochim. Acta. 2003;404:163–76.

44. Friedman HL. Kinetics of thermal degradation of char-forming plastics from thermogravimetry. Application to a phenolic plastic. J. Polym. Sci. Part C Polym. Symp. 1964;6:183–95.

45. Ozawa T. A New Method of Analyzing Thermogravimetric Data. Bull. Chem. Soc. Jpn. 1965;38:1881–6.

46. Kissinger HE. Reaction Kinetics in Differential Thermal Analysis. Anal. Chem. American Chemical Society; 1957;29:1702–6.

47. Akahira T, Sunose T. Method of determining activation deterioration constant of electrical insulating materials. Res. Rep. Chiba Inst. Technol. 1971;16:22–31.

48. Vyazovkin S, Sbirrazzuoli N. Isoconversional kinetic analysis of thermally stimulated processes in polymers. Macromol. Rapid Commun. 2006;27:1515–32.

49. Ferreira CI, Dal Castel C, Oviedo MAS, Mauler RS. Isothermal and non-isothermal crystallization kinetics of polypropylene/exfoliated graphite nanocomposites. Thermochim. Acta. Elsevier B.V.; 2013;553:40–8.

CHAPTER 5

ELECTRICAL AND DIELECTRIC PROPERTIES OF POLY(VINYL ALCOHOL)/STARCH/GRAPHENE NANOCOMPOSITES

Osamah A. Bin-Dahman[1], Mostafizur Rahaman[2], Dipak Khastgir[3] and Mamdouh A. Al-Harthi[1]

[1]Department of Chemical Engineering, King Fahd University of Petroleum and Minerals, Dhahran, Saudi Arabia

[2]Department of Chemistry, College of Science, King Saud University, Riyadh, Saudi Arabia

[3]Rubber Technology Centre, Indian Institute of Technology, Kharagpur, India

[*]Corresponding Author: Mamdouh A. Al-Harthi, E-mail address: mamdouh@kfupm.edu.sa

This chapter has been submitted to journal of "Polymer Science Series A"

Abstract

Electrical and dielectric properties of poly(vinyl alcohol) (PVA) films, and PVA/starch blend and its nanocomposites with graphene were investigated. The tested materials were prepared via solution mixing and an evaporative casting technique using glycerol as a plasticizer. Differential scanning calorimetric (DSC) measurement data was used to calculate the percentage of crystallinity and glass transition temperature (T_g). Distribution of starch and graphene in the PVA matrix was determined from field emission scanning electron microscopy (FESEM). Effects of the plasticizer and graphene loading on the DC and AC electrical conductivities of the PVA/starch blend were studied. The impact of graphene loadings on the dielectric permittivity (ε'), dielectric loss tangent (tan δ), complex electric modulus (M^*), and complex impedance (Z^*) as a function of frequency were reported. The DC conductivity of PVA was increased with the addition of glycerol and starch. The permittivity of PVA films and PVA/starch/graphene nanocomposites showed a strong frequency-dependent behavior in a low frequency zone. The addition of graphene to the PVA/starch blend reduced the area under the semicircles of the Nyquist plot.

Keywords Nancomposites / Electrical conductivity / Dielectric properties / Electric modulus / Electrical impedance

5.1 Introduction

Non-biodegradable polymers are a potential risk to the environment and they require petroleum resources for their production. Development of composites from degradable polymers and renewable materials for diverse applications has attracted attention in scientific and technological communities. Recently, graphene has been extensively used by researchers in making novel nanocomposites with unique functional properties [1–8]. Two-dimensional graphene nanosheets have advanced one step ahead of the conventional nanofillers such as nanoclays and carbon nanotubes due to their excellent electrical and mechanical properties, ultra-high aspect ratio, and low density [9–11].

Poly(vinyl alcohol) (PVA) is a non-toxic polymer which has unique properties such as biocompatibility, biodegradability, hydrophilicity, and chemical resistance. It also has good barrier properties against the passage of gases and liquids [12]. PVA can be smoothly mixed with natural polymers and fillers to make biodegradable composites. Starch is a renewable biodegradable polymer and possesses numerous benefits such as availability, lower cost compared to synthetic polymers, and complete compostability without producing poisonous residue [13]. Starch can be used to improve the features of final products as well as to reduce the cost [14,15]. However, pure starch film has certain drawbacks such as brittleness and high water absorption [16]. Blends of PVA with starch have been extensively studied [17–20]. Recently, further studies have been conducted on studying the thermal and mechanical properties of PVA/starch system using carbon nanotubes and graphene as nanofillers [21–23].

The study of electrical and dielectric properties of polymers is imperative because conductive polymer composites can compete with metals as materials for electrical and electronic devices as a result of their unique mechanical and electrical properties. Electrically conductive polymer composites have been used in a broad range of practical applications. These include capacitors, sensors, conductive coatings, and as anti-static, microwave absorbing, and electromagnetic interference shielding materials [24–32].

We reported that a PVA/starch blend (70/30 parts by weight) had optimum compatibility and enhanced mechanical properties where glycerol was used as a plasticizer [17–19]. In this chapter, we studied the effects glycerol and starch on DC and AC conductivities of PVA films. Special emphasis was given to investigate the effect of graphene loading on the electrical and dielectric properties of the PVA/starch blend.

5.2 Experimental

5.2.1 Materials

Poly(vinyl alcohol) (PVA) with a molecular weight of 27,000 and glycerol were purchased from Sigma Aldrich. Corn starch was acquired from ARASCO Corn Products, Dammam, Saudi Arabia. Graphene with an oxygen content of 1%, surface area of about 13-15 m^2/g, and thickness from 50 to100 nm was obtained from Grafen Chemical Industries Co., Turkey.

5.2.2 Preparation of Blends

PVA films and nanocomposites composed of PVA/starch blends with graphene were fabricated via a solution mixing and evaporative casting method. A constant weight ratio for PVA/starch (70/30) was used. PVA (4.2 g) in 50 mL of deionized water was completely dissolved. Starch (1.8 g) was dispersed in deionized water (50 mL) with a fixed amount of glycerol (3 g) added as a plasticizer. A stable dispersion of graphene in deionized water (according to the formulations shown in Table 5-1) was prepared via ultra-sonication using an ultrasonic probe (Ultrasonica Q 700) for 2 min at an amplitude of 30 %. After that, starch and graphene dispersions were added to the dissolved PVA solution. The whole mixture was continually stirred for four hours at 400 rpm. Then the mixture was degassed for 10 min to remove any traces of air from the solution. The mixture was decanted into a flat glass plate and put in an air oven overnight at 50 ^oC. After drying, the films of about 0.3 mm thickness were pulled off from the glass plates and stored in a desiccator filled with silica gel to prevent moisture absorption.

Table 5-1: Formulations used in preparing the PVA/starch/graphene nanocomposites

Sample code	Graphene (wt. %)	Sample code	Graphene (wt. %)
PVA	-	PVASG7	7
PVAg	-	PVASG 10	10
PVASG0	-	PVASG12.5	12.5
PVASG0.25	0.25	PVASG15	15
PVASG0.5	0.5	PVASG17.5	17.5
PVASG1	1	PVASG20	20
PVASG3	3	PVASG25	25
PVASG5	5		

All the samples contain 3 g glycerol except the PVA sample. PVA refers to poly(vinyl alcohol), g to glycerol, S to starch and G to graphene.

5.3 Characterization

5.3.1 Thermal analysis

Differential scanning calorimetric tests were performed with a DSC-Q1000, Universal V4.2E TA instrument. The tests were conducted at a heating rate of 10 °C/min from -70 °C to 200 °C in a nitrogen atmosphere. The percentage of crystallinity was estimated according to the following equation [33,34]:

$$\%\ of\ crystallinity = \frac{\Delta H_{fus}/\emptyset_{PVA}}{\Delta H^{o}_{fus}} \times 100 \qquad (5\text{-}1)$$

Where, ΔH_{fus} is the enthalpy of fusion of the composites, ΔH^{o}_{fus} is the enthalpy of fusion of the 100 % crystalline PVA, and $\emptyset_{PVA}$ is the PVA content in the composites. The value of ΔH^{o}_{fus} of PVA was reserved as 142 J/g [35].

5.3.2 Electrical and dielectric properties

DC resistivity of the films was measured using Agilent 4339B (High-resistance meter connected with an Agilent 16008B resistivity cell). AC electrical resistivity, dielectric constant, and dielectric loss of the nanocomposites were calculated using a Novocontrol Alfa-A instrument, where the frequency was varied from 1 or 10 Hz to 10^7 Hz.

5.3.3 Field emission scanning electron microscopy (FESEM)

FESEM micrographs were taken using MIRA3 TESCAN Field Emission SEM. The films were cryo-fractured with liquid nitrogen before testing. The fractured cross-sections of the films were coated with platinum (5 nm thickness).

5.4 Results and discussion

5.4.1 DSC results

The results of the DSC analysis of PVA films (with and without glycerol) and PVA/starch blends with different loading of graphene are shown in Table 4-2. The addition of a plasticizer increases the flexibility of the polymer chains. As a result a decrease in the glass transition temperature (T_g) was observed in case of PVAg and PVASG samples. The presence of glycerol may disturb the interaction between PVA molecules by occupying the chain free volume which in turn decreased the crystalline phase of the pure PVA [18,36,37]. Furthermore, hydrogen bonding between PVA and

glycerol suppresses the formation of crystallites in the blend films [38]. The incorporation of graphene decreased the T_g of the PVA/starch blend. This may be because of weakening of the hydrogen bonding between PVA and starch as a result of adding graphene [39].

Table 5-2: Glass transition temperature and degree of crystallinity for PVA and PVA/starch/graphene nanocomposites

Sample code	Glass transition temperature (T_g) (^{o}C)	Crystallinity [a)] (%)
PVA	72.00	43.30
PVAg	36.00	18.15
PVASG0	46.50	23.77
PVASG1	38.8	24.02
PVASG5	39.82	24.58
PVASG10	41.86	25.23
PVASG15	43.00	25.56
PVASG20	44.91	25.90

[a] Based on equation (1)

5.4.2 Field emission scanning electron microscopic (FESEM) studies

Scanning electron micrographs of PVA (pure and with glycerol), PVA/starch blend, and selected PVA/starch/graphene nanocomposites are shown in Fig. 5-1(a-f). The surface of PVA became more smooth and softer after the addition of the plasticizer as shown in Fig. 5-1(b). It is clear that the granules of starch were homogenously distributed in the PVA matrix. At a low loading of graphene (Fig. 5-1(d)), there are small number of graphene

aggregates spread in the PVA/starch matrix and the interfacial distance between these aggregates is very high. At high loadings of graphene (Fig. 5-1(f)), a continuous conductive phase of graphene aggregates was formed within the insulating PVA/starch matrix.

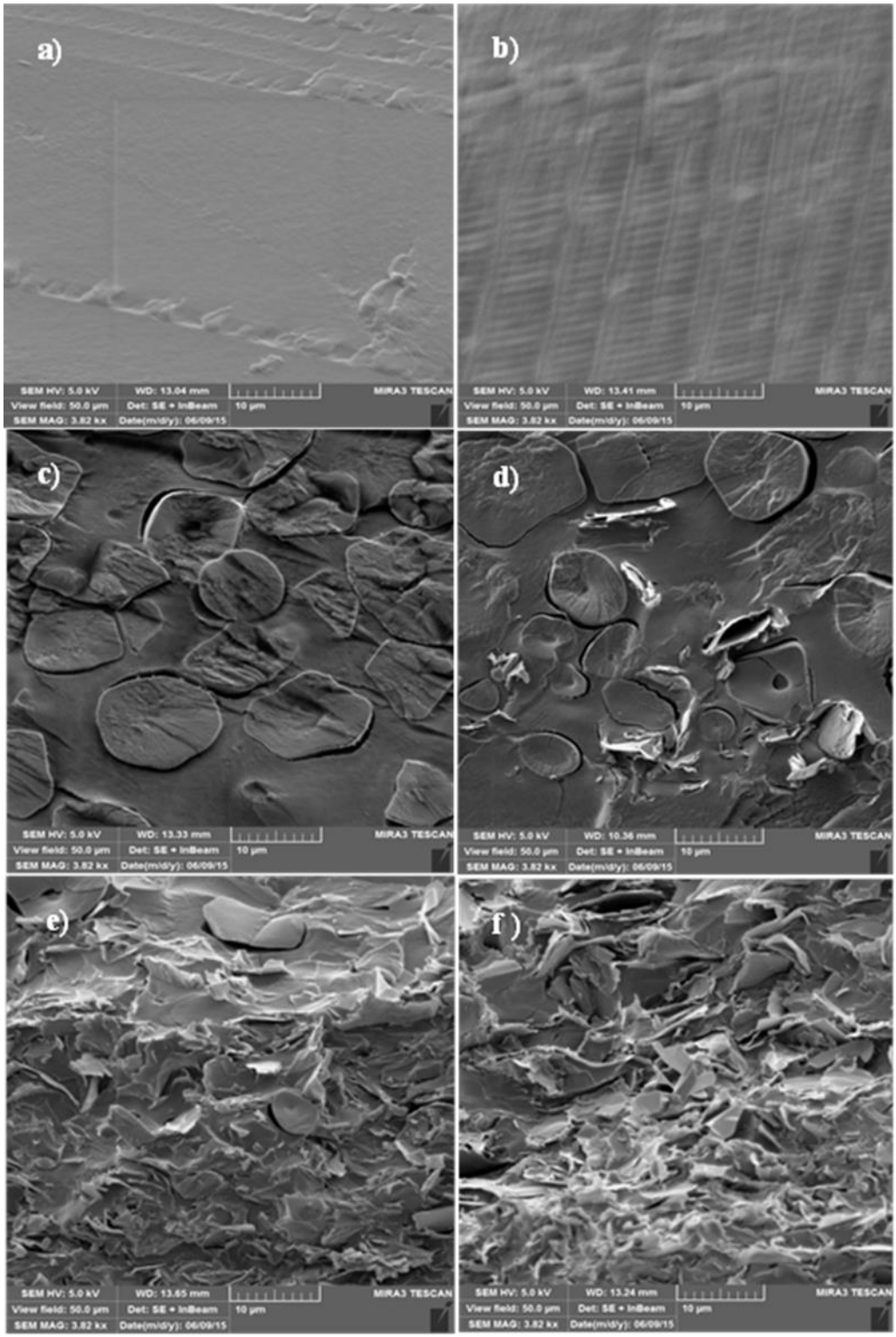

Fig 5-1: FESEM micrographs for (a) PVA; (b) PVAg; (c) PVASG0; (d) PVASG1; (e) PVASG10; (f) PVASG20

5.4.3 DC conductivity

The effect of glycerol, starch and graphene loading on DC conductivity of PVA and their nanocomposites are presented in Fig. 5-2. It is clear that the DC conductivity of neat PVA increased with the addition of glycerol. The DC conductivity of the plasticized PVA can be explained qualitatively according to the following equation:

$$\sigma_{dc} = \mu\, n\, q \qquad (5\text{-}2)$$

where μ is the charge mobility, n is the charge carrier concentration/density and q is the charge. The addition of glycerol to PVA offsets the DC conductivity in two ways. Firstly, it leads to an increase in ionic charge concentration/charge carrier concentration which increases macroscopic conductivity. Secondly, glycerol results in reduced T_g and crystallinity [36]. The reduction in the T_g of polymer leads to an increase in the segmental mobility of polymer chains. This segmental movement is closely related to the charge carrier mobility of the polymer system. Both the factors result in the increase in conductivity of the PVA according to equation (5-2). Also, it is seen that the addition of starch increased the conductivity of the PVA. Buraidah and Arof reported that a host of two polymers can increase the electrical conductivity of electrolytes [30]. According to the authors, blending of two polymers can offer more complexation sites for ion hopping and exchange. Consequently, the blend of PVA and starch results in an increase in conductivity. In addition to that, the gelatinized starch increases the number of hydroxyl groups which results in an increase in conductivity due to the increase in ionic charge [40].

It is also seen from Fig. 5-2 that the addition of graphene into the PVA/starch blend affected the DC conductivity. Initially, the increase in conductivity with the addition of

graphene is very marginal. After a certain loading, however, there is a significant increase in the DC conductivity. The graphene loading point at which this increase in conductivity is observed is known as the percolation threshold of electrical conductivity. According to the theory of percolation, the DC conductivity of composite systems can be presented via the power law model [41]:

$$\sigma_{dc} = k(P_f - P_{fc})^t \qquad for\ P_f > P_{fc} \qquad or \tag{5-3}$$

$$log\sigma_{dc} = logk + t\ log(P_f - P_{fc}) \tag{5-4}$$

Where, σ_{dc} is the DC conductivity, k is a constant known as the pre-exponential factor, P_f is the weight fraction of the filler, P_{fc} is the weight fraction of the filler at critical concentration at which percolation occurs, and t is the critical exponent of conductivity. The pre-exponential factor depends on the conductivity of filler, contact resistance, and characteristics of conductive networks. The critical exponent of conductivity depends on the connectivity of conductive networks in the composite system. The universal values of t for two and three-dimensional composite systems are $t \approx 1.33$ and $t \approx 2.0$, respectively [42,43]. For the present composite system, the value of P_{fc} and t are 11.5 wt. % and 0.95, respectively. Deviation of the experimentally obtained value of t from its universal value is widely reported [44–46]. Though the actual reason of non-universality of t is unknown, in some reports it has been attributed to the complex tunnelling transport process in the real polymer composites [47,48]. Initially, the added graphene particles in the PVA/starch blend remain isolated or separated from other graphene particles due to very small loading of graphene. Hence, the increase in DC conductivity is very marginal. But at or around the percolation threshold, there is a formation of a continuous conductive network or pathway with the aggregation of graphene inside the nanocomposite blend. Hence, a

clear increase in electrical conductivity is observed. Further addition of graphene into the nanocomposite blend, increases only the number of such conductive pathways inside the nanocomposites. Thus, the increase in electrical conductivity becomes marginal.

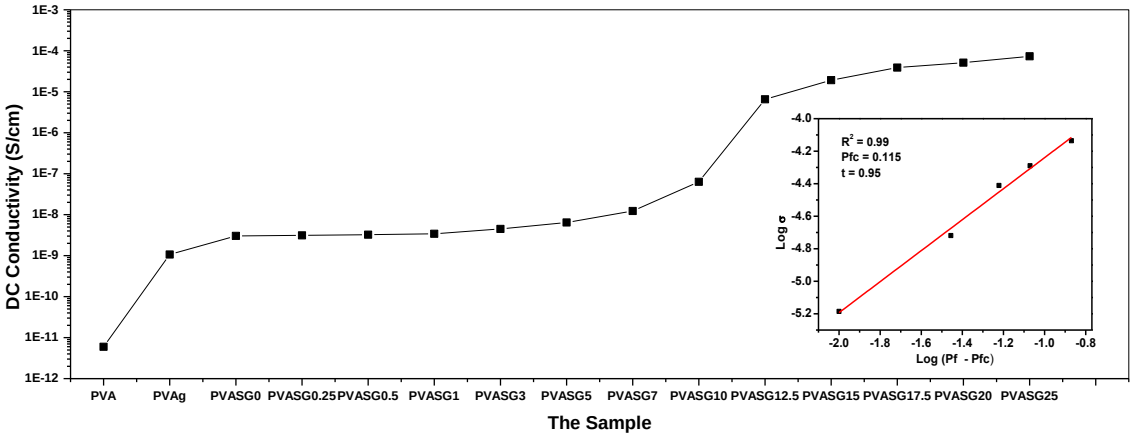

Fig 5-2: The effects of glycerol and graphene on DC conductivity at room temperature

5.4.4 AC conductivity

The effects of frequency on AC electrical conductivity (σ_{ac}) at room temperature of PVA, PVA/starch blend and their nanocomposites are presented in Fig. 5-3. All the samples showed frequency-dependent behavior under investigation. However, the nature of the frequency dependency differs according to sample characteristics. PVA and PVAg showed a higher range of frequency-dependency behavior as compared to the frequency-dependency behavior of graphene loaded PVA/starch blends. That is, the frequency dependency decreases as the graphene loading in the PVA/starch blend increases. The AC conductivity of PVAg is lower than that of PVA/starch blend, but after a certain frequency the AC conductivity of PVAg crosses the conductivity of the PVA/starch blend and some lower loaded PVA/starch/graphene composites. This high frequency-dependency behavior of PVAg is due to its lower T_g value and crystallinity as shown earlier in Table 5-2. The increase in frequency means more energy is exerted on the charge carrier. The hopping or tunneling of the charge carrier is increased with an increase in frequency. Therefore, the AC conductivity increases with the increase in frequency for all components. As the flexibility of PVAg is higher compared to the PVA/starch blend, the relative tendency of hopping of charge carriers present in PVAg is higher compared to the charge carriers present in the PVA/starch blend when the frequency is increased. Thus the AC conductivity of PVAg crosses the AC conductivity of the PVA/starch blend after a certain frequency. The AC electrical conductivity of the PVA/starch/graphene nanocomposites is improved with increasing filler loading. At low filler content, there is a marginal increase in conductivity of nanocomposites compared to the PVA/starch blend. At lower graphene loading, the conductivity is primarily governed

by the hopping or tunneling mechanisms of electrical conductivity [49]. At higher filler loading, there is a considerable increase in the value of σ_{ac} compared to the nanocomposites of lower filler loadings. This can be attributed to the increase in the formation of continuous conductive pathways within the PVA/starch matrix due to the increase in the continuous network structure among filler aggregates [50]. The increase in the σ_{ac} with frequency is more noticeable in the frequency range of 10^6-10^7 Hz. This can be attributed to the fact that some charge carriers that were inactive in lower frequency ranges become activated in this frequency range and that results in the increase in conductivity.

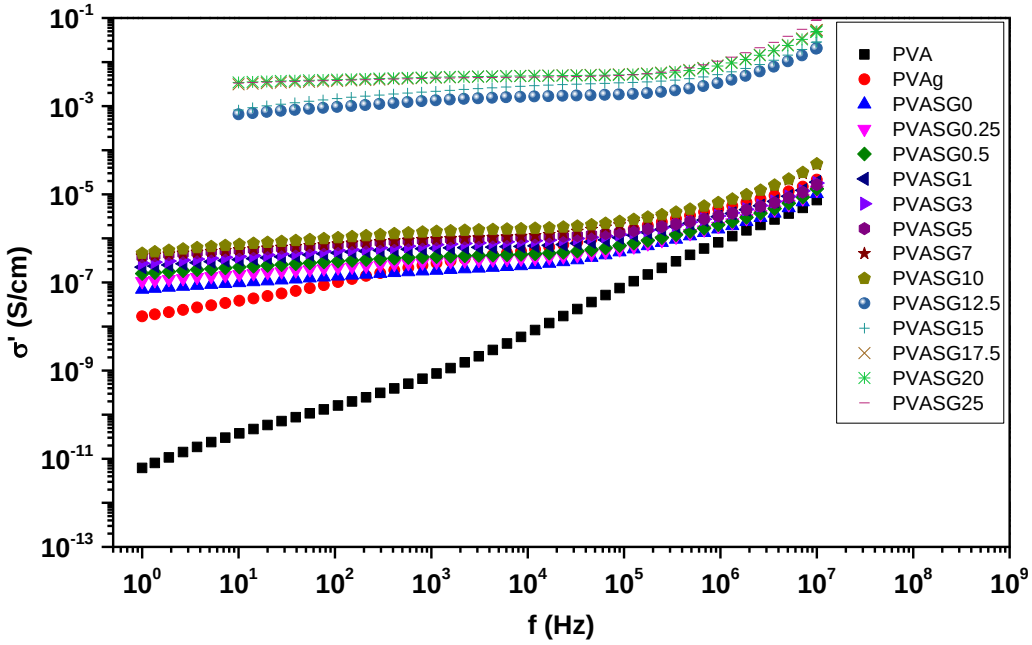

Fig 5-3: Variation of AC conductivity with frequency for PVA, PVA with glycerol and PVA/starch films with different content of graphene at room temperature

5.4.5 Dielectric permittivity

Dielectric permittivity or dielectric constant (ε') provides an important understanding about the polarization effect and displays the ability of a system to store charges under the impact of an electric field [51]. Figure 5-4 displays the variation of dielectric constant versus frequency for PVA, PVA/starch blend, and their nanocomposites at room temperature. PVA without glycerol showed a weak frequency-dependent behavior over the entire range of frequency. PVA with glycerol and PVA/starch nanocomposites showed a strong frequency-dependent behavior in the low frequency zone. The frequency-dependent behavior is stronger in films with high amounts of graphene. At the low frequency zone, the dielectric constant decreased sharply and reached an almost constant value at a frequency of around 10^5 Hz. This may be ascribed to the ability of dipoles to adjust themselves in the direction of the applied field at the low frequency region [31,50]. At the high frequency zone, the dipoles are unable to adjust themselves rapidly in the direction of the applied field because of reduced time for re-orientation [50,52]. The effect of interface polarization at the low frequency zone is a dominant factor for the high value of dielectric constant. This effect is minimized when the frequency is increased [31]. The addition of graphene into the PVA/starch blend increased the value of the dielectric constant. This promotion in dielectric constant can be essentially ascribed to a gradual formation of microcapacitor networks in the PVA/starch matrix as the amount of graphene increases [53,54]. The decrease in the value of the dielectric constant at high frequency may be because of the strong decrease in the diffusion of dipoles in the electric field direction and the accumulation of space charge [50].

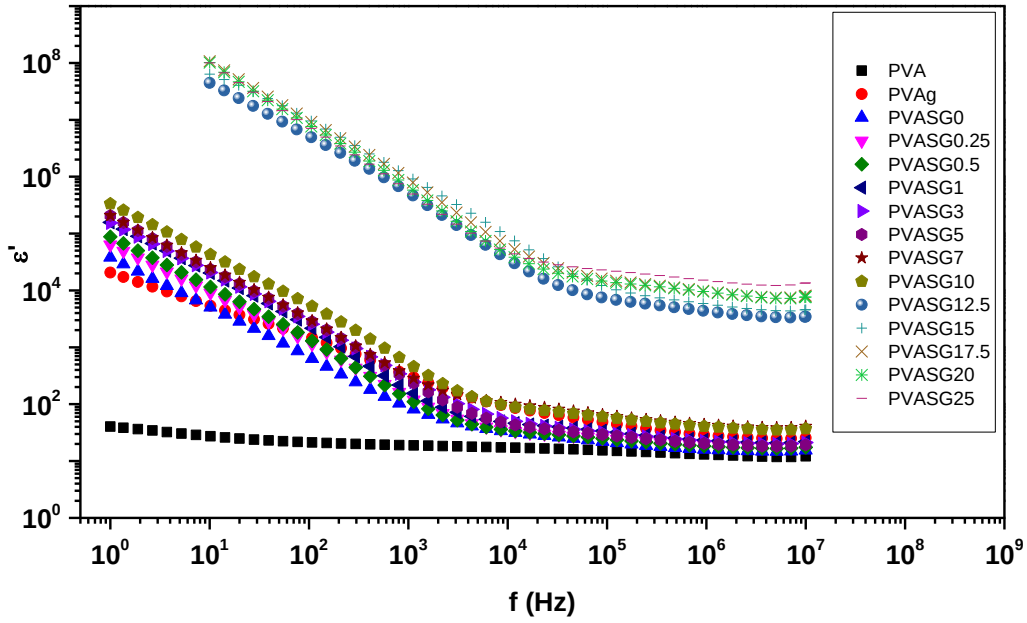

Fig 5-4: Variation of dielectric constant versus frequency at room temperature for PVA, PVA with glycerol and PVA/starch films with different content of graphene

5.4.6 Dielectric loss tangent

The dielectric loss tangent or loss factor (tan δ) measures the dissipation of electromagnetic energy and it is a parameter of the dielectric material [50]. Figure 5-5 depicts the variation of loss tangent versus frequency for PVA, PVA/starch blend, and their nanocomposites at room temperature. The loss spectrum of plasticizer-free PVA did not show any characteristic peak over the whole range of the frequency. The loss spectra of plasticized PVA, PVA/starch blend and their nanocomposites showed peaks at a characteristic frequency. Characteristic properties of dipolar relaxation play an essential role in affecting the strength and frequency of relaxation. The addition of plasticizer led to the appearance of a peak frequency in the PVA. This can be ascribed to an increase in the amorphous content in the PVA polymer. The polymer chains in the amorphous phase are more flexible than those in the crystalline phase and are rapidly able to adjust themselves in the applied field [51]. The insertion of graphene into the PVA/starch matrix shifted the peak frequency towards a higher frequency. This is due to a decrease in relaxation time associated with increasing the filler loading [50].

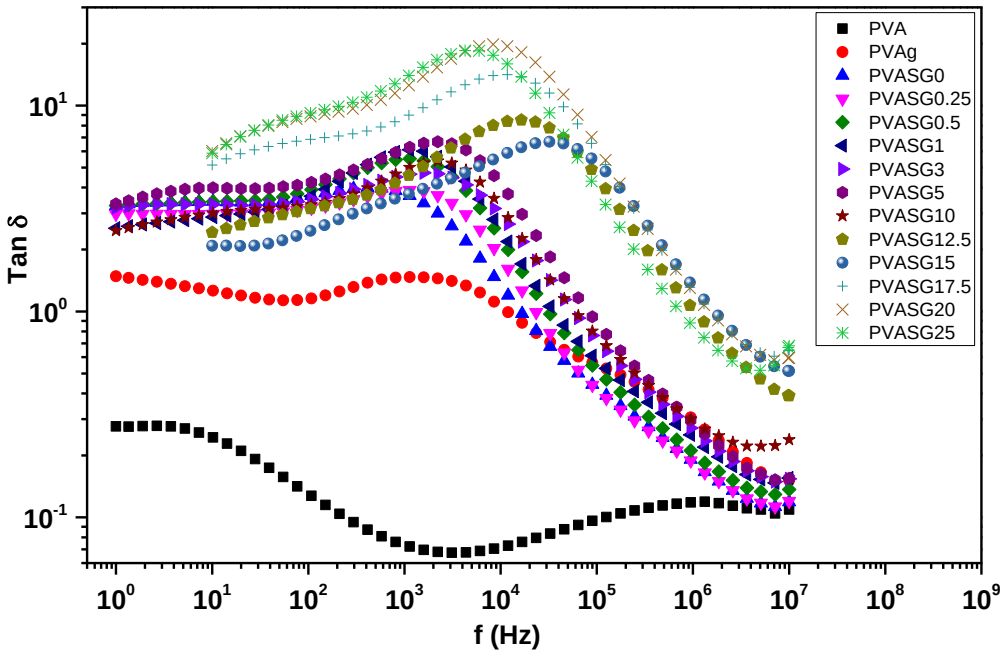

Fig 5-5: Variation of dielectric loss factor (tan δ) as a function of frequency at room temperature for PVA, PVA with glycerol and PVA/starch films with different content of graphene.

5.4.7 Electric modulus

The complex electric modulus (M^*) is defined as the reverse of the complex permittivity (ε^*) and can be expressed as following:

$$M^* = \frac{1}{\varepsilon^*} = \frac{\varepsilon'}{\varepsilon'^2 + \varepsilon''^2} + j\frac{\varepsilon''}{\varepsilon'^2 + \varepsilon''^2} = M' + jM'' \qquad (5\text{-}5)$$

Where, ε' and ε'' are the real (dielectric permittivity) and imaginary (dielectric loss) parts of permittivity and M' and M'' are the real and imaginary parts of the electric modulus, respectively. The interfacial polarization or Maxwell-Wagner-Sillars (MWS) effect is found in heterogeneous materials consisting of two or more phases such as is found in polymer nanocomposites [55]. The electric modulus formalism is introduced to overcome the difficulties resulting from the study of interfacial polarization at a low frequency zone. The difficulties are due to a large variation in conductivity and dielectric permittivity. Figure 5-6 displays the variation of real and imaginary parts of the electric modulus for the PVA, PVA/starch blend, and their nanocomposites as a function of frequency at room temperature. The real part of the electric modulus for all samples increased with increasing frequencies and reached a constant value. The presence of the step-like transitions indicated the existence of a relaxation process. An increase in the graphene loading caused a decrease in the values of M'. This indicates that the dielectric permittivity increased with increasing graphene content, which is in agreement with the dielectric permittivity plot (Fig. 5-4). The constant value of M' is attributed to the inability of large dipoles that developed at the interfaces to follow the electric field at higher frequencies [55]. The observed transitions in the curves of the imaginary part of electric modulus are associated with a loss peak. This peak is slightly shifted towards the

right side of frequency spectrum. The more intense relaxation peak takes place in the curves of the imaginary part at the intermediate frequency region. This peak was found to be dependent on the graphene filler loading and its loss maxima is reduced at higher filler loadings.

Figure 5-7 displays the Cole-Cole plots between the real and imaginary parts of the electric modulus for all samples. The curves represent a suppressed semicircle indicating a non-Debye behavior with the PVA specimen showing the higher deviation. The movement of semicircles towards the origin after the addition of graphene is due to the increase of relaxation time with the increased heterogeneity of the system [56].

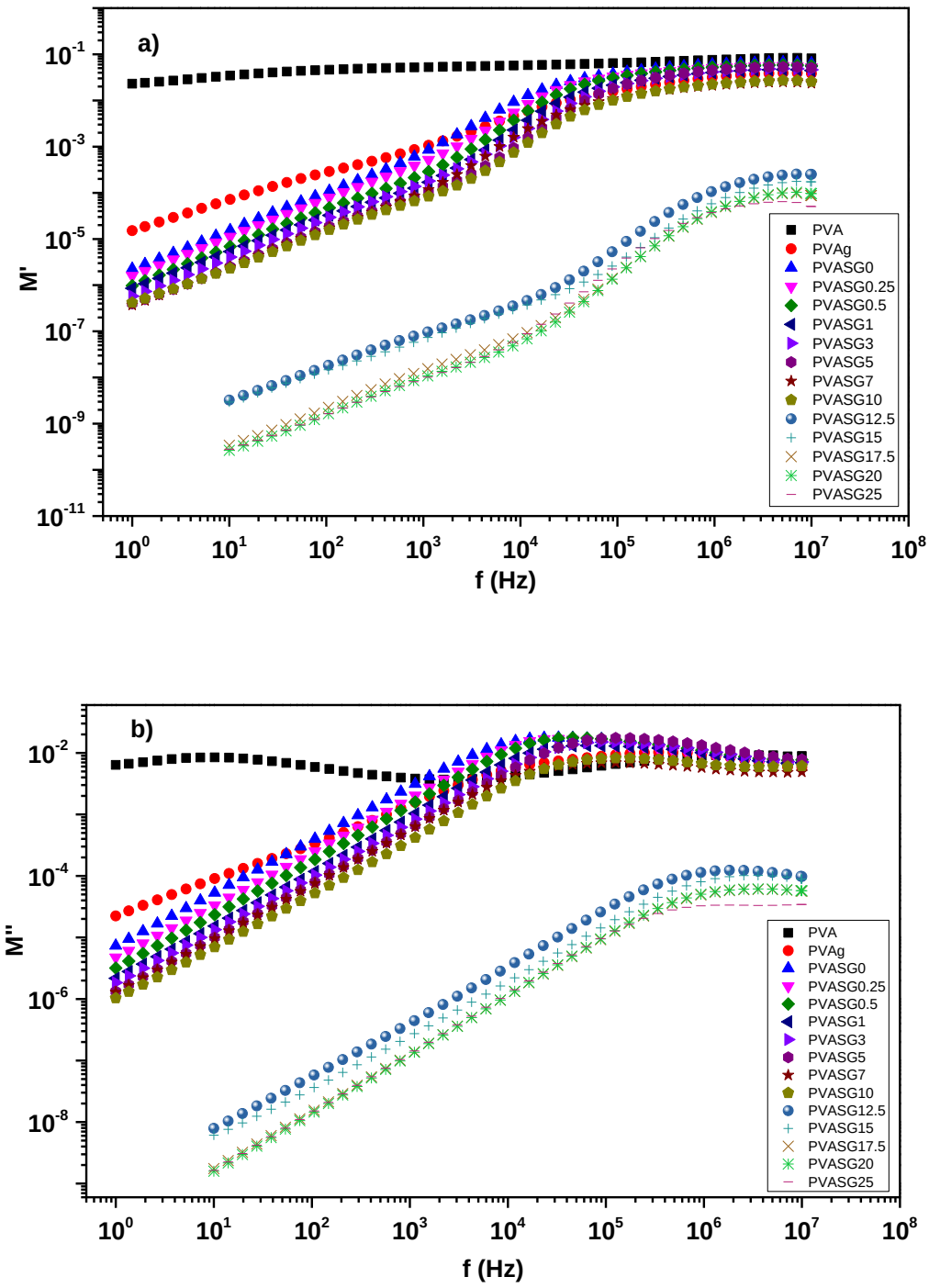

Fig 5-6: Plots of (a) the real (M′) and (b) imaginary (M″) parts of electric modulus versus frequency for PVA, PVA with glycerol and PVA/starch films with different content of graphene at room temperature.

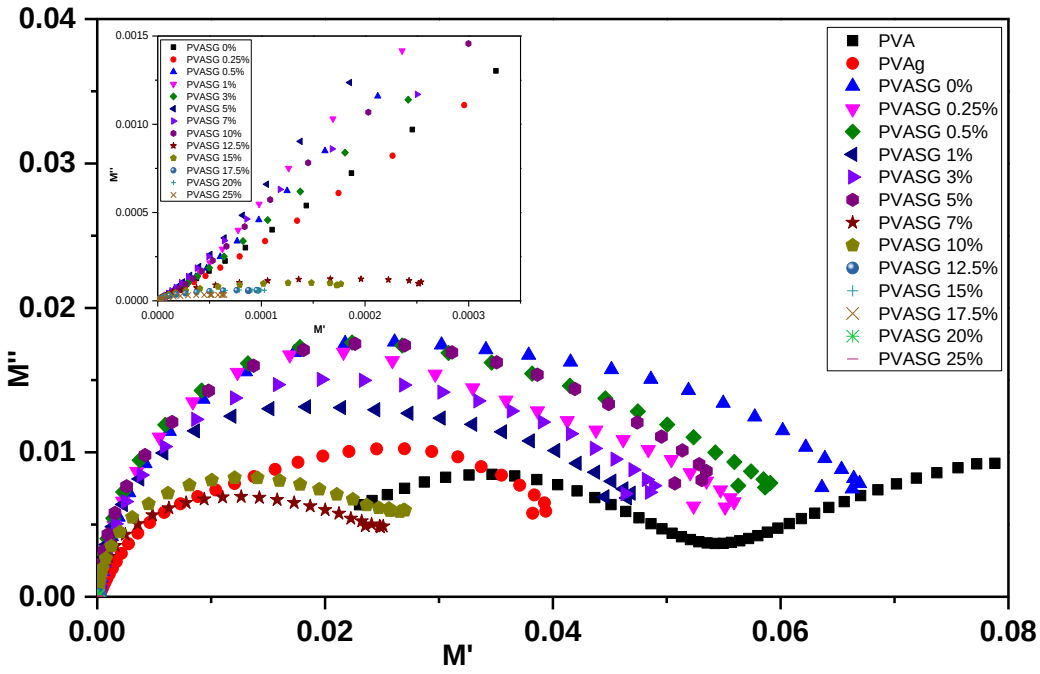

Fig 5-7: Cole-Cole plot between the real (M′) and imaginary (M″) parts of the electric modulus of PVA and PVA/starch/graphene nanocomposites.

5.4.8 Electrical impedance

The electrical conductance (G) was calculated from the measured AC conductivity (σ_{ac}) using the following expression:

$$G(\omega) = \frac{\sigma_{ac} A}{d} \qquad (5\text{-}6)$$

where A is the cross-sectional area of the electrode and d is the thickness of the sample. The calculated conductance (G) and measured capacitance (C) were used to determine the real (Z') and imaginary (Z'') parts of the electrical complex impedance (Z^*) using the following equation:

$$Z^*(\omega) = \frac{G(\omega)}{G^2(\omega)+\omega^2C^2(\omega)} - j\frac{\omega C(\omega)}{G^2(\omega)+\omega^2C^2(\omega)} = Z'(\omega) + jZ''(\omega) \qquad (5\text{-}7)$$

where ω is the angular frequency, $\omega = 2\pi f$. Z' represents the capacitance or storage of charges and Z'' accounts for the loss of accumulated charges (the conductive part) of the system [50]. Figure 5-8 displays the variation of real and imaginary parts of the electrical impedance for the PVA, PVA/starch blend, and their nanocomposites as a function of frequency at room temperature. The value of Z' is decreased with increasing graphene loading as well as with frequency, and this trend is similar for all nanocomposites (Fig. 5-8(a)). At low filler loading, the interphase formed between the polymer and filler hinders the molecular mobility due to the distinct properties [57]. While at high filler loading, a continuous conductive pathway is formed within the insulating polymer matrix owing to the homogeneous distribution of agglomerated conductive fillers. In addition to that, the electron hopping is more important in microwave frequency which is a significant phenomenon of conduction [58].

The variation of the imaginary part of impedance (Z'') with frequency is shown in Fig. 5-8(b). It is clear that Z'' showed similar trend as Z'. It decreases with increasing frequency

for all graphene loadings. This behavior may be ascribed to the identical dielectric relaxation process of all the nanocomposites [50].

The Nyquist plot for the PVA, PVA/starch blend, and their nanocomposites at room temperature at room temperature is shown in Fig. 5-9. For a polymer/composite system, the Z' accounts for bulk resistance (R_B) and Z'' accounts for maximum value of angular frequency (ω_{max}) at the top of the semicircle and is defined as [50]:

$$\omega_{max} = 1/R_B C_B \quad (5\text{-}8)$$

There is a decrease in the value of R_B with increasing graphene loadings; consequently, the conductivity of the nanocomposites is considerably increased. This is in agreement with the AC conductivity plot (Fig. 5-3). There is also a significant enhancement in the bulk capacitance (C_B). The addition of graphene reduced the area under the semicircles of the Nyquist plot and this reduction increased with increasing the filler content.

The system with a single relaxation time is characterized by an excellent semicircle on a Nyquist plot. The semicircular nature specifies the capacitive characteristic of the system. This phenomenon may occur because of the formation of secondary structures (aggregates) created from the aggregation of the graphene sheets [59]. By increasing the filler content, the space between the aggregates decreases. The gap between the graphene aggregates governs the electron conduction through non-Ohmic connections between graphene aggregates [50].

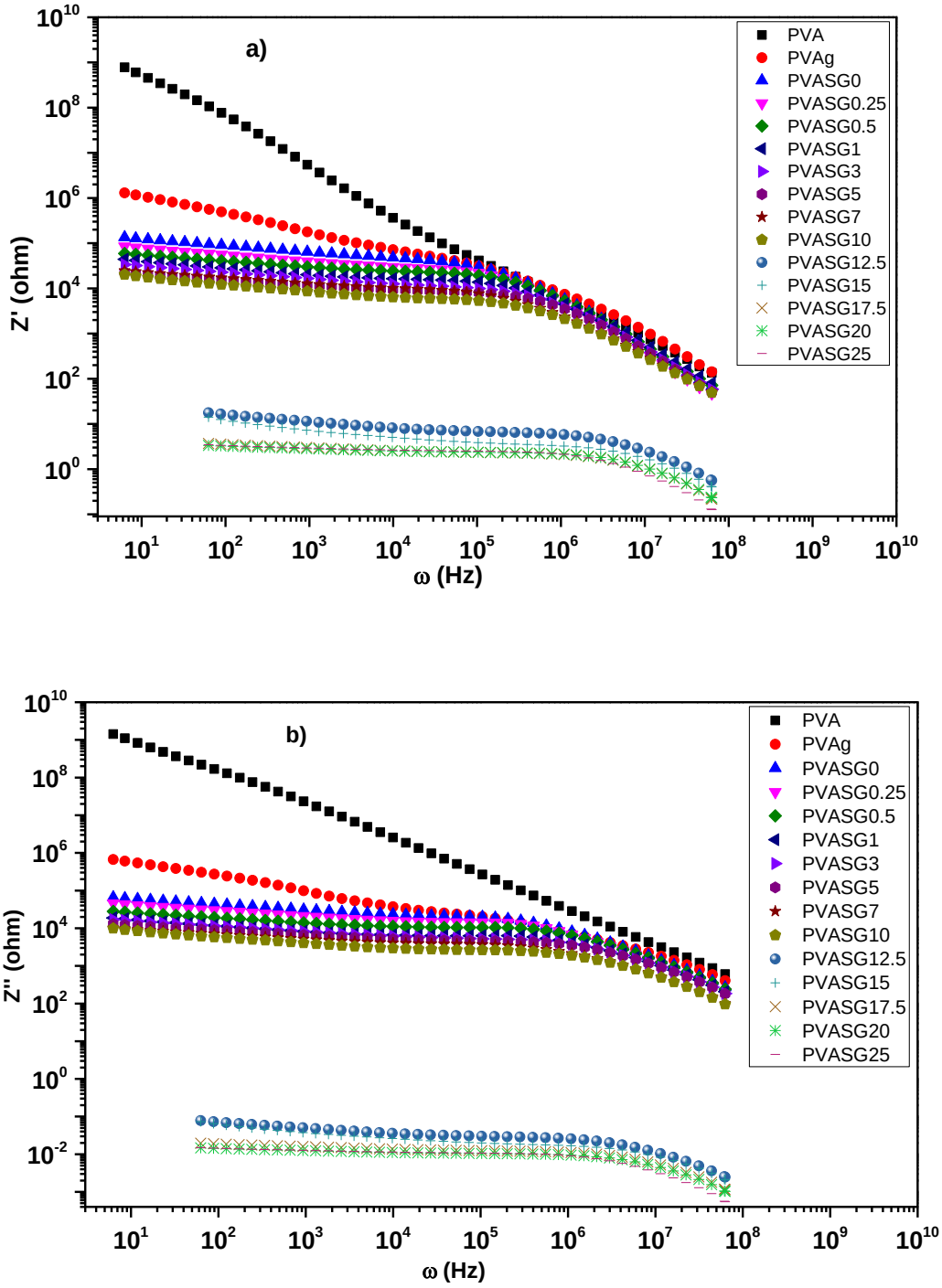

Fig 5-8: Variations of (a) the real (Z′) and (b) imaginary (Z″) parts of the electrical impedance as a function of frequency for PVA, PVA/starch blend, and their nanocomposites at room temperature.

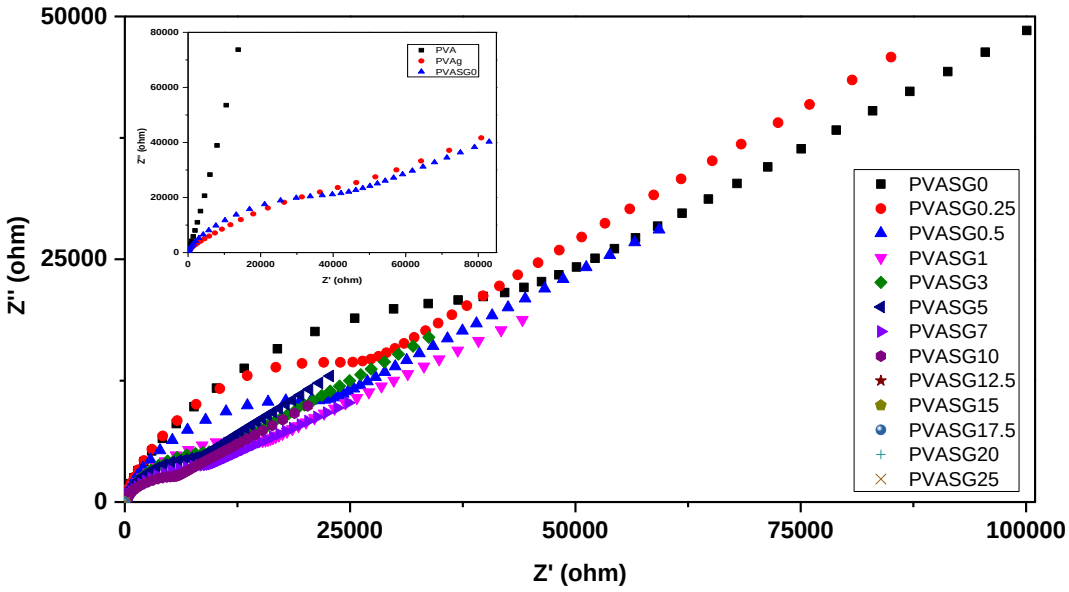

Fig 5-9: Nyquist plot (Z′ vs. Z″) for PVA, PVA/starch blend, and their nanocomposites at room temperature

5.5 Conclusion

The DC conductivity of PVA has been increased with the addition of glycerol and starch. Initially, the increase in conductivity with the addition of graphene was low. After a certain loading (known as percolation threshold), a drastic increase in DC conductivity was observed. For the present system, the value of percolation threshold was 11.5 wt. %. The AC conductivity of the PVA/starch/graphene nanocomposites was improved with the increase in both graphene loading and frequency. At lower graphene loading, the AC conductivity is primarily governed by the hopping and tunnelling mechanisms of electrical conductivity. At higher graphene loading, there is a substantial increase in the value of both DC and AC conductivity due to the formation of continuous conductive network pathways of graphene aggregates within the PVA/starch blend. The dielectric permittivity of PVA without glycerol showed a weak frequency-dependent behavior over the whole range of frequencies. However, the permittivity of PVA films with glycerol and PVA/starch/graphene nanocomposites showed a strong frequency-dependent behavior in the low frequency zone because of the higher magnitude of interface polarization. This frequency-dependent behavior is stronger in films with high amounts of graphene. The addition of a plasticizer in PVA led to the presence of peak frequency in the PVA loss factor spectrum. This can be attributed to an increase in the amorphous content in the PVA polymer. The insertion of graphene into the PVA/starch blend shifted the peak frequency towards the higher frequency side. The Cole-Cole plots showed a suppressed semicircle indicating a non-Debye behavior and the PVA specimen showed the higher deviation. The PVA showed a gradual decrease in the value of Z' with increase in frequency. The value of Z' slowly decreases with increasing filler loading as well as

with increasing frequency and this trend was similar for all nanocomposites. Similar behavior was detected for Z''. The addition of graphene reduced the area under the semicircles of the Nyquist plot and this reduction increased with increasing the filler content because of the increase in conductivity. The semicircles at higher frequency are due to the bulk properties and the spikes at lower frequency are due to interface properties of the composite materials.

References

1. B. Indumathi, S. Thamizharasan, J. Gopinathan, K.K. Karthikeyan, and A. Bhattacharyya, Polym. Sci. Ser. A (2016) doi:10.1134/S0965545X16050035

2. L. Wan, B. Wang, S. Wang, X. Wang, Z. Guo, B. Dong, L. Zhao, J. Li, Q. Zhang, and T. Luo, J. Mater. Sci. **50**, 2148 (2015).

3. S. Shang, L. Gan, C.W.M. Yuen, S. Jiang, and N.M. Luo, Compos. Part A Appl. Sci. Manuf. **68**, 149 (2015).

4. I. Sen, Y. Seki, M. Sarikanat, L. Cetin, B.O. Gurses, O. Ozdemir, O.C. Yilmaz, K. Sever, E. Akar, and O. Mermer, Compos. Part B Eng. **69**, 369 (2015).

5. P.K. Ghosh, A. Kumar, and K. Kumar, Polym. Sci. Ser. A **57**, 829 (2015).

6. C.R. Arza, P. Jannasch, and F.H.J. Maurer, Eur. Polym. J. **59**, 262 (2014).

7. S. Sayyar, E. Murray, B.C. Thompson, S. Gambhir, D.L. Officer, and G.G. Wallace, Carbon N. Y. **52**, 296 (2013).

8. T. Nezakati, A. Tan, A.M. Seifalian, and J. Colloid Interface Sci. **435**, 145 (2014).

9. O.C. Compton and S.T. Nguyen, Small **6**, 711 (2010).

10. S. Sheshmani, A. Ashori, M.A. Fashapoyeh, Int. J. Biol. Macromol. **58**, 1 (2013).

11. S. Sheshmani and R. Amini, Carbohydr. Polym. **95**, 348 (2013).

12. M.I. Baker, S.P. Walsh, Z. Schwartz, B.D. Boyan, and J. Biomed. Mater. Res. B. Appl. Biomater. **100**, 1451 (2012).

13. F. Xie, E. Pollet, P.J. Halley, and L. Avérous, Prog. Polym. Sci. **38**, 1590 (2013).

14. O.A. Bin-Dahman, J. Jose, and M.A. Al-Harthi, Starch/Staerke **67**, 1061 (2015).

15. M. Maiti, B.S. Kaith, R. Jindal, and A.K. Jana, Polym. Degrad. Stab. **95**, 1694 (2010).

16. B. Chatterjee, N. Kulshrestha, and P.N. Gupta, Phys. Scr. **90**, 025805 (2015).

17. P. Sreekumar, M. a. Al-Harthi, and S. K. De, J. Compos. Mater. **46**, 3181 (2012).

18. P.A. Sreekumar, M.A. Al-Harthi, and S.K. De, J. Appl. Polym. Sci. **123**, 135 (2012).

19. P.A. Sreekumar, M.A. Al-Harthi, and S.K. De, Polym. Eng. Sci. **52**, 2167 (2012).

20. S.P. Appu, S.K. De, M.J. Khan, and M.A. Al-Harthi, J. Polym. Eng. **33**, 1 (2013).

21. J. Jose, S.K. De, M.A. AlMa'adeed, J.B. Dakua, P.A. Sreekumar, R. Sougrat, and M.A. Al-Harthi, Starch /Stärke **66**, 1 (2014).

22. J. Jose, M.A. Al-Harthi, M.A.-A. AlMa'adeed, J. Bhadra Dakua, and S.K. De, J. Appl. Polym. Sci. **132**, 41827 (2015).

23. O.A. Bin-Dahman, J. Jose, and M.A. Al-Harthi, Starch - Stärke (2016) DOI: 10.1002/star.201600005.

24. X. Feng, Z. Yan, R. Li, X. Liu, and W. Hou, Polym. Bull. **70**, 2291 (2013).

25. V. Panwar, B. Kang, J.-O. Park, S. Park, and R.M. Mehra, Eur. Polym. J. **45**, 1777 (2009).

26. C. Basavaraja, P.X. Thinh, W.J. Kim, M. Revanasiddappa, and D.S. Huh, Polym. Compos. **33**, 1534 (2012).

27. N.A. Aal, F. El-Tantawy, A. Al-Hajry, and M. Bououdina, Polym. Compos. **29**, 125 (2008).

28. M. Rahaman, T.K. Chaki, and D. Khastgir, J. Mater. Sci. **46**, 3989 (2011).

29. A.A. Al-Ghamdi, O.A. Al-Hartomy, F. El-Tantawy, and F. Yakuphanoglu, Microsyst. Technol. **21**, 859 (2014).

30. M.H. Buraidah, A.K. Arof, and J. Non. Cryst. Solids **357**, 3261 (2011).

31. Y.M. Yusof, M.F. Shukur, H.A. Illias, and M.F.Z. Kadir, Phys. Scr. **89**, 035701 (2014).

32. M.A. Soto-Oviedo, O.A. Araújo, R. Faez, M.C. Rezende, and M.A. De Paoli, Synth. Met. **156**, 1249 (2006).

33. J. Cheng, J. Zhang, and X. Wang, J. Appl. Polym. Sci. **127**, 3997 (2013).

34. B. Chieng, N. Ibrahim, W. Yunus, and M. Hussein, Polymers. **6**, 93 (2013).

35. Y. Nishio, T. Haratani, T. Takahashi, and R.S.J. Manley, Macromolecules **22**, 2547 (1989).

36. I. Kelly, J.R. Owen, and B.C.H. Steele, J. Electroanal. Chem. Interfacial Electrochem. **168**, 467 (1984).

37. D.R. MacFarlane, J. Sun, P. Meakin, P. Fasoulopoulos, J. Hey, and M. Forsyth, Electrochim. Acta **40**, 2131 (1995).

38. X. Luo, J. Li, and X. Lin, Carbohydr. Polym. **90**, 1595 (2012).

39. E. R. Kenawy, E.A. Kamoun, M.S. Mohy Eldin, and M.A. El-Meligy, Arab. J. Chem. **7**, 372 (2014).

40. P. Sarazin, G. Li, W.J. Orts, and B.D. Favis, Polymer. **49**, 599 (2008).

41. S. Barrau, P. Demont, A. Peigney, C. Laurent, and C. Lacabanne, Macromolecules **36**, 5187 (2003).

42. D. Stauffer, A. Aharony, Introduction To Percolation Theory, Taylor & Francis, 1994.

43. M. Sahini, M. Sahimi, Applications Of Percolation Theory, Taylor & Francis, 1994.

44. W. Bauhofer and J.Z. Kovacs, Compos. Sci. Technol. **69**, 1486 (2009).

45. M. Rahaman, T.K. Chaki, and D. Khastgir, Compos. Sci. Technol. **72**, 1575 (2012).

46. R. Ram, M. Rahaman, and D. Khastgir, Compos. Part A Appl. Sci. Manuf. **69**, 30 (2015).

47. I. Balberg, Phys. Rev. Lett. **59**, 1305 (1987).

48. I. Balberg, J. Phys. D. Appl. Phys. **42**, 064003 (2009).

49. J. Li, and J.K. Kim, Compos. Sci. Technol. **67**, 2114 (2007).

50. B.P. Sahoo, K. Naskar, R.N.P. Choudhary, S. Sabharwal, and D.K. Tripathy, J. Appl. Polym. Sci. **124**, 678 (2012).

51. N. Gondaliya, D.K. Kanchan, P. Sharma, and M.S. Jayswal, Polym. Compos. **33**, 2195 (2012).

52. N. Gondaliya, D.K. Kanchan, P. Sharma, M. Pant, M.S. Jayswal, D.K. Aswal, and A.K. Debnath, in:, Int. Conf. Phys. Emerg. Funct. Mater., AIP Publishing, 2010, pp. 112–114.

53. F. He, S. Lau, H.L. Chan, and J. Fan, Adv. Mater. **21**, 710 (2009).

54. Z. M. Dang, L. Wang, Y. Yin, Q. Zhang, and Q. Q. Lei, Adv. Mater. **19**, 852 (2007).

55. G.M. TSANGARIS and G.C. PSARRAS, J. Mater. Sci. **33**, 2027(1998) .

56. G.M. Tsangaris, G.C. Psarras, and A.J. Kontopoulos, J. Non. Cryst. Solids **131-133**, 1164 (1991).

57. L. Karasek and M. Sumita, J. Mater. Sci. **31**, 281 (1996).

58. G.T. Mohanraj, T.K. Chaki, A. Chakraborty, and D. Khastgir, Polym. Eng. Sci. **46,** 1342 (2006).

59. D. Xu, V. Sridhar, S.P. Mahapatra, and J.K. Kim, J. Appl. Polym. Sci. **111**, 1358 (2009).

CHAPTER 6

COMPATIBILITY OF POLY(ACRYLIC ACID)/STARCH BLENDS

Osamah A. Bin-Dahman[1], Jobin Jose[2] and Mamdouh A. Al-Harthi[1, 3]

[1]Department of Chemical Engineering, King Fahd University of Petroleum & Minerals, Dhahran, Saudi Arabia

[2]Center for Engineering Research, King Fahd University of Petroleum & Minerals, Dhahran, Saudi Arabia

[3]Center for Research Excellence in Nanotechnology, King Fahd University of Petroleum & Minerals, Dhahran, Saudi Arabia

[*]Corresponding Author: Mamdouh A. Al-Harthi, E-mail address: mamdouh@kfupm.edu.sa

This chapter has been published in "Starch/Stärke" on June 22, 2015

Abstract

Compatibility of poly(acrylic acid) (PAA) and corn starch blends was studied by various techniques. Blends were prepared by using solution mixing and casting method with the aid of glycerol as a plasticizer. The molecular level interactions between the blend components were analyzed with Fourier transform infrared spectroscopy (FTIR). Dynamic mechanical analysis (DMA) showed that the introduction of starch into PAA matrix contributed substantially to the increase of the storage modulus. Differential scanning calorimetry (DSC) studies revealed that the PAA/starch blends were partially miscible and had an amorphous structure. The thermal gravimetric analysis (TGA) confirmed that the blends had higher thermal stability than the individual polymers. Water uptake experiments showed that the degree of swelling was mainly dependent on the PAA content in the blend. X-ray diffraction (XRD) studies showed that the incorporation of the PAA into starch destructed its crystalline structure. The morphology of the blends was changed by varying the composition. Scanning electron microscopic (SEM) analysis showed that at higher loads of starch, the PAA was formed as layers around starch granules. Blends containing higher amount of starch showed more homogenous and compatible behaviors relative to those with lower starch contents.

Keywords:

Biodegradable polymer / Compatibilization / Plasticizer / Poly(acrylic acid) / Starch

6.1 Introduction

Most polymeric materials are non-biodegradable, and thus may be accumulated in the natural environment if they are not disposed properly. This problem can be addressed by developing biodegradable polymer products that naturally degrade. Biodegradable water soluble polymers are being used for various industrial applications such as textiles, paints, papers, adhesives, water treatment, pharmaceuticals, and others [1]. However, substitution of polymers with biodegradable materials requires attention to mechanical features, thermal stability, water resistance, and chemical properties.

Poly(acrylic acid) (PAA), a water soluble polymer, forms the base of a class of materials termed "super absorbent polymers" because of PAA's ability to absorb water up to many times of its original volume and also retain water under pressure [1]. As a result of these unique features, PAA is widely used in numerous applications such as release devices, disposable diapers, ion exchange resins, tissue engineering, toothpastes, membranes, and others [2]. The swelling performance of the PAA can be controlled by crosslinking reaction and copolymerization or via preparing composites that incorporate suitable nanofillers through solution polymerization [3]. The mechanical properties of the PAA can be improved by mixing with different polymers such as poly(2-hydroxyethyl vinyl ether) (PHEVE) or poly(vinyl alcohol) (PVA) by processing them with solution mixing and casting [2, 4]. Developed blends of PAA and poly(ethylene glycol) are potential materials for thermal energy storage applications at their miscibility conditions [5]. Starch is a natural biodegradable polymer and has several advantages such as wide availability, lower cost than synthetic materials, and total compostability with no toxic residue byproducts [6]. Starch is brittle without the presence of an appropriate plasticizer.

Plasticized starch or modified starch is frequently used to enhance the final features of products [7]. Blends of starch with synthetic polymers upgrade the mechanical properties [8–11] and give biodegradable property to plastics [12–15]. Blends of starch with natural and synthetic biodegradable polymers such as chitosan [16–21], poly(lactic acid) (PLA) [22–24], polycaprolactone (PCL) [25, 26], and poly(vinyl alcohol) (PVA) [27–33] were reported. These blends are biodegradable, and are used in applications such as energy storage devices, packaging, agriculture, water treatment, and medicine.

The current chapter aims to study the compatibility of poly(acrylic acid) and corn starch blend at different blend ratios in the presence of glycerol as a plasticizer. Comprehensive characterizations using different techniques were presented in this work.

6.2 Materials and methods

6.2.1 Materials

Corn starch (CAS number: 9005-25-8) with a 27% amylose was obtained from ARASCO Corn products, Dammam, Saudi Arabia. Poly(acrylic acid) (CAS number: 9003-01-4) with an average molecular weight of 1 250 000 was procured from Winlab, UK. Glycerol (CAS number: 56-81-5) and ethanol (CAS number: 64-17-5) were obtained from Sigma–Aldrich Company.

6.2.2 Preparation of blends

Blends of poly(acrylic acid) and starch for 6 g were prepared by means of solution mixing and casting method based on the formulations shown in Table 6-1. PAA was dissolved in ethanol (200 mL) at a temperature below 70°C under stirring. Native starch

was dispersed separately in ethanol (50 mL) and a fixed amount of glycerol (2.4 mL equivalent to 3 g) was added as a plasticizer and kept at 70°C under stirring for 0.5 h. Then the plasticized starch was added to the PAA solution. The whole mixture was kept under stirring (400 rpm) at 70°C for 6 h. After that, the mixture was degassed for 10 min and then decanted into a glass plate located on a flat surface and kept for drying overnight in an air oven at 50°C. After drying, the blend film was carefully peeled-off from the plates and compressed at 150°C for 7 min using a Carver press. The samples have rectangular shapes with an average size 18×10×0.9 mm^3. Finally, the samples were kept in a desiccator filled with silica gel to avoid any moisture uptake.

Table 6-1: Formulations utilized in preparing the PAA/starch blends

Sample code	Ratio of PAA/starch
PAA	100/0
PAAS-1	90/10
PAAS-2	70/30
PAAS-3	50/50
PAAS-4	30/70
PAAS-5	10/90
Starch	0/100

6.2.3 Fourier transform infrared spectroscopy (FTIR)

A Thermo NICOLET 6700 FTIR Spectrometer was used to collect the IR spectra. The spectra were obtained by average 32 scans, at a resolution of 4 cm^{-1} from 500 to 4000 cm^{1}.

6.2.4 Dynamic mechanical analysis (DMA)

The change in the storage modulus with temperature in the range of 40–130°C was studied by a Perkin Elmer DMA Q-800 at a load of 5 N. The experiments were implemented under a nitrogen environment at a heating rate of 5°C/min and a 1Hz frequency using tensile mode.

6.2.5 Differential scanning calorimetry analysis (DSC)

Differential scanning calorimetric (DSC) studies were carried out using a DSC-Q1000, Universal V4.2E TA machine in nitrogen at a heating rate of 10°C/min and in the temperature range of -70 to 200°C. In the first scanning, the sample was heated till 100°C to remove any moisture and thermal history. This temperature was selected to avoid cyclic anhydride formation of PAA which may start forming beyond that temperature [34]. The glass transition temperature was recorded in the second heating scan.

6.2.6 Thermogravimetric analysis (TGA)

Thermal degradation analyses were carried out using Perkin Elmer, Thermogravimetric Analyzer, Pyris-6. Samples of about 10mg were heated in a nitrogen environment at a heating rate of 10°C/min over the range of 25–550°C.

6.2.7 Measurements of the degree of swelling (DS) and the absorbed water

The degree of swelling was carried out by immersing rectangular-shaped strips at room temperature in distilled water for 24 h. The initial weight was recorded after conditioning the samples in an air oven at 50°C for 24 h and then placed in a desiccator for cooling. The swollen samples were removed from water and gently wiped by using a tissue paper to remove the excess water before weighing in a sensitive balance. The swelling experiments were continued at specific intervals until a constant weight was reached. The relative degree of swelling was calculated as follows:

$$DS = \frac{W_t - W_i}{W_i} \quad (6\text{-}1)$$

where W_t and W_i are the weights of the swollen sample at any time and before swelling, respectively.

After 24 h, the samples weighed and then reconditioned at 50°C for 24 h. The percentage of water absorbed at equilibrium for each sample was calculated according to ASTM D 570-98(2010) E1 as follows:

The equilibrium degree of swelling was calculated using the constant weight as follows:

$$DS_{eq} = \frac{W_{eq} - W_i}{W_i} \times 100 \quad (6\text{-}2)$$

where *Weq* is the weight of the sample at equilibrium . The water-soluble matter loss was measured as follows:

$$\text{Soluble matter lost} = \frac{W_{Conditioned} - W_{Reconditioned}}{W_{Conditioned}} \times 100 \quad (6\text{-}3)$$

The percentage of water absorbed at equilibrium was calculated from the summation of Eqs. (6-2) and (6-3).

6.2.8 X-ray diffraction (XRD)

The X-ray diffraction (XRD) measurements were carried out using a LABX XRD-6000, Shimadzu diffractometer operating at 40 kV and 40 mA. X-rays of 1.541A^{o} wavelengths produced by the Cu K_{α} source. The angle of diffraction (2θ) was varied from 5^{o} to 40^{o} in order to detect any changes in the crystal structure.

6.2.9 Scanning electron microscopic (SEM)

The samples were cryo-fractured using liquid nitrogen. The cross sections of the fractures were coated with gold for 2 min to render the surface conductive. Scanning electron micrographs were taken using a LYRA3 TESCAN Field Emission SEM.

6.3 Results and discussion

6.3.1 Fourier transform infrared spectroscopy analysis (FTIR)

The FTIR spectra of poly(acrylic acid) and starch are shown in Fig. 6-1(a). The spectrum of pure PAA demonstrates a wide band between 3600 and 2800 cm^{-1}. The bands between 3600 and 3300 cm^{-1} reflect the O–H stretching vibration of the carboxyl groups [3, 35]. In addition, the bands at 3100–2800 cm^{-1}, superimposed upon the O–H bands, correspond to –CH_2– and –CH and stretching vibrations of acrylate units in the PAA [36]. Also, there is a strong peak at 1718 cm^{-1} corresponding to the –C=O stretching vibration of the carboxyl group of acrylate units [3]. The absorption peak at 2928 cm^{-1} in a pure starch spectrum, superimposed upon the O–H bands, reflects C–H stretching vibration in the starch molecules [29]. The peak at 1640 cm^{-1} in the starch spectrum refers to the δ-O–H

band of absorbed water [37] and the bands at 1156 and 1083 cm^{-1} are assigned to the stretching vibration of C–O in C–O–H groups [38]. The band at 998 cm^{-1} refers to C–O in C–O–C bending of α-1,4-glycosidic bond [39].

For the spectra of poly(acrylic acid) and starch blends (Fig. 6-1(b)), the peak corresponding to C–H stretching vibration (at 2928 cm^{-1}) in the starch was present in the blends containing higher amounts of starch (PAAS-4 and PAAS-5). However, in the blends of the lower amount of starch (PAAS-1, PAAS-2, and PAAS-3), this peak coalesced with the band of the O–H stretching vibration. The intensity of the characteristic peak of the C=O group in the PAA increased in the blends PAAS-1, PAAS-2, PAAS-3, and PAAS-4 which gives an indication of the nature of interaction between PAA and starch via hydrogen bonding. Moreover, in the blend containing the highest amount of starch (PAAS-5) both bands of the C=O (at 1722 cm^{-1}) in the PAA and that of the δ-O–H (at 1640 cm^{-1}) in starch exist. These bands coalesced with each other in the rest of the samples.

The spectra of PAAS blends showed new peaks in the range from 1200 to 800 cm^{-1} such as the more pronounced peaks at 1105 and 1079 cm^{-1}. These peaks correspond to a C–O stretch of the glycerol [40]. It is clear that the existence of glycerol led to an increase in intensity of O–H and C=O peaks because of the increase in the hydrogen bonding between the molecules [29].

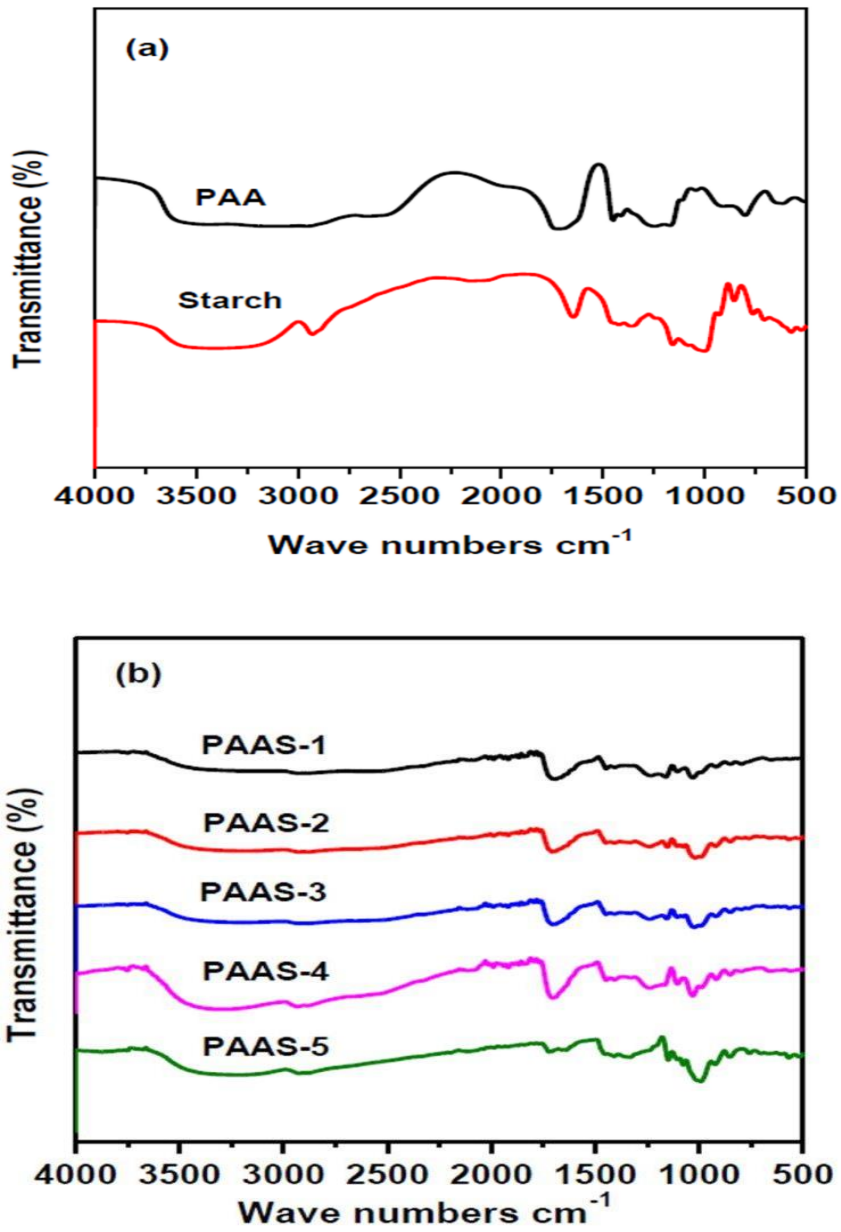

Fig 6-1: FTIR spectra of: (a) PAA, starch, and (b) their blends.

6.3.2 Dynamic mechanical analysis (DMA)

Dynamic mechanical analysis of the poly(acrylic acid) and starch blends are carried out in the temperature range from 40 to 130°C and the variations in the storage modulus with temperature are given in Fig. 6-2. The results showed that the storage modulus for the blends of larger or equal concentration of PAA compared to starch (Fig. 6-2(a–c)) decreased with increasing temperature up to 50–80°C and then increased again. The increase in storage modulus in these blends at higher temperature may be due to the formation of the intermolecular interaction through the reaction between the carboxyl group of poly(acrylic acid) and the hydroxyl group of starch to form ester bonds [4, 41]. For the blends containing lower content of PAA (Fig. 6-2(d) and (e)), thermal softening dominates over the formation of the intermolecular interaction in the whole range of temperature examined.

The results showed that the stiffness of the PAA/starch blends increased with increasing the starch content. This trend may be attributed to the larger modulus of starch granules [13, 37]. The extraordinary increase in the stiffness of the PAA/starch blends, particularly for the composition 10/90 is due to the formation of the adhesive layer of the melted PAA around the starch granules as shown in SEM micrograph study (Fig. 6-8).

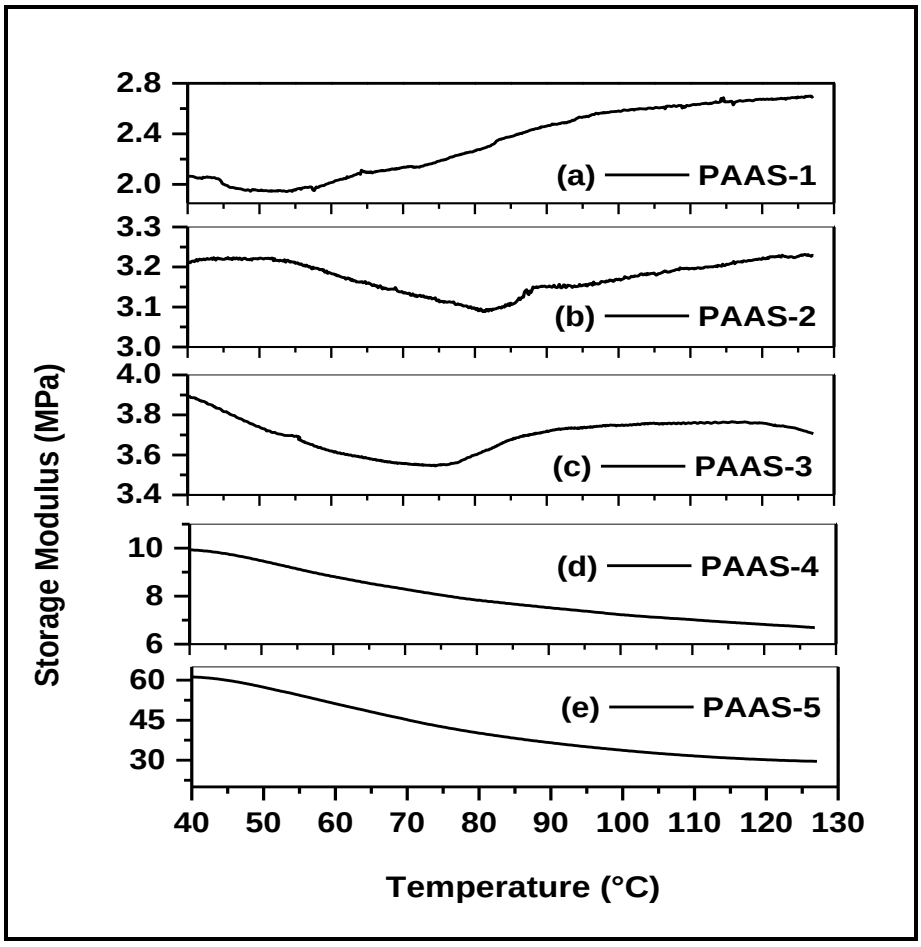

Fig 6-2: Dependence of storage modulus of PAA/starch blends on temperature.

6.3.3 Differential scanning calorimetry (DSC) analysis

The results of the DSC analysis of PAA, starch, and their blends are shown in Table 6-2. The PAA showed a glass transition temperature (T_g) of 131°C. There is a substantial discrepancy regarding the Tg of PAA that was reported. This difference may be attributed to the degree of intermolecular hydrogen bonding and the acquiring of bound water during the PAA preparation process [34, 42].

The glass transition temperature of PAA has been shifted toward lower temperature with increase in starch content. Corn starch showed a glass transition temperature of 78°C. It is interesting to see that the blends having low amounts of starch (PAAS-1, PAAS-2, and PAAS-3) showed two glass transition temperatures contrary to those with large amounts of starch (PAAS-4 and PAAS-5), which showed single T_g behavior. This behavior may be attributed to the existence of higher amounts of free glycerol in those compositions compared to the blends of large amount of starch where the whole content of glycerol was consumed during the plasticization of starch.

Table 6-2: Summary of DSC analysis results of the second heating scan

Blend	T_{g1} (°C)	T_{g2} (°C)
PAA	131	-
PAAS-1	0	107
PAAS-2	1	105
PAAS-3	7	102
PAAS-4	95	-
PAAS-5	90	-
Starch	78	-

6.3.4 Thermogravimetric analysis (TGA)

Figure 6-3 shows thermal degradation profiles of poly(acrylic acid), starch, and their blends. Poly(acrylic acid) demonstrated a three-stage degradation thermogram [43]. The first stage (60–140°C) of about 4% weight loss is mainly related to the release of moisture. Also, this stage reflects the formation of anhydride bonds. The second stage (180–340°C) of about 30% weight loss is related to the formation of unsaturated molecules due to the decarboxylation process of the anhydride structures formed in the prior stage and the release of carbon dioxide. The third stage (340–480°C) of about 43% weight loss is related to the full decomposition of the poly(acrylic acid) molecules [43].

Pure starch showed a two-step degradation thermogram. The initial weight loss (45–115°C) refers to the release of moisture. However, the major decomposition of starch of about 80% occurred in the temperature range of 250–400°C [29].

Blends of PAA/starch displayed a trend of multi-step degradation thermograms. The first step is assigned to the volatilization of water as well as glycerol. The second stage of degradation is mainly contributed to the decomposition of starch whereas the third stage weight loss is dominated by the main chain scission of the PAA molecules.

Figure 6-4 shows the first-order derivative of TGA curves. The results of the maximum degradation temperature (T_d) are shown in Table 6-3. The value of the difference between the temperature of the end and the beginning of the maximum degradation temperature at the derivative TG of 0.2%, ΔT, also is reported in Table 6-3. The increase in ΔT reflects the increase in the degree of the blend heterogeneity as reported by Sreekumar et al. [28, 30]. The maximum degradation temperature of the blends contains higher or equal content of PAA shifted toward high temperature causing an increase in ΔT. The blends that contain a higher amount of starch look more similar to that of the pure starch. Poly(acrylic acid) and starch blends of the compositions of 30/70 and 10/90 are more homogenous and compatible than those of the compositions of 90/10, 70/30, and 50/50. The increase of the degree of the heterogeneity of the latter set of blends may be attributed to the occurrence of phase separation due to the dissociation of hydrogen bonds [44].

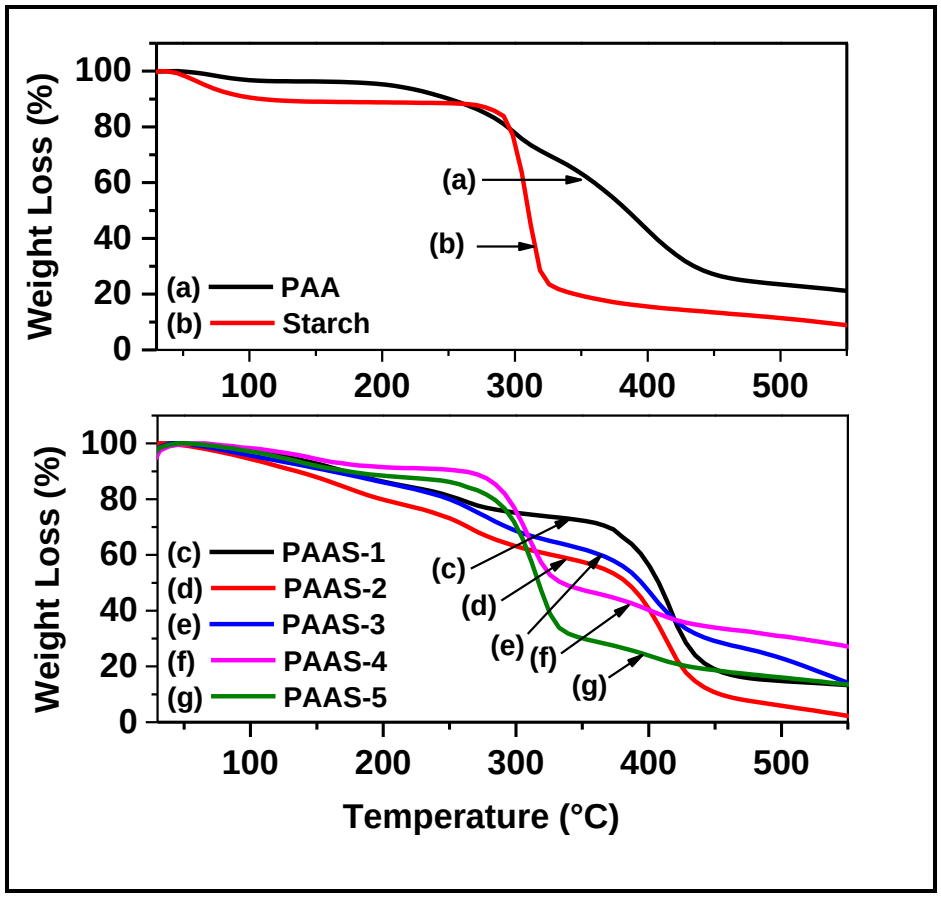

Fig 6-3: TGA thermograms for PAA, starch, and their blends.

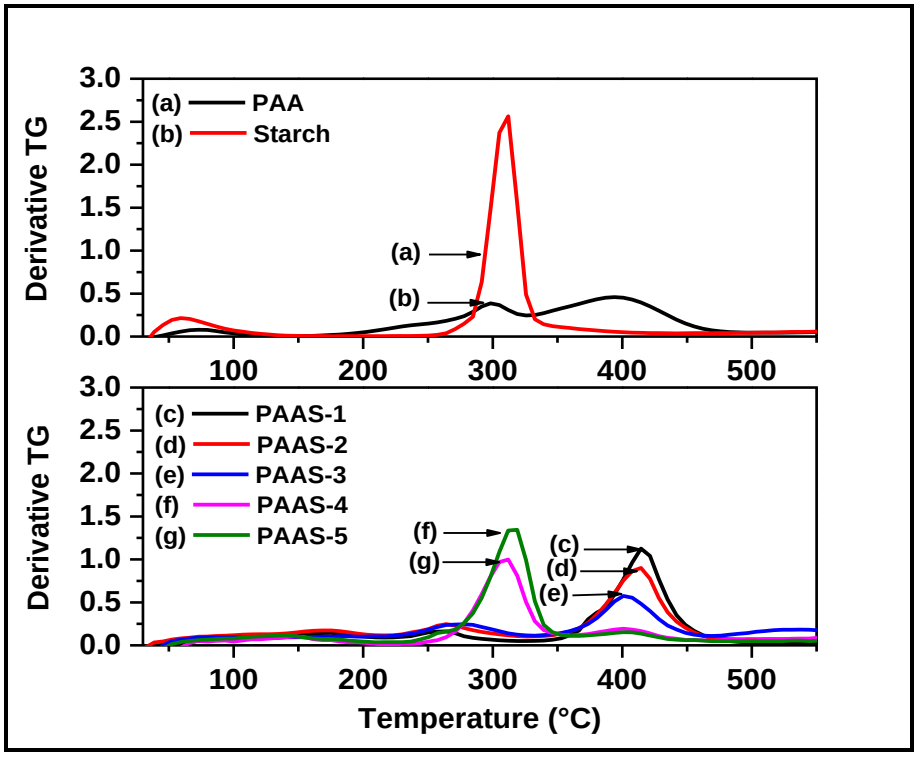

Fig 6-4: First-order derivatives of TGA curves for PAA, starch, and their blends.

Table 6-3: Summary of the temperature of the maximum loss in weight, ΔT and percent of residue at 550°C for PAA, starch, and their blends

Sample	T_d (°C)	ΔT (°C)	Residue at 550 °C (%)
PAA	396	171	20
PAA/S-1	416	86	13
PAA/S-2	414	83	3
PAA/S-3	403	74	14
PAA/S-4	314	65	27
PAA/S-5	312	67	15
Starch	311.5	51	9

6.3.5 Degree of swelling and the absorbed water

Figure 6-5 shows the swelling rate behavior of PAA/starch films in distilled water for 24 h at room temperature. Initially, the swelling rate of all samples increased sharply and finally reached an equilibrium state. The time to reach equilibrium decreased with increasing the starch content.

It is evident that the degree of swelling depends on the concentration of the PAA in the blends. The degree of swelling increased with increasing PAA amount in the blend. Poly(acrylic acid) is a hydrophilic anion polymer and possesses large swelling ratios due to the carboxyl groups present in the polymer chain [35]. The amount of water absorbed at the equilibrium of the films increased with increasing the PAA content. The results are summarized in Table 6-4.

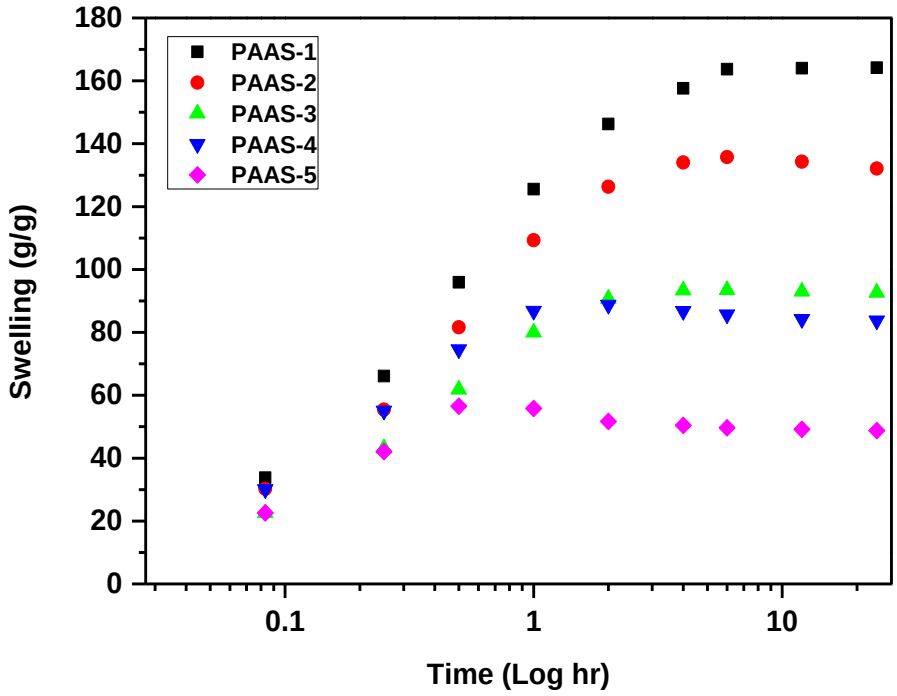

Fig 6-5: Swelling rate behavior for PAA/starch blends.

Table 6-4: The percentage of water absorbed at equilibrium for PAA/starch blends

Blend	The percentage of water absorbed (%) [a)]
PAAS-1	189
PAAS-2	163
PAAS-3	118
PAAS-4	114
PAAS-5	78

a) Calculated using equation (2) and (3).

6.3.6 X-ray diffraction (XRD) studies

Figure 6-6 shows the XRD diagrams of PAA, starch, and PAA/starch blends. The PAA is an amorphous polymer while corn starch contains semicrystalline granules with mainly polyhedral shape. These polyhedrons characterized by nearly perfect left-handed, six-fold double helices [45]. The characteristic peaks of starch appeared in 15.2, 17.2, 18.1, and 23^{o} 2θ represent the XRD pattern of a mixture of A-type and V-hydrate (V_h) type crystal structure in starch [28, 30].

The incorporation of the PAA into starch has destructed its crystalline structure and the blends have been converted to an essentially amorphous material. This effect was predominant with increase in PAA content. This may be attributed to the higher amounts of glycerol relative to starch in those compositions [29, 46].

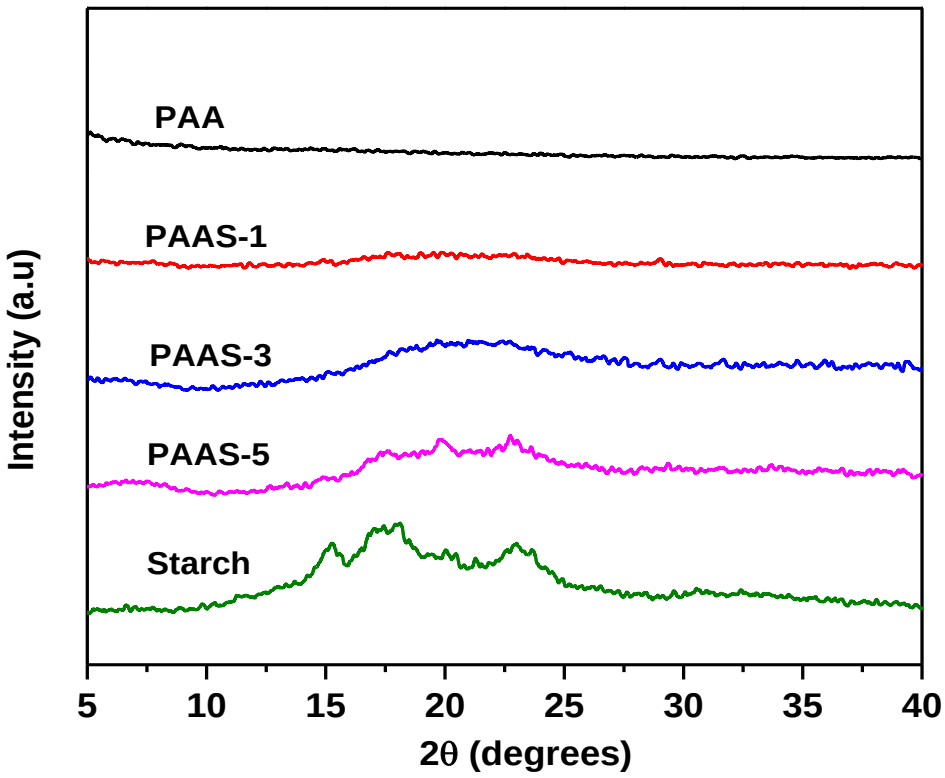

Fig 6-6: XRD plots of PAA, starch, and PAA/starch blends.

6.3.7 Scanning electron microscopic (SEM) studies

Scanning electron micrographs of PAA/starch blends are shown in Fig. 6-7. Starch granules have almost spherical shape with an average size of 10 mm. At lower concentrations of starch, SEM micrographs showed non-uniform dispersion of starch in the PAA matrix with clear spots of agglomerations (Fig. 6-7(a) and (b)). At higher content of starch in the blends, particularly PAAS-5, the PAA flowed around the starch granules and formed binding layers during the solidification step (Fig. 6-8). This form of PAA/starch interface caused starch granules to hold one another in the matrix and eventually led to an increase in the storage modulus as discussed previously in the DMA analysis (Fig. 6-2).

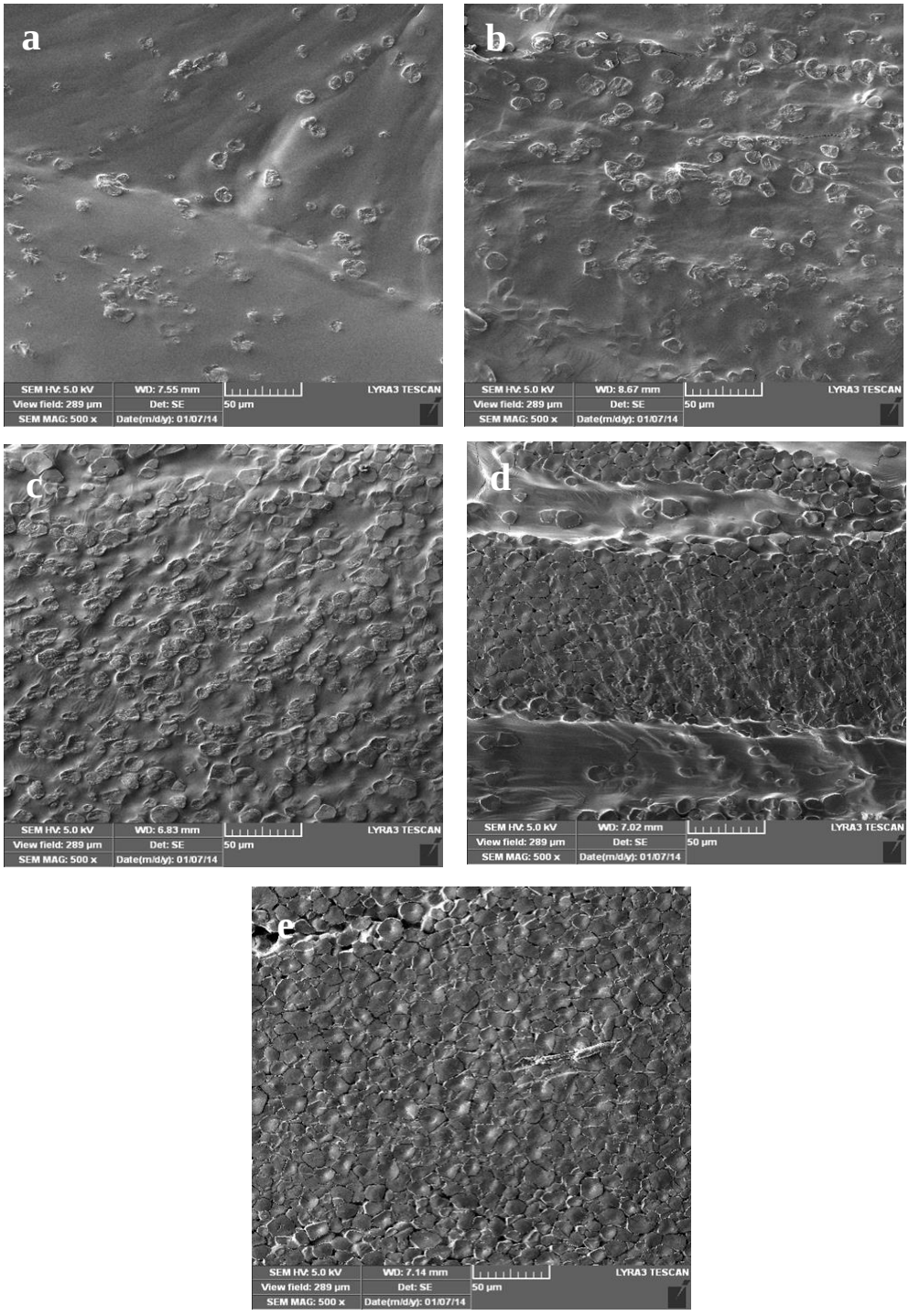

Fig 6-7: SEM micrographs for PAA/starch blend prepared at different ratios: (a) 90/10; (b) 70/30; (c) 50/50; (d) 30/70; (e) 10/90.

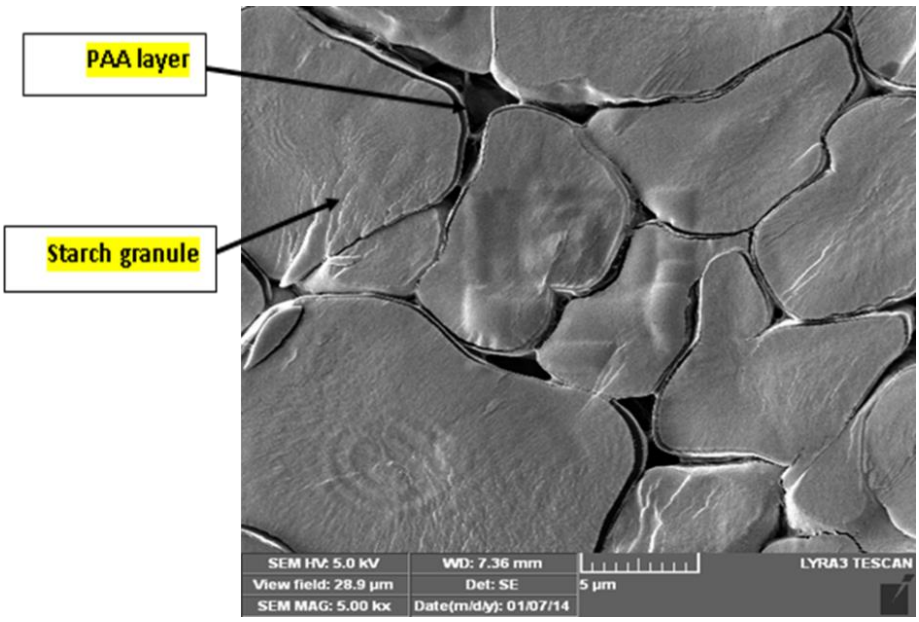

Fig 6-8: SEM micrograph for PAA/starch 10/90 blend.

6.4 Conclusion

Poly(acrylic acid)/starch blends were successfully prepared through solution mixing and casting process. The incorporation of glycerol into the blend increased the intermolecular hydrogen bonding between PAA and starch. The stiffness of the PAA/starch blends was increased with the increase of starch content. The blends were partially miscible and have fully amorphous structures. The thermogravimetric studies showed that the blends with higher amount of starch were more homogenous and compatible than those of the lower content of starch. The water uptake measurements demonstrated that the degree of swelling was a function of the PAA content in the blend. The crystalline structure of starch was destroyed after incorporating the PAA. The morphology of the blends was changed by varying the composition of the blend. At higher loading of starch, the lower phase PAA was formed as layers around all granules of starch.

References

[1] Kadajji, V. G., Betageri, G. V., Water soluble polymers for pharmaceutical applications. *Polymers* 2011, *3*, 1972–2009.

[2] Jose, J., Shehzad, F., Al-Harthi, M. A., Preparation method and physical, mechanical, thermal characterization of poly(vinyl alcohol)/poly(acrylic acid) blends. *Polym. Bull*.2014, *71*, 2787–2802.

[3] Zhu, Z. Q., Sun, H. X., Qin, X. J., Jiang, L., Pei, C. J. et al., Preparation of poly(acrylic acid)–graphite oxide superabsorbent nanocomposites. *J. Mater. Chem*. 2012, *22*, 4811–4817.

[4] Khutoryanskiy, V. V., Cascone, M.G., Lazzeri, L., Barbani, N. et al., Hydrophilic films based on blends of poly(acrylic acid) and poly(2-hydroxyethyl vinyl ether): Thermal, mechanical, and morphological characterization. *Macromol. Biosci*. 2003, *3*,117–122.

[5] Alkan, C., Günther E., Hiebler S., Himpel, M., Complexing blends of polyacrylic acid-polyethylene glycol and poly(ethylene-co-acrylic acid)-polyethylene glycol as shape stabilized phase change materials. *Energy. Convers. Manag.* 2012, *64*, 364 – 370.

[6] Xie, F., Pollet, E., Halley, P. J., Avérous, L., Starch-based nano-biocomposites. *Prog. Polym. Sci.* 2013, *38*, 1590 –1628.

[7] Maiti, M., Kaith, B. S., Jindal, R., Jana, A. K., Synthesis and characterization of corn starch based green composites reinforced with Saccharum spontaneum L graft copolymers prepared under micro-wave and their effect on thermal, physio-chemical and mechanical properties. *Polym. Degrad. Stab*. 2010, *95*, 1694 –1703.

[8] Prachayawarakorn, J., Hommanee, L., Phosee, D., Chairapaksatien, P., Property improvement of thermoplastic mung bean starch using cotton fiber and low-density polyethylene. *Starch/Stärke* 2010, *62*, 435 – 443.

[9] Li, J., Luo, X., Lin, X., Zhou, Y., Comparative study on the blends of PBS/thermoplastic starch prepared from waxy and normal corn starches. *Starch/Stärke* 2013, *65*,831– 839.

[10] Gupta, A. P., Kumar, V., Sharma, M., Formulation and characterization of Bbiodegradable packaging film derived from potato starch & LDPE grafted with maleic anhydride—LDPE composition. *J. Polym. Environ*. 2010, *18*,484 – 491.

[11] Sharif, A., Aalaie, J., Shariatpanahi, H., Hosseinkhanli, H., Khoshniyat, A., Study on the structure and properties of nanocomposites based on high-density polyethylene/starch blends. *J. Polym. Res.* 2011, *18*, 1955 –1969.

[12] Raquez, J. M., Bourgeois, A., Jacobs, H., Degée, P. et al., Oxidative degradations of oxodegradable LDPE enhanced with thermoplastic pea starch: Thermo-mechanical properties, morphology, and UV-ageing studies. *J. Appl. Polym. Sci.* 2011, *122*, 489 – 496.

[13] Amin, R. M., Sreekumar, P. A., Al-Harthi. M. A., De, S. K., Abu-Sharkh, B. F., Natural weather ageing of the low-density polyethylene: Effect of polystarch N. *J. Appl. Polym. Sci*. 2013, *127*, 1122–1127.

[14] Majid, R. A., Ismail, H., Taib, R. M., The effects of natural weathering on the properties of linear density polyethylene (LDPE)/thermoplastic sago starch (TPSS) blends. *Polym. Plast. Technol. Eng*. 2010, *49*, 1142–1149.

[15] Vieyra Ruiz, H., Martínez, E. S. M., Mendez, M. A. A., Biodegradability of polyethylene-starch blends prepared by extrusion and molded by injection: Evaluated by response surface methodology. *Starch/Stärke* 2011, *63*, 42–51.

[16] Shukur, M. F., Kadir, M. F. Z., Hydrogen ion conducting starch-chitosan blend based electrolyte for application in electrochemical devices. *Electrochimica Acta* 2015, *158*, 152 –165.

[17] Sudhakar,Y.N., Selvakumar, M., Lithium perchlorate doped plasticized chitosan and starch blend as biodegradable polymer electrolyte for supercapacitors. *Electrochim. Acta.* 2012, *78*, 398 – 405.

[18] Shukur, M.F., Ithnin, R., Kadir, M.F.Z., Electrical properties of proton conducting solid biopolymer electrolytes based on starch–chitosan blend. *Ionics* 2013, *20*, 977–999.

[19] Duan, B., Sun, P., Wang, X., Yang, C., Preparation and properties of starch nanocrystals/carboxymethyl chitosan nanocomposite films. *Starch/Stärke* 2011,*63*, 528–535.

[20] Liu, H., Adhikari, R., Guo, Q., Adhikari, B., Preparation and characterization of glycerol plasticized (high-amylose) starch–chitosan films. *J. Food Eng.* 2013, *116*, 588 –597.

[21] Yusof, Y. M., Shukur, M. F., Illias, H. A., Kadir, M. F. Z., Conductivity and electrical properties of corn starch–chitosan blend biopolymer electrolyte incorporated with ammonium iodide. *Physica Scripta* 2014, *89*, 035701, 1– 10.

[22] Oza, H., Thompson, M. R., Hrymak, A. N., Liu, Q., Influence of di-functional versus multi-functional chain extenders on the foamability of a potato starch-based biopolymer. *Starch/Stärke* 2012, *64*, 944 – 954.

[23] Ouyang, C., Wang, Y., Zhao, N., Liu, X. et al., Preparation of poly(lactic acid) and modified starch composites. *Polym. Bull.* 2012, *68*, 2009–2019.

[24] Xiong, Z., Yang, Y., Feng, J., Zhang, X. et al., Preparation and characterization of poly(lactic acid)/starch composites toughened with epoxidized soybean oil. *Carbohydr. Polym.* 2013, *92*, 810 – 816.

[25] Nor, F. M., Kurniawan, D., Seo, Y. K., Park, J. K. et al., Polycaprolactone-starch blends with corn-based coupling agent: physical properties and in vitro analysis. *Proc. Inst. Mech. Eng. H.* 2012, *226*, 693 – 698.

[26] Ali Akbari Ghavimi, S., Ebrahimzadeh, M. H., Solati-Hashjin, M., Osman, A., Azuan, N., Polycaprolactone/starch composite: Fabrication, structure, properties, and applications. *J. Biomed. Mater. Res. A* 2014, DOI: 10.1002/jbm.a.35371.

[27] Palma-Rodríguez, H. M., Aguirre-Álvarez, G., Chavarría-Hernández, N., Rodríguez-Hernández, A. I. et al., Oxidized banana starch-polyvinyl alcohol film: Partial characterization. *StarchlStärke* 2012, *64*, 882 – 889.

[28] Sreekumar, P. A., Al-Harthi, M. A., De, S. K., Reinforcement of starch/polyvinyl alcohol blend using nano-titanium dioxide. *J. Compos. Mater.* 2012, *46*, 3181–3187.

[29] Sreekumar, P. A., Al-Harthi, M. A., De, S. K., Effect of glycerol on thermal and mechanical properties of polyvinyl alcohol/starch blends. *J. Appl. Polym. Sci.* 2012, *123*, 135 – 142.

[30] Sreekumar, P. A., Al-Harthi, M. A., De, S. K., Studies on compatibility of biodegradable starch/polyvinyl alcohol blends. *Polym. Eng. Sci*. 2012, *52*, 2167–2172.

[31] Appu, S. P., Kumar De, S., Khan, M. J., Al-Harthi, M. A., Natural weather ageing of starch/polyvinyl alcohol blend: effect of glycerol content. *J. Polym. Eng*. 2013, *33*, 257–263.

[32] Jose, J., De, S. K., AlMa'adeed, M. A. A., Dakua, J. B. et al., Compatibilizing role of carbon nanotubes in poly(vinyl alcohol)/starch blend. *Starch/Stärke* 2014, *67*, 147–153.

[33] Jose, J., Al-Harthi, M. A., AlMa'adeed, M. A. A., Bhadra Dakua, J., De, S. K., Effect of graphene loading on thermomechanical properties of poly(vinyl alcohol)/starch blend. *J. Appl. Polym. Sci.* 2015, DOI: 10.1002/app.41827.

[34] Maurer, J. J., Eustace, D. J., Ratcliffe, C. T., Thermal characterization of poly(acrylic acid). *Macromolecules* 1987, *20*, 196 – 202.

[35] Huang, Y., Yu, H., Xiao, C., pH-sensitive cationic guar gum/poly (acrylic acid) polyelectrolyte hydrogels: Swelling and in vitro drug release. *Carbohydr. Polym.* 2007, *69*, 774 –783.

[36] Dubinsky, S., Grader, G. S., Shter, G. E., Silverstein, M. S., Thermal degradation of poly(acrylic acid) containing copper nitrate. *Polym. Degrad. Stab*. 2004, *86*, 171–178.

[37] Chandra, R., Rustgi, R., Biodegradation of maleated linear low-density polyethylene and starch blends. *Polym. Degrad. Stab.* 1997, *56*, 185 – 202.

[38] Xiong, H., Tang, S., Tang, H., Zou, P., The structure and properties of a starch-based biodegradable film. *Carbohydr. Polym*. 2008, *71*, 263 – 268.

[39] Flores-Morales, A., Jiménez-Estrada, M., Mora-Escobedo, R., Determination of the structural changes by FT-IR, Raman, and CP/MAS 13C NMR spectroscopy on retrograded starch of maize tortillas. *Carbohydr. Polym.* 2012, *87*, 61– 68.

[40] Cerqueira, M. A., Souza, B. W., Teixeira, J. A., Vicente, A. A., Effect of glycerol and corn oil on physicochemical properties of polysaccharide films – A comparative study. *Food Hydrocoll*. 2012, *27*, 175 – 184.

[41] Herrera-Kao, W., Aguilar-Vega, M., Storage modulus changes with temperature in poly(vinyl alcohol), PVA,/poly(acrylic acid), PAA, blends. *Polym. Bull*. 1999, *42*, 449 –456.

[42] Park, J. K., Kim, D. W., Kim, C. H., Maeng, K. S., Hwang, T. S., Kim, Y. C., Effect of drying conditions on the glass transition of poly(acrylic acid). *Polym. Eng. Sci.* 1991, *12*, 867 –72.

[43] Khutoryanskiy, V. V., Cascone, M. G., Lazzeri, L., Barbani, N. et al., Morphological and thermal characterization of interpolymer complexes and blends based on poly(acrylic acid) and hydroxypropylcellulose. *Polym. Int.* 2004, *53*, 307–311

[44] Zhang, X., Takegoshi, K., Hikichi, K., Phase separation and thermal degradation of poly(vinyl alcohol)/poly(methacrylic acid) and poly(vinyl alcohol)/poly(acrylic acid) systems by 13C c.p./m.a.s. n.m.r. *Polymer* 1992, *33*,718 – 724.

[45] Matzinos, P., Tserki,V., Kontoyiannis, A., Panayiotou, C., Processing and characterization of starch/polycaprolactone products. *Polym. Degrad. Stab.*2002, *77*, 17–24.

[46] Zhang,Y., Han, J.H., Crystallization of high-amylose starch by the addition of plasticizers at low and intermediate concentrations. *J. Food Sci.* 2010,*75*, N8 – N16.

CHAPTER 7

CONCLUSIONS AND RECOMMENDATIONS

7.1 Conclusions

The environmental effects primarily affect the crystallinity of all biodegradable polymers. In the early stages of exposure, the degradation was mainly because of dissolution of the amorphous phase, while in the later stages the degradation process has been extended even to the crystalline phases. The incorporation of graphene into PVA/starch matrix led to a remarkable increase in the value of the change in percentage of crystallinity during the exposure. Graphene accelerates the dissolution rate of the amorphous portion of the PVA/starch blend by weakening the interaction between the molecules. As the ageing process progressed, the polymer chain scission might have taken place due to the exposure to the sunlight. The shorter polymer chains thus generated could be easily re-arranged in the polymer matrix and hence increase in percentage crystallinity.

The non-isothermal crystallization behavior of the nanocomposites was investigated using differential scanning calorimetry (DSC). Ozawa and Mo models have been applied to study the non-isothermal kinetics. The Ozawa model was failed to adequately describe the crystallization behavior of the system owing to the inappropriate assumption of ignoring the secondary stage crystallization. Mo model had successfully described the non-isothermal crystallization process of poly(vinyl alcohol)/starch/graphene

nanocomposites. It was observed that incorporation of graphene into the PVA/starch composite acts as a nucleating agent and shifted its crystallization onset temperature (T_{on}) and crystallization peak temperature (T_c) to higher values as well as enhanced its crystallization enthalpy (ΔH_{cry}). However, the addition of graphene confined the movement of chain transfers and hindered the growth of crystals, and consequently retarded the overall rate of crystallization. The activation energy (E_A) was evaluated by using the differential Friedman method, which shows the dependence of E_A on temperature and extent of transformation. Also, it was observed that incorporation of graphene into the PVA/starch composite considerably lowers the effective E_A for crystallization, therefore proving the nucleation.

The DC conductivity of PVA has been increased with the addition of glycerol and starch. Initially, the increase in conductivity with the addition of graphene was very low. After a certain loading (known as percolation threshold), a drastic increase in DC conductivity was observed. For the present system, the value of percolation threshold was 11.5 wt. %. The AC conductivity of the PVA/starch/graphene nanocomposites was improved with the increase in both graphene loading and frequency. At lower graphene loading, the AC conductivity is mainly governed by the hopping and tunnelling mechanisms of electrical conductivity. At higher graphene loading, there is a substantial increase in the value of both DC and AC conductivity owing to the formation of continuous conductive network pathways of graphene aggregates within the PVA/starch blend. The dielectric permittivity of PVA without glycerol showed a weak frequency-dependent behavior over the whole range of frequencies. However, the permittivity of PVA films with glycerol and PVA/starch/graphene nanocomposites showed a strong frequency-dependent behavior in

the low frequency zone because of the higher magnitude of interface polarization. This frequency-dependent behavior is stronger in films with high amounts of graphene. The addition of a plasticizer in PVA led to the presence of peak frequency in the PVA loss factor spectrum. This can be attributed to an increase in the amorphous content in the PVA polymer. The insertion of graphene into the PVA/starch blend shifted the peak frequency towards the higher frequency side. The Cole-Cole plots showed a suppressed semicircle indicating a non-Debye behavior and the PVA specimen showed the higher deviation. The PVA showed a gradual decrease in the value of Z' with increase in frequency. The value of Z' slowly decreases with increasing filler loading as well as with increasing frequency and this trend was similar for all nanocomposites. Similar behavior was detected for Z''. The addition of graphene reduced the area under the semicircles of the Nyquist plot and this reduction increased with increasing filler content because of the increase in conductivity. The semicircles at higher frequency are due to the bulk properties and the spikes at lower frequency are due to interface properties of the composite materials.

Poly(acrylic acid)/starch blends were successfully prepared through solution mixing and casting process. The incorporation of glycerol into the blend increased the intermolecular hydrogen bonding between PAA and starch. The stiffness of the PAA/starch blends was increased with the increase of starch content. The blends were partially miscible and have fully amorphous structures. The thermogravimetric studies showed that the blends with higher amount of starch were more homogenous and compatible than those of the lower content of starch. The water uptake measurements demonstrated that the degree of swelling was a function of the PAA content in the blend. The crystalline structure of

starch was destroyed after incorporating the PAA. The morphology of the blends was changed by varying the composition of the blend. At higher loading of starch, the lower phase PAA was formed as layers around all granules of starch.

7.2 Recommendations

The following steps can be recommended in order to further improve the properties of graphene reinforced eco-friendly water soluble polymers:

1. Development of graphene reinforced PAA/starch nanocomposites and characterization of the prepared composites by studying mechanical, thermal, electric and water transport properties as well as morphological changes.
2. Investigating the ageing behavior of the graphene reinforced PAA/starch composites under natural weathering conditions.
3. Development of graphene reinforced PVA/starch and PAA/starch nanocomposites by modifying graphene surface using several chemical functional groups and characterization of the prepared composites by studying the mechanical, thermal, electric and water transport properties as well as morphological changes.
4. Studying the dynamic viscosity of selected nanocomposites of graphene reinforced PVA/starch and PAA/starch composites in order to examine the feasibility of using conventional plastics processing equipment.

Vitae

Name: Osamah Awadh Bin Dahman.

Nationality: Yemeni.

Date and Place of Birth: July 08th, 1978, Hadhramout, Yemen.

Marital Status: Married

Permanent Address: Al-Shihr, Hadhramout, Yemen.

Mobile: +966-530059085

+967-773685559

Email: o.bindahman@gmail.com

bindahman@kfupm.edu.sa

Education

- **Doctor of Philosophy in Chemical Engineering**, King Fahd University of Petroleum and Minerals, Dhahran, Saudi Arabia, (December, 2016).
  Thesis Title: Graphene Reinforced Eco-Friendly Water Soluble Polymers.
- **Master of Science in Chemical Engineering**, King Fahd University of Petroleum and Minerals, Dhahran, Saudi Arabia, (June, 2011).
  Thesis Title: Experimental Investigation of Heat Transfer Characterization for CNT-Nanofluid in Heat Exchangers.
- **Bachelor of Science in Chemical Engineering**, Hadhramout University, Yemen (May, 2003), with 1st class honors.

Research papers

1. **Bin-Dahman, O. A.,** Jose, J., Al-Harthi, M. A., Compatibility of poly(acrylic acid)/starch blends. *Starch/Stärke* 2015,*67*,1061–1069.

2. **Bin-Dahman, O. A.,** Jose, J., Al-Harthi, M. A., Effect of natural weather aging on the crystallinity of poly(vinyl alcohol)/starch/graphene nanocomposite. *Starch/Stärke* 2016, DOI: 10.1002/star.201600005.

3. **Bin-Dahman, O. A.,** Shehzad, F., Al-Harthi, M. A., Influence of graphene on non-isothermal crystallization kinetics of poly(vinyl alcohol)/starch composite. Journal of thermal analysis and calorimetry (Submitted).

4. **Bin-Dahman, O. A.,** Rahaman, M., Khastgir, D., Al-Harthi, M. A., Electrical and dielectric properties of poly(vinyl alcohol)/starch/graphene nanocomposites. Polymer Science Series A (Submitted).

Patents

No.	Patent Title	Inventors	Status
1.	Poly(Acrylic Acid)-Glycerol Blends	Mamdouh A. Al-Harthi, **Osamah A. Bin-Dahman**, Jobin Jose, Sadhan Kumar De	Issued patent, Patent No. : US 9346938 B1
2.	Nanocomposite Films with Conducting and Insulating Surfaces	Mamdouh A. Al-Harthi, **Osamah A. Bin-Dahman**, Mostafizur Rahaman	Filed patent, Appl. No. : US 14/877623
3.	Nanocomposite Films and Methods of Preparation Thereof	Mamdouh A. Al-Harthi, **Osamah A. Bin-Dahman**,	Filed patent, Appl. No. : US 62/280459